MEASURING HEMOGLOBIN OXYGENATION BY TIME RESOLVED REFLECTANCE

DUAL WAVELENGTH TIME RESOLVED REFLECTANCE MEASUREMENTS FOR THE DETERMINATION OF HEMOGLOBIN OXYGENATION IN TISSUE

by

ROBERT HUNTER, B.SC.

A Thesis

Submitted to the School of Graduate Studies

in Partial Fulfillment of the Requirements

for the Degree

Master of Science

McMaster University

MASTER OF SCIENCE (1998) McMaster University

(Physics) Hamilton, Ontario

TITLE: Dual Wavelength Time Resolved Reflectance Measurements For The Determination Of Hemoglobin Oxygenation in Tissue

AUTHOR: Robert Hunter, B.Sc. Hons. (McMaster University, Canada)

SUPERVISOR: Dr. Michael S. Patterson

NUMBER OF PAGES: xiv, 183

ABSTRACT

The aim of this work was to develop and test a system to measure the optical properties of tissue *in vivo*, with the specific goal of monitoring hemoglobin oxygenation in tissue. Since it is desirable to determine these properties noninvasively, it is necessary to use the information retained in the light that is scattered out of the tissue, i.e. the reflectance, to estimate values for the scattering and absorption coefficients of the tissue. It is possible to use these properties to study many physiological functions, including hemoglobin saturation and tissue metabolism.

Methods for the indirect measurement of tissue optical properties fall into three categories: continuous wave (cw), frequency domain and time domain techniques. Regardless of which technique is used to measure the reflectance, a suitable model of light transport is needed to provide the best estimates of the optical properties of the medium investigated. The diffusion equation has been shown to have good agreement with both phantom measurements and Monte Carlo simulations under certain conditions.

This thesis discusses a two wavelength system which operates in time-correlated single photon counting mode to measure noninvasively the optical properties of tissue. By exploiting the known differences in absorption between oxyhemoglobin and deoxyhemoglobin at 750 nm and 810 nm, this system will be used to monitor hemoglobin saturation. However, prior to performing oxygenation measurements, the performance of the system was compared to a continuous wave (cw) and a frequency domain system in our lab. This thesis will outline the instrumentation of the time-resolved system, results from fitting Monte Carlo data and the results of various measurements which investigate the response of the system to different factors. The two main experiments study the ability of the system to predict variations in either the scattering

or the absorption coefficient. Following the success of the system in predicting optical properties of tissue simulating phantoms, *in vivo* measurements were performed on the palm of the hand. The system proved sensitive enough to reflect changes in oxygenation induced in the tissue.

ACKNOWLEDGEMENTS

I am grateful to Dr. Michael Patterson for sharing his insight into this project and providing excellent guidance throughout its duration. I would also like to thank Dr. Tom Farrell and Dr. William Prestwich for their help with this thesis. I also wish to express my thanks to Dr. Joe Hayward, Dr. Robert Weersink and Jody Bruulsema for their assistance in setting up the apparatus and general knowledge around the lab. I wish to acknowledge Ed Hull for providing the Mie theory programs, David Moulton and Steen Madsen for the use of some of their programs and Phil Eles for his help with the Monte Carlo data. In addition, I am thankful to Derek Hyde and Lee Chin for their contributions to the project. I am also indebted to Colleen and Rob for many conversations and coffees which are so essential to any successful project. Finally, I would like to thank my family for their continued support over the years.

TABLE OF CONTENTS

ABSTRACT iii

ACKNOWLEDGEMENTS v

LIST OF FIGURES x

LIST OF TABLES xiii

1 INTRODUCTION 1

1.1 Motivation 1

1.2 Interaction of light with biological tissue 3

1.3 Measurement of optical properties 6

1.3.1 Steady State Methods *7*

1.3.2 Frequency-Domain Methods *9*

1.3.3 Time-Domain Methods *11*

1.4 Models for light transport 14

1.4.1 Zero Boundary Condition *19*

1.4.2 Extrapolated Boundary Condition *20*

1.4.3 Partial Current Boundary Condition *22*

1.5 Hemoglobin oxygenation measurements 23

1.6 Thesis proposal 29

2	**EXPERIMENTAL**	**31**
2.1	Apparatus	31
2.1.1	*Time correlated photon counting system*	*31*
2.1.2	*Pulsed diode lasers*	*36*
2.1.3	*Photomultiplier tube*	*37*
2.1.4	*Control circuitry*	*38*
2.1.5	*Phantoms for measurement*	*39*
2.2	Analysis	40
2.2.1	*Non linear least squares fitting in time domain*	*43*
2.2.2	*Boundary Conditions*	*65*
2.2.3	*Fitting phase and amplitude in frequency space*	*69*
3	**RESULTS**	**89**
3.1	System Characterization	89
3.2	Preliminary Phantom Measurements using Intralipid	92
3.2.1	*Characterization*	*93*
3.2.2	*Intralipid Dilutions*	*94*
3.2.3	*Increasing Concentration of Melanin Ink*	*96*
3.3	Phantom Measurements using Solid Phantoms	100
3.3.1	*Short Term Stability*	*101*
3.3.2	*Effect of Statistics on Optical Properties*	*103*
3.3.3	*Boundary Conditions*	*106*

3.3.4 Source Detector Separation *108*

3.3.5 Measurements using 750 nm Diode Laser *109*

3.4 Polystyrene Spheres 111

3.4.1 Variation with Concentration *112*

3.4.2 Phantom Size and Boundary Effects *118*

3.4.3 Variation of Results with ρ *119*

3.4.4 Investigation of Performance of 750 nm Diode Laser *120*

3.5 Variation of absorption 121

3.5.1 Variation of Absorption with Ink Concentration *122*

3.5.2 Variation of Absorption with Indocyanine Green Concentration *125*

3.6 Results from Dual Wavelength System 132

3.6.1 Dual Wavelength Measurements on Tissue Simulating Phantoms *133*

3.6.2 Dual Wavelength Measurements Performed in vivo *134*

3.6.3 Further in vivo Measurements *138*

4 DISCUSSION **142**

4.1 Polystyrene Spheres 142

4.1.1 Effect of Source-detector separation on estimated scattering *142*

4.1.2 Further Measurements using Large Volume Phantom *144*

4.1.3 Investigations on Total Attenuation Coefficient of Polystyrene *150*

4.1.4 Comparison of Theoretical Data from Time Domain and CW Fitting Programs *151*

4.1.5 Effect of Scattering Time Delay on Estimates of μ_s' *153*

4.2 Variation of Absorption with added ICG in the Frequency Domain 155

4.3 *in vivo* Dual Wavelength Measurements 160

4.4 Uncertainties 163

5 CONCLUSIONS 166

6 REFERENCES 176

LIST OF FIGURES

Figure 1.1: Variation of absorption of oxyhemoglobin and deoxyhemoglobin with. wavelength. 4

Figure 1.2: The principle of spatially resolved measurements. 8

Figure 1.3: The principle of the frequency domain system. 9

Figure 1.4: The principle of time domain measurements. 12

Figure 1.5: Representation of the extrapolated boundary condition (EBC). 21

Figure 2.1: Diagram of the time correlated photon counting system. 34

Figure 2.2: Control diagrams for dual measurement system. 39

Figure 2.3: Algorithm used to estimate μ_a and μ_s' in the time domain. 42

Figure 2.4: Fit of diffusion data with noise at $\rho = 15$ mm. 46

Figure 2.5: Fit of diffusion data with noise at $\rho = 20$ mm. 50

Figure 2.6: Diffusion theory fit to Monte Carlo (MC) data at 10 mm ($\mu_a = 0.01$ mm^{-1}, $\mu_s' = 1.0$ mm^{-1}). 53

Figure 2.7: Diffusion theory fit to Monte Carlo data at 20 mm. 54

Figure 2.8: Variation of optical properties with start of fit for MC data. 56

Figure 2.9: Diffusion theory fit to MC data at 20 mm ($\mu_a = 0.02$, $\mu_s' = 1.0$ mm^{-1}). 59

Figure 2.10: Diffusion theory fit to Monte Carlo data with IRF at 10 mm. 61

Figure 2.11: Diffusion theory fit to Monte Carlo data with IRF at 20 mm. 62

Figure 2.12: Variation of optical properties with start time for MC data with IRF. 64

Figure 2.13: Comparison of reflectance from diffusion model using EBC and ZBC with Monte Carlo reflectance at 10 mm. 66

Figure 2.14: Comparison of reflectance from different boundary conditions. 68

Figure 2.15: Diffusion theory data fit in the frequency domain at 15 mm. 75

Figure 2.16: Diffusion fit for phase and modulation to MC data (15/10 mm). 78

Figure 2.17: Variation of optical properties with maximum frequency fit for Monte Carlo data 2 using relative distance approach. 79
Figure 2.18: Frequency domain fit of Monte Carlo data 10 mm. 82
Figure 2.19: Variation of optical properties with maximum frequency fit for Monte Carlo data at a single distance. 83
Figure 2.20: Fit to Monte Carlo data with an IRF at 20 mm. 85
Figure 2.21: Variation of optical properties with maximum frequency fit for Monte Carlo data convolved with an IRF at one distance. 86
Figure 3.1: Comparison of IRF from R5600U PMT. 91
Figure 3.2: Variation of (a) μ_s' and (b) μ_a with Melanin ink concentration. 98
Figure 3.3: Fit and residuals for Intralipid with 0.02% ink at $\rho = 20$ mm. 99
Figure 3.4: Fit and residuals for Marley 8 phantom at $\rho = 10$ mm. 102
Figure 3.5: Variation of optical properties and standard deviation with number counts in the peak of the reflectance. 104
Figure 3.6: A typical fit from a measurement using polystyrene spheres. 113
Figure 3.7: Results from polystyrene sphere measurements using spatial and time domain methods. 116
Figure 3.8: Variation of measured absorption versus ink concentration. 124
Figure 3.9: An example of a fit for polystyrene spheres with ICG. 128
Figure 3.10: Variation of absorption and scattering for polystyrene and ICG. 129
Figure 3.11: Variation of μ_s' estimated with source-detector separation. 130
Figure 3.12: Diffusion fit to *in vivo* data measured on the palm of the hand at 750 nm with a source detector separation of 10 mm. 136
Figure 3.13: Variation of measured oxygenation status over time following arterial occlusion. 141
Figure 4.1: Example of a typical frequency domain fit on polystyrene. 147
Figure 4.2: Results from fitting three distances (20, 30 and 40 mm) relative to 10 mm simultaneously on polystyrene phantom. 148

Figure 4.3: Measured versus expected μ_t values for varying concentrations of polystyrene spheres in water. 151

Figure 4.4: Variation of the predicted DC amplitude of the reflectance with ρ using two different fitting methods. 153

Figure 4.5: Frequency domain fit to polystyrene phantom with added ICG. 156

Figure 4.6: Variation of optical properties with concentration of ICG in polystyrene phantoms. 158

LIST OF TABLES

Table 2.1: Estimated optical properties with varying ρ. 47

Table 2.2: Results of fits varying optical properties for ρ=20 mm. 48

Table 2.3: Variation of estimated optical properties from MC data. 57

Table 2.4: Results of frequency domain fits of diffusion data. 74

Table 3.1: Variation of estimated μ_a and μ_s' with Intralipid concentration from different methods. 95

Table 3.2: Summary of thirty measurements on Marley 8. 101

Table 3.3: Variation of optical properties with statistics. 103

Table 3.4: Variation of optical properties of solid phantoms with different measurement techniques and boundary conditions. 107

Table 3.5: Variation of optical properties with wavelength. 110

Table 3.6: Estimates of μ_a and μ_s' from time and spatially-resolved reflectance measurements on varying concentrations of polystyrene. 114

Table 3.7: Results from linear regression of measured versus expected scattering coefficients from different methods. 115

Table 3.8: Variation of results from two polystyrene phantoms with ρ. 120

Table 3.9: Results on polystyrene phantom measured at 750 nm. 121

Table 3.10: Results from linear regression of measured versus expected absorption coefficients from two techniques with ink. 124

Table 3.11: Results of linear regression of measured versus expected absorption coefficients from two techniques with ICG. 131

Table 3.12: Phantom measurements performed at two wavelengths. 133

Table 3.13: Optical properties estimated from in vivo measurements on the hand at two wavelengths. 135

Table 3.14: Measured oxygenation parameters under different oxygenation conditions as estimated by time domain measurements. 137

Table 3.15: Optical properties of the hand measured during various stages of arterial occlusion. 139
Table 3.16: Variation of measured oxygenation parameters with time. 140
Table 4.1: Results of frequency domain fits on polystyrene phantoms. 143
Table 4.2: Results of frequency domain fits on large volume phantom. 146
Table 4.3: Theoretical predictions, from two different methods for the amplitude of the DC component of the reflectance. 152
Table 4.4: Results of linear regression of μ_a versus ICG concentration. 159

1 INTRODUCTION

1.1 Motivation

In the fields of therapeutic and diagnostic medicine, there are various reasons for studying the optical properties of tissue. In therapeutic applications, the biological effects are dependent on the fluence of the light, which is in turn determined by the optical properties of the tissue. The use of light for therapeutic purposes is becoming increasingly popular; two examples are photodynamic therapy (Wilson and Patterson 1986) and laser surgery (Jacques and Prahl 1987). With respect to diagnostic applications, the absorption coefficient may be useful in calculating the concentration of exogenous chromophores (e.g. photosensitizing drugs Patterson *et al.* 1990) or endogenous chromophores, such as hemoglobin or cytochrome aa_3 (Chance *et al.* 1988a and Cope and Delpy 1988). It would clearly be advantageous to be able to perform noninvasive *in vivo* measurements in tissue. It is this particular aspect of the study of light propagation that is addressed in this thesis.

Hemoglobin saturation represents the percentage of hemoglobin which is oxygenated within a region and is defined as:

$$SO_2 = \frac{[HbO_2]}{[HbO_2]+[Hb]} \times 100\% \qquad (1)$$

where [HbO_2] is the concentration of oxyhemoglobin and [Hb] is the concentration of deoxyhemoglobin. The noninvasive examination of oxygenation has uses in many areas of medicine. One major area is the study of the causes of neurodevelopmental problems in newborn infants. It is believed that damage to the brain of infants can be linked to low oxygen levels in the blood or poor cerebral blood flow, or a combination of these two problems (Cope 1991). In addition, photodynamic therapy techniques could benefit from a knowledge of the oxygen levels in the tumor. Although much effort has been put into the characterizing the fluence distribution and the concentration of photosensitizer in the tumor, dose models have only recently included oxygen levels, despite the fact that singlet oxygen ($^1O_2$) is believed to be the main cytotoxic product (Weishaupt *et al.* 1976). As well, it is thought that response to radiation therapy is dependent on oxygen concentration within the treatment region (Hall 1988). Moreover, apart from being less traumatic than invasive measurements, these methods, due to their rapid time response can be performed simultaneously with treatment and/or continuously to allow for a constant monitoring of oxygen concentration within the area of interest (Ferrari *et al.* 1985 and Brazy *et al.* 1985). These are two specialized, yet important areas where the noninvasive measurement of hemoglobin saturation would be an asset. Further discussion of the history and current status of hemoglobin oxygenation measurements can be found in section 1.5.

1.2 Interaction of light with biological tissue

Prior to discussion of specific applications of the determination of tissue optical properties, a general introduction to the concepts involved is necessary. The optical properties of interest must first be defined. There exist a variety of models regarding light propagation in tissue. A model of light transport should detail the dielectric nature of the medium and its effect upon the electromagnetic field. Unfortunately, due to the complexity of this approach, it is not used. Instead, photons are considered neutral particles whose only interactions with tissue are absorption and elastic scattering (Patterson 1995). The probabilities corresponding to these interactions are represented by the absorption coefficient, μ_a and the scattering coefficient, μ_s respectively. The absorption coefficient is the probability per unit pathlength of a photon being absorbed; similarly, the scattering coefficient is the probability per unit pathlength of a photon being scattered. A complete description of a scattering interaction also requires a probability density function representing the angular dependence of the scatter. The first moment of this function is g, the anisotropy parameter, which is the mean cosine of the angle of scattering. In practice, photons in a turbid medium will scatter many times before detection. Different combinations of g and μ_s will result in similar distributions of photons. Hence they are often combined into one parameter, the reduced scattering coefficient μ_s', where $\mu_s'=(1-g)\ \mu_s$ (van de Hulst 1980).

In tissue, the total probability of absorption is related to the sum of the individual probabilities of absorption by specific chromophores within the region.

$$\mu_a = \ln(10) \sum_i C_i \varepsilon_i \qquad (2)$$

where C_i is the concentration of chromophore i and ε_i is the extinction coefficient of chromophore i. Absorption is extremely high in the UV region due to proteins and nucleic acids. As wavelength increases, absorption becomes dominated by specific molecules, such as hemoglobin, myoglobin and melanin (Madsen 1993). Naturally occurring, or endogenous chromophores have characteristic absorption spectra. Figure 1.1 shows the absorption spectra of hemoglobin. The absorption of these chromophores is sensitive to their oxygenation states and these differences can be exploited to determine the oxygenation state of the tissue through optical means. For wavelengths greater than 1 μm, absorption increases due to the strong absorption by water.

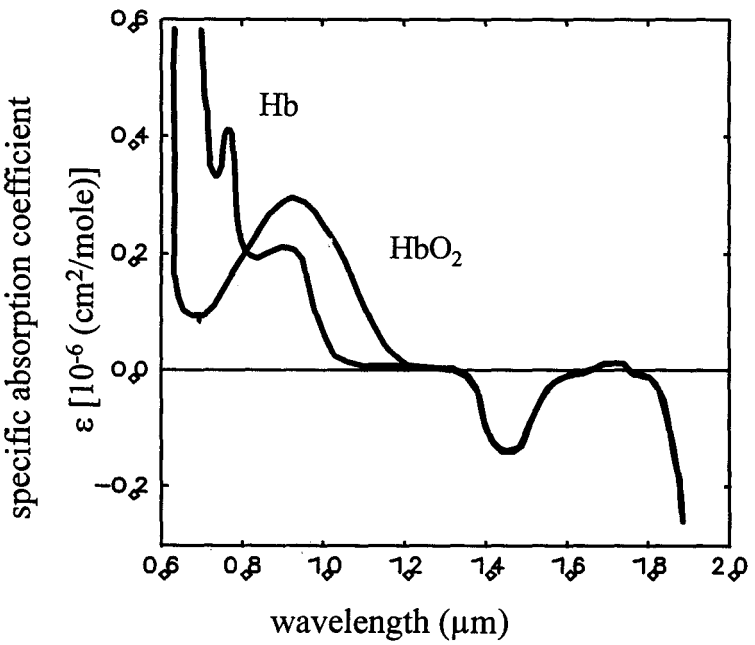

Figure 1.1: Variation of absorption of oxyhemoglobin and deoxyhemoglobin with wavelength.

In the region of interest for this work, the absorption coefficient of tissue ranges from approximately 0.01 to 0.05 mm^{-1} (Cheong *et al.* 1990).

In contrast, it is much more difficult to associate the reduced scattering coefficient with a distinct physical property. Scattering by particles of comparable or larger size than the wavelength of the incident light is known as Mie scattering and it is this type of scattering that best represents that observed in tissue in the near infrared region. The reduced scattering coefficient for tissue ranges from about 0.5 to 7 mm^{-1} in this region (Cheong *et al.* 1990). The effective size of the scattering particle is of the order of microns, indicating that scattering is probably attributable to cells or large organelles (Madsen 1993). Once more it must be noted that this is a very simple picture of scattering in biological tissue and is not a true representation of the actual nature of tissue. On the microscopic level, scattering is due to fluctuations in the refractive index, so it is necessary to have some knowledge of the index of refraction of the medium of interest. In the near infrared region the index of refraction, n varies from about 1.3 to 1.5. This determines the speed of light in the medium according to the equation

$$c=\frac{c_o}{n} \qquad (3)$$

where c_o is the speed of light in a vacuum, 0.3 mm/ps. In addition, mismatches in indices of refraction, for example at an air-tissue interface, result in specular reflection at the boundaries. This reflection can be incorporated into a light propagation model with the use of Fresnel's equations. Thus, the three main variables with which tissue is characterized are the average index of refraction, the absorption and the reduced scattering coefficients.

1.3 Measurement of optical properties

The two major categories of optical properties which are of interest are fundamental and derived. The fundamental optical properties are the basis for the derived properties. They are the absorption coefficient, the scatter coefficient and the scattering phase function. The derived properties can be defined in terms of these parameters, through the application of an appropriate model. Derived properties include the anisotropy parameter, the reduced scattering coefficient, the total attenuation coefficient (μ_t), the effective attenuation coefficient (μ_{eff}), the mean free path (mfp), the effective penetration depth, the local and total diffuse reflectance and transmittance.

There are two groups of procedures that are used to determine these properties. Direct techniques use thin samples, such that single scattering dominates. The optical properties can then be calculated from a transmission measurement or with the use of an integrating sphere. However, the methods of obtaining adequately thin samples are likely to change the properties of the sample and they are also invasive measurements. The more clinically useful class of measurements is known as indirect methods (Wilson *et al.* 1987). These techniques are based on *in vivo* measurements of the derived properties. With the application of a model of light transport it is then possible to determine the fundamental optical properties of interest. These indirect methods can further be broken down into internal and external methods, external methods being preferred as they are noninvasive. Within the class of external methods, there exist photothermal techniques,

mainly photothermal radiometry (Prahl *et al.* 1992) and photoacoustic spectroscopy (Fainchtein *et al.* 1997), which are useful only in dermatological studies (Wilson *et al.* 1987) . The other branch of external methods are known as radiometric techniques which are measurements of either diffuse reflectance or transmittance and are the best means for the near infrared regime. There are three general radiometric techniques which will be discussed in this thesis: steady state, frequency and time-resolved measurements.

1.3.1 Steady State Methods

Steady state measurements have two observable quantities: the spatially resolved diffuse reflectance or the angle resolved reflectance. Measurement of the latter is impractical *in vivo*. The principle behind the spatially resolved methods is shown in Figure 1.2. Light enters the medium and is scattered until it is either absorbed or remitted from the medium. The measurements are integrated over the solid angle of the detector.

However, there exist an infinite number of combinations of μ_a and μ_s' that can result in the identical reflectance at a given source detector separation, ρ (Patterson 1995). Since one measurement is insufficient to determine the optical properties of the sample and although two measurements of the absolute reflectance in principle would be sufficient, in practice measurements at many different source detector separations are performed. The observed reflectance per unit area per unit time is then compared to a suitable model of reflectance. Values for μ_a and μ_s' are found by minimizing the difference between the theoretical and experimental curves for all values of ρ measured.

One of the first groups to perform such measurements were Groenhuis *et al.* (1983a and 1983b) They were able to derive Green's function for the photon current

resulting from an isotropic point source at a given depth in a semi-infinite medium. By integrating Green's function over the tissue volume and treating each scatter site as an isotropic point source,

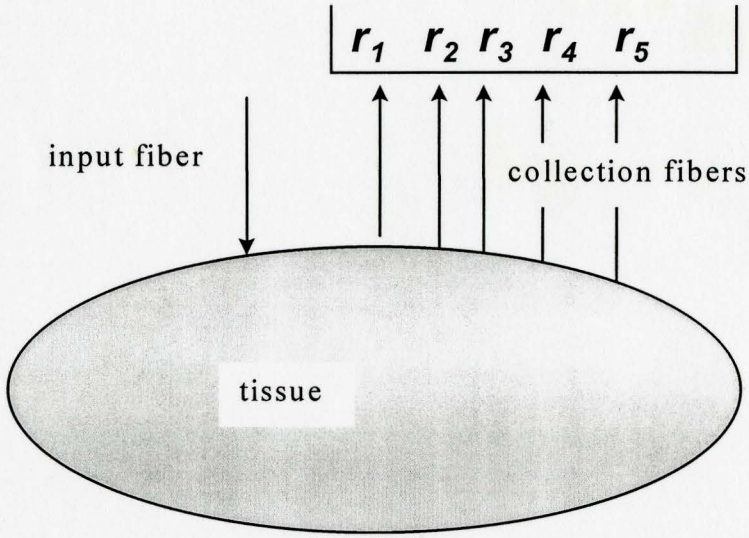

Figure 1.2. The principle of spatially resolved measurements. Light enters the tissue through an input fiber and is collected at various distances, for example $r_{1\text{-}5}$.

they were able to determine the radial reflectance. Schmitt *et al.* (1990) extended this idea to derive an expression for the reflectance for a multi-layer medium such as skin. Patterson *et al* (1989b). developed a simple model where the observed quantities are relative reflectance at numerous distances and total diffuse reflectance. Analytical expressions for the reduced scattering and absorption coefficients were derived from diffusion theory in terms of the measured quantities. More recent additions to the model by Farrell *et al.* (1992) incorporate correct boundary conditions and are in agreement with Monte Carlo data and experiments performed on phantoms.

Advantages of this system include simple, inexpensive apparatus and the capability of real time measurements. There are also some limitations to the steady state system. They include: (a) sensitivity to boundary conditions, (b) requirement for measurements at multiple locations and (c) unknown effect of tissue heterogeneity

1.3.2 Frequency-Domain Methods

These techniques use the information contained within the distribution of photon transit times between the source and detector. A schematic diagram of the principle behind frequency domain measurements is shown in Figure 1.3.

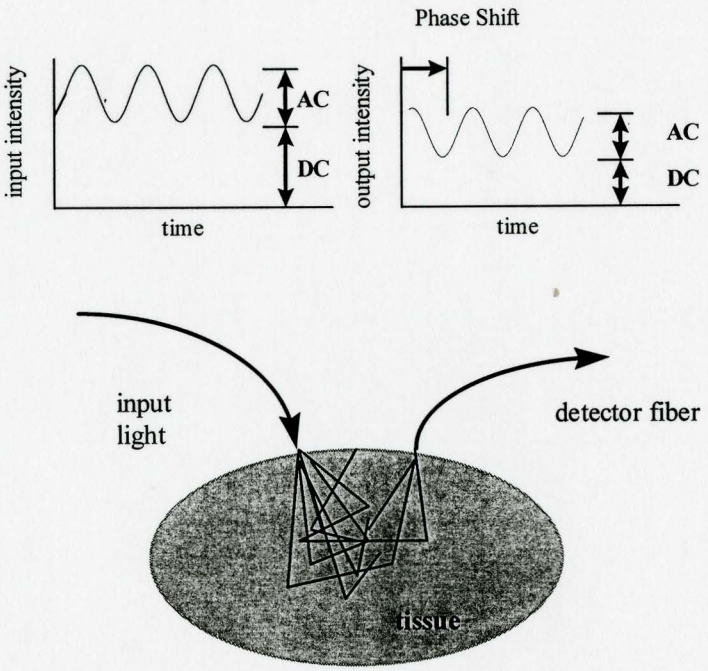

Figure 1.3 The principle of frequency domain measurements. Modulated light enters the tissue and the reflectance is collected. The phase and the modulation of the light are changed by the optical properties of the medium.

The source can be any high frequency intensity modulated continuous wave light, but in all cases, the detected light will be out of phase (delayed) with respect to the

source. In addition, the ratio of AC amplitude to DC amplitude, known as the modulation, will be reduced. These two quantities, the phase and modulation, depend upon the optical properties of the medium and on the source detector separation. Expressions predicting the phase and modulation from a suitable model are then compared to the experimental values to estimate the values of μ_a and μ_s'.

The first frequency domain measurements were made by Lakowicz *et al.* (1988). Different approaches to the problem have since been attempted (Patterson *et al.* 1991a, Sevick *et al.* 1991, Madsen *et al.* 1994, Fantini *et al.* 1995 and Pogue *et al.* 1996). Perhaps the most appealing of these methods is employed by Fantini *et al.* and requires two detectors at different distances. The phase difference between the detectors and the ratio of signals is then measured. This technique has the advantage that it is not necessary to establish a baseline for the phase and modulation, as required by methods with one detector (Fantini *et al.* 1995). Despite differences in approaches, all these methods exploit the following advantages of the frequency domain system: (a) phase and modulation can be measured in about 1 second, (b) for frequencies below 300 MHz inexpensive photomultiplier tubes can be used and (c) corrections for the impulse response of the measurement system, which is convolved with the true signal in the time domain, are algebraic operations not deconvolution. Of course, there are disadvantages to the frequency system which include insufficient demodulation for small ρ values, establishing reference values for phase and modulation with one detector or the need for two, or more detectors.

1.3.3 Time-Domain Methods

Time-resolved measurements seek to overcome the two main problems of the steady state system, the need for absolute measurements and for multiple measurements. The concept of these measurements is shown in Figure 1.4. The incident light is a brief pulse, of the order of picoseconds, and the observed quantity is the diffuse reflectance versus time at a given ρ value. Similar models to those used in steady-state methods define $R(\rho,\lambda,t)$ as a function of ρ, t, μ_a, μ_s' and n. The original narrow pulse undergoes multiple scatters in the medium. This results in a distribution of pathlengths which broadens the pulse in the time domain. Typical photon transit times are on the order of one nanosecond. During early times, on the order of picoseconds, the photons will have undergone fewer scattering events and the angular dependence of the scattering will dramatically affect the pulse shape. Because the pathlength corresponding to early times is short, the absorption will have little influence on the signal when $\mu_a << \mu_s'$. For these times the photons penetrate only a few mm. At later times, i.e. nanoseconds, the light is highly diffuse and absorption will have the principle influence on the shape of the remitted signal. As well, the photons will be able to penetrate deeper into the tissue at longer times, to the order of 10 mm or more. The observed pulse shape is then fit using a time dependent model. The difference between the collected signal and the predicted pulse shape is minimized by choosing the best estimates for μ_a and μ_s'. Within the observed reflectance is convolved the instrument response function (IRF) which must be accounted for by deconvolution of the experimental results or convolution of the modeled data with the experimental IRF.

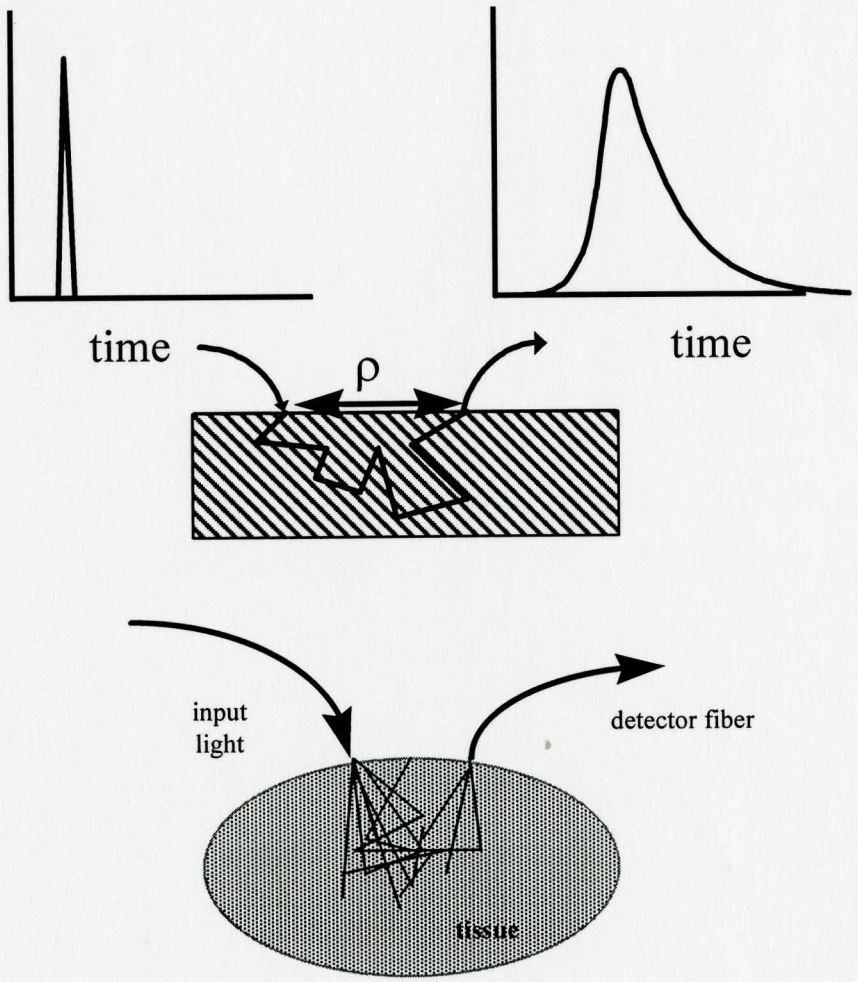

Figure 1.4: The principle of time-domain measurements. A short pulse of light enters the tissue in a pencil beam geometry It is broadened and attenuated due to scattering and absorption. The reflectance is collected at a specific distance, ρ.

Time-resolved experiments became possible in the 1980's with the advent of picosecond light sources, such as mode-locked lasers or diode lasers and fast photodetectors such as microchannel plate photomultiplier tubes. Studies in living tissue

were performed by Chance *et al.* (1988a and 1988b) and Delpy *et al.* (1988) to determine oxygenation in human brain and muscle and the optical pathlength in rat brain, respectively. A simple model was proposed to fit the collected signal by Patterson *et al.* which showed good agreement with their results (Patterson *et al.* 1989a). Since then more complex models which take into account Fresnel reflections at mismatched boundaries have been developed (Patterson *et al.* 1991b, Haskell *et al.* 1994, Hielscher *et al.* 1995 and Kienle and Patterson 1997a) and limitations of the approach have been identified (Madsen *et al.* 1992a, Papazoglou *et al.* 1995, Hielscher *et al.* 1996 and Cubeddu *et al.* 1996).

The main disadvantage to time domain techniques is the fact that there does not exist a clinically useful tunable picosecond light source. Thus far most measurements have been performed with mode-locked solid state pumped dye lasers or Ti:sapphire lasers. Although they offer excellent tunability and time resolution, they are expensive and too complex for practical clinical applications. Furthermore microchannel plate photomultiplier tubes used for the detection of diffusely reflected light are expensive devices. It is the purpose of this study to investigate the feasibility of using time-domain measurements with inexpensive pulsed diode lasers and a less expensive type of photomultiplier tube to monitor hemoglobin saturation.

There do exist advantages to the time domain system which are only recently being explored. The potential advantages of a time-resolved system are: (a) for small ρ values, as in an endoscope, a frequency domain system cannot extract useful phase and modulation information due to the short separation distance. However, it has been shown

that the time-resolved pulse contains information regarding the absorption coefficient (Jacques and Flock 1991). (b) since the time of flight determines the penetration depth of the light, this depth can be controlled by varying the detection time, (c) the measurements are less sensitive to boundary conditions, which affect the absolute signal value, than steady-state techniques and (d) since photon counting is used, these techniques are excellent for situations where light levels are low, as in tissue measurements. It is these advantages of the time-resolved system which prompted this study into the potential of designing a system at a reasonable cost which could be employed in clinical situations.

1.4 Models for light transport

Many models can, in theory, be used to describe light propagation. The most exact approach would be to solve Maxwell's equations for a heterogeneous dielectric, however, there do not exist any available solutions for realistic cases. As mentioned earlier, it is more common to model light using solutions to the neutral particle transport equation. In a homogeneous medium, this equation has the following form:

$$\frac{1}{c}\frac{\delta L(\mathbf{r},\hat{\Omega},t)}{\delta t} + \hat{\Omega}\cdot\nabla L(\mathbf{r},\hat{\Omega},t) + (\mu_a+\mu_s)L(\mathbf{r},\hat{\Omega},t) = \mu_s \int_{4\pi} L(\mathbf{r},\hat{\Omega}',t) f(\Omega'\cdot\Omega) d\Omega' + S(\mathbf{r},\hat{\Omega},t) \quad (4)$$

where $L(\mathbf{r},\Omega,t)d\Omega dA$ is the number of photons passing through a perpendicular area dA per unit time in the solid angle $d\Omega$ about the direction Ω at location $\mathbf{r}$ and time t. The speed of light is c and the source term is $S(\mathbf{r},\Omega,t)$. This equation can be solved

numerically or, under certain conditions, analytically. Numerical solutions to the transport equation include: (a) the method of discrete ordinates (Duderstadt and Hamilton 1976) (b) random walk (Bonner *et al.* 1987) and (c) Monte Carlo (MC) simulations (Wilson and Adam 1983, Tinet *et al.* 1996 and Kienle and Patterson 1996). Simplifications of the transport equation which allow for analytical solutions are the 2-flux models for a tissue slab (Reichman 1973 and Mudgett and Richards 1972) and diffusion theory (Reynolds *et al.* 1976, Hemenger 1977 and Svaasand and Ellingson 1983). The most powerful method is probably the Monte Carlo method, which is extremely general, but is computationally expensive when few photons are detected. Recent advances in this area may change this limitation under some circumstances (Kienle and Patterson 1996).

The diffusion equation is arrived at by assuming that $L(\mathbf{r},\Omega,t)$ is close to isotropic and that the source itself is isotropic. By ignoring terms which are not significant for typical μ_a and μ_s' values and by using the following approximation:

$$L(\mathbf{r},\hat{\Omega},t) \cong \frac{1}{4\pi}[\Phi(\mathbf{r},t) + 3\mathbf{J}(\mathbf{r},t)\cdot\hat{\Omega}] \tag{5}$$

a differential equation for the fluence rate, $\Phi(\mathbf{r},t)$, in a homogeneous medium can be derived which has the following form (Duderstadt and Hamilton 1976):

$$\frac{1}{c}\frac{\delta\Phi(\mathbf{r},t)}{\delta t} - D\nabla^2\Phi(\mathbf{r},t) + \mu_a\Phi(\mathbf{r},t) = S(\mathbf{r},t) \tag{6}$$

where

$$\mathbf{J}(\mathbf{r},t) = -D\nabla\Phi(\mathbf{r},t) \tag{7}$$

and

$$D = \frac{1}{3(\mu_a + \mu_s')} \tag{8}$$

For uniform tissues and simple geometries, it is possible to solve (6) analytically, while for other geometries or in inhomogeneous media numerical methods may be employed (Madsen *et al.* 1991).

Although the diffusion equation provides a simple model of light propagation in a turbid medium it does have limitations. The first requirement is that photon radiance must be close to isotropic which is not true when the absorption and scattering coefficients are comparable. In general, it is prudent to have $\mu_a < 0.1\mu_s'$ which is true for biological tissue in the near infrared region, with the exception of pigmented tissue or those with large amounts of exogenous chromophores. The radiance will not be isotropic close to highly anisotropic sources, therefore the theory is best suited to situations where $\mu_s'\rho >> 1$. Hielscher *et al.* (1995) showed that the reduced scattering coefficient derived from time dependent solutions to the diffusion equation for small source-detector separations was not accurate. In addition, the diffusion equation is not valid at any times comparable to the ballistic limit which is the minimum photon transit time between the source and the collection fibers. Finally, boundaries, like an air-tissue boundary, may cause the radiance to be anisotropic due to a lack of backscatter from the air. Before applying the diffusion equation , the above four assumptions must be validated. If results

are suspect, Monte Carlo methods may be required to ascertain the accuracy of the model.

If the diffusion model is valid, then it must be determined how accurately it predicts optical properties. This is done by comparison to direct measurements or to Monte Carlo simulations. In general, it has been found that for adequately large volumes, such that a semi-infinite model can be applied, the errors in estimating scattering and absorption coefficients are less than 10% (Kienle and Patterson 1997a). For small volumes, the semi-infinite model breaks down and it becomes necessary to solve the diffusion equation for the finite volume of interest, for example, a sphere. Detailed time-resolved studies have been performed by Cubeddu *et al.* (1996) investigating the applicability of the diffusion model. Four different models were compared: the simple diffusion model, the diffusion model modified to contain a time shift parameter which accounts for variations between the temporal position of the experimental and theoretical data, the random walk model and the special case of the diffusion theory with time shift where one optical coefficient is known. For optical properties similar to those found in tissue at distances comparable to those used in experiments $\geq$ 10 mm, for the range of wavelengths from 600 to 900 nm, the absolute error in μ_a was typically less than 10%, while the error in μ_s' was less than 20%; the larger errors were observed for ρ=10 mm. The linearity error was determined by keeping one parameter constant and varying the other by a small increment. The linearity error in μ_a was generally less than 2% and slightly higher, up to 4%, for the scattering. The diffusion model also showed good reproducibility overall; the variation in the results decreased with an increase in the

number of counts collected. Furthermore, the reproducibility in determining the absorption was always better than the scattering coefficient. Since, in this thesis the most essential feature is determination of relative changes in μ_a, and absolute values, especially for the scatting coefficient are less critical, the best method to use is the simple diffusion model due to the small linearity error in μ_a (Cubeddu *et al.* 1996).

A topic that has received much attention in this field recently is the application of appropriate boundary conditions with the time-resolved diffusion equation (Farrell *et al.* 1992, Haskell *et al.* 1994, Kienle and Patterson 1997a, Svaasand *et al.* 1993 and Wang and Jacques 1993). The following discussion will deal only with volumes which can be considered semi-infinite. Boundary effects can be accounted for by assuming that the tissue-medium boundary is a plane where, in agreement with Fresnel's equations, refraction and specular reflection take place. The other medium is either air or a solid depending on the nature of the probe used. Although the incorporation of reflection into Monte Carlo calculations is fairly simple (Flock *et al.* 1989), problems arise in the case of the diffusion model. Unlike Monte Carlo, a partially reflecting plane boundary cannot be applied exactly because this would imply a known relationship between the outgoing and incoming radiance. This is impossible in the diffusion approximation as it assumes the radiance depends only the fluence rate and its gradient (see equation 6). The solution is to define a relationship between the outgoing and incoming photon currents (Svaasand *et al.* 1993 and Duderstadt and Hamilton 1976) . There are various ways to define this relationship, all of which must account for the decrease in fluence rate near a boundary as a result of a lack of backscatter. The three most common boundary conditions which will

be discussed here are the zero boundary condition (ZBC), the extrapolated boundary condition (EBC) and the partial current boundary condition (PCBC). Although all of the following expressions have been derived in the time domain, similar solutions can be obtained in frequency space by applying Fourier transforms to the time domain expressions.

1.4.1 Zero Boundary Condition

The problem is to solve equation (6) where the light is introduced by a small source, for example, an optical fiber and is collected by another fiber with separation ρ. The finite size of both source and detector are ignored and it is assumed that a photon source is formed within the medium due to the initial scattering of all incident photons at a depth

$$z_o = \frac{1}{\mu_a + \mu_s'} \tag{9}$$

The simplest method to solve equation (6) is to set the fluence to zero on the tissue boundary, $\Phi(\rho, z = 0)=0$. Although this has no completely satisfactory physical foundation, when combined with the method of images, it does allow for a simple solution to the problem which has the form (Patterson *et al.* 1989a and Moulton 1990):

$$R(\rho,t) = \frac{z_o}{(4\pi Dc)^{3/2}} t^{-5/2} \exp\left[-\frac{\rho^2+z_o^2}{4Dct}\right] \exp(-\mu_a ct) \tag{10}$$

It should be stated that this does not make corrections for reflection at the boundary. This model has been shown to produce adequate results in determining μ_a, within about 1%,

but errors of up to 12 % in μ_s' (Kienle and Patterson 1997a). The errors in μ_s' are considerable higher than the deviations seen with other models.

1.4.2 Extrapolated Boundary Condition

The extrapolated boundary condition also uses the method of images to solve the boundary problem. Closer to the boundary, the fluence rate decreases due to less backscatter from the air. In this case, the fluence is set to zero at some distance beyond the actual boundary in accordance with a common approach in transport theory (Duderstadt and Hamilton 1976). Once more, the photons are assumed to be isotropically scattered at a mean distance z_o within the medium and the fluence rate can be forced to zero on the extrapolated boundary by placing a negative image source on the other side of the interface, as illustrated in Figure 1.5. The fluence rate is thus the sum of contributions from these two source terms.

The resulting equation for the fluence rate is (Patterson *et al.* 1989a and Moulton 1990):

$$\Phi(\rho,z,t)=\frac{c}{(4\pi Dct)^{3/2}}\exp(-\mu_a ct)\left\{\exp\left[-\frac{(z-z_o)^2+\rho^2}{4Dct}\right]-\exp\left[-\frac{(z+z_o+2z_b)^2+\rho^2}{4Dct}\right]\right\} \quad (11)$$

For the EBC the z_b value is given by

$$z_b=\frac{1+R_{eff}}{1-R_{eff}}2D \quad (12)$$

where R_{eff} is the fraction of photons that are internally diffusely reflected at the boundary.

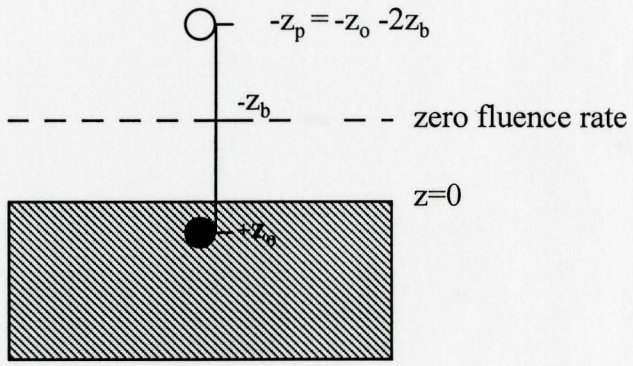

Figure 1.5· Source and image configurations for the extrapolated boundary condition (EBC) using the semi-infinite geometry

This value has been calculated by Haskell *et al.* (1994) and depends on the mismatch in refractive indices between the two media. Previous researchers have calculated the diffuse reflectance as the current across the boundary (Hielscher *et al.* 1995 and Moulton 1990) The reflectance is then defined by the following equation.

$$R_f(\rho,t) = -D\nabla\Phi(\rho,z,t)\ (-\mathbf{z})\ \Big|_{z=0} \qquad (13)$$

Insertion of equation (11) into (13) gives:

$$R_f(\rho,t) = \frac{t^{-5/2}}{2(4\pi\ Dc)^{3/2}} \exp(-\mu_a ct)\left\{ z_o \exp\left[-\frac{r_1^{\,2}}{4Dct}\right] + (z_o + 2z_b)\exp\left[-\frac{r_2^{\,2}}{4Dct}\right]\right\} \qquad (14)$$

where $r_1^{\,2} = z_o^{\,2} + \rho^2$ and $r_2^{\,2} = (z_o + 2z_b)^2 + \rho^2$

The ZBC equation (10) can be obtained by substituting $z = 0$ and $z_b = 0$ into this equation.

However, Haskell *et al.* (1994) concluded that it is more correct to express the reflectance as the integral of the radiance over the backward hemisphere. The radiance is a sum of two terms, one proportional to fluence rate and the other proportional to the current (see equation 5). The integral for the time-resolved reflectance is (Haskell *et al.* 1994):

$$R(\rho,t) = \frac{1}{4\pi}\int_{2\pi}\left[\Phi(\rho,z=0,t) + 3D\frac{\delta\Phi(\rho,z=0,t)}{\delta z}\cos\right][1 - R_{fres}(\theta)]\cos\theta\, d\Omega \quad (15)$$

where $R_{fres}(\theta)$ is the Fresnel reflection coefficient for a photon incident on the boundary at an angle θ to the normal. The value of this integral depends on the mismatch between the two media. In general, the accurate EBC reflectance expression will have the form:

$$R(\rho,t) = m_1\Phi(\rho,z=0,t) \quad + \quad m_2 R_f(\rho,t) \quad (16)$$

where m_1 and m_2 are determined from equation (15). For example, for n =1.4, m_1=0.118 and m_2=0.306, while for n=1, i.e. a matched boundary, m_1=0.25 and m_2=0.5. This approach is more justifiable than the ZBC and produces more accurate results.

1.4.3 Partial Current Boundary Condition

The most correct treatment of the boundary condition relates the flow of energy across the boundary in either direction. The irradiance at the surface is set equal to the integral of the reflected radiance. The equation for the time dependent fluence rate is shown below (Haskell *et al.* 1994)

$$\Phi(\rho, z, t) = \frac{c}{(4\pi Dct)^{3/2}} \exp(-\mu_a ct) \times$$
$$\left\{ \exp\left[-\frac{(z - z_o)^2 + \rho^2}{4Dct} \right] + \exp\left[-\frac{(z + z_o + 2z_b)^2 + \rho^2}{4Dct} \right] - \frac{2}{z_b} \int_0^\infty dl \exp(-l/z_b) \times \exp\left[-\frac{(z + z_o + l)^2 + \rho^2}{4Dct} \right] \right\} \quad (17)$$

The origin of these terms is discussed by Haskell *et al.* (1994). The first term is from the original source at $z = z_o$, the second term is from the image source of the same magnitude and sign but at $z = -z_o$ and the third term is from a continuous line of sinks stretching from $z = -z_o$ to $z = -\infty$ with negative charge. The sinks are exponentially damped but their total strength is equal to the strength of the source plus the image terms.

Following the same approach as used with the EBC, the PCBC expression for fluence rate can be used to derive an expression for the time-resolved reflectance. Although this approach is most accurate, differences from the EBC are small (Haskell *et al.* 1994 and Kienle and Patterson 1997a) and the integral in equation (17) must be calculated numerically making this method computationally expensive.

1.5 Hemoglobin oxygenation measurements

The general goal of spectroscopy in tissue is to measure the absorption of the tissue chromophores and relate this to a physiological quantity of interest. According to a review paper by Chance, tissue absorbers have been studied with optical methods since the 1930's (Chance 1991). Over the years the focus has moved from *in vitro* to *in vivo* measurements in accordance with the trend in medicine away from invasive procedures. Potential applications of non invasive measurements include (a) the study of the

distribution of photosensitizers used in photodynamic therapy (Patterson *et al.* 1990), (b) monitoring glucose concentration in diabetics (Maier *et al.* 1994, Kohl and Cope 1994 and Bruulsema *et al.* 1997) and (c) determining hemoglobin oxygenation (Cope and Delpy 1988 and Chance *et al.* 1988a). This section will detail the developments that brought the field of tissue oximetry via optical methods to its current state.

In his thesis, Cope gives a detailed history of measuring blood and tissue oxygenation (Cope 1991). A summary of the relevant aspects will be presented here. One of the first molecules to be studied with optical techniques was hemoglobin; in 1914 the absorption bands were observed by Hartridge and Hills. It took eighteen years before hemoglobin oxygenation measurements in tissue were initiated by Nicolai. Three years later, in 1935, the first commercial instruments were designed. The system used by Kramer had one red wavelength and thus was unable to adjust for changes in hemoglobin saturation. However, Matthes designed a system with two wavelengths, one green which was not dependent on oxygenation, and a red one similar to Kramer. He continued to experiment with hemoglobin *in vitro* until he came up with a system that used an infrared wavelength which was not oxygen dependent.

The measurements made by Kramer and Matthes were performed *in vitro* and this trend continued, using small volumes of blood such that Beer's Law could be applied and scattering in that small volume was ignored. However, this changed during World War II when the need for *in vivo* measurements arose. The military was concerned about the oxygenation of their pilots in the unpressurised cabins of aircraft and, to monitor this, built an oximeter which fit on the hand in 1940. The next step in the evolution of the *in*

vivo monitor was the ear oximeter built by Milikan in 1942, also for aviation purposes. This was improved by Wood and Geraci in 1949 to enable determination of absolute oxygen saturation. The final innovation was the Hewlett Packard Ear Oximeter which measured attenuation at eight wavelengths but, although it worked adequately, it was not clinically useful due to high cost and bulky ear attachment. More recently, in the mid 1970's, the pulse oximeter was developed. This monitors fluctuations in light transmission across a vascular bed due to the beating of the heart. With this instrument absolute arterial saturation can be determined using two wavelengths. Indeed, this system is reliable and is widely used today (Cope 1991). Many review papers exist which detail the current state of the field (Tremper and Barker 1989, Kelleher 1989, Sevinghuis and Kelleher 1992 and Lindberg *et al.* 1995). All of the systems described so far have relied on transmission measurements through a cuvette or a narrow tissue section, such as the ear lobe.

The state of the field in the 1970's was as follows. The near infrared absorption bands of hemoglobin had been accurately measured, as had the bands of cytochrome c oxidase, the final member of the respiratory chain (Cope 1991). However, the excellent penetration of infrared light in tissue had not yet been exploited to its potential. In 1977, Jöbsis measured the oxygen related changes in transillumination across a cat brain and concluded that the primary infrared absorbers were hemoglobin and cytochrome aa_3 (Jöbsis 1977). Many subsequent experiments were conducted by Jöbsis on animals but it was not until 1985 that clinical publications began to appear (Ferrari *et al.* 1985 and Brazy *et al.* 1985). These studies compared changes in the concentration of hemoglobin

and deoxyhemoglobin with other monitored physiological parameters and were able to see the effect of clinical procedures on the oxygen status of the brain. It also became clear that there were problems with this method. The first was that the concentrations determined were relative, not absolute. Secondly, the units of chromophore concentration used were arbitrary ones due to the fact that scattering occurs within the brain and hence the optical pathlength is an unknown.

The methods employed in these preliminary studies were continuous-wave methods and did not detail the scattering spectra It was assumed to be constant, an assumption that is most likely violated in a variety of situations due to the variability in tissue scattering. Since these continuous-wave techniques, in general, contain insufficient information to detail both the scattering and the absorption in the measurement, it was necessary to employ more expensive time domain methods. Time-resolved measurements can determine the optical pathlength by measuring the time delay in the arrival of an optical pulse thus allowing for the determination of both scattering and absorption coefficients. Of course, steady state methods based on diffusion theory or frequency domain techniques which are capable of measuring μ_a and μ_s' can also be used to measure absolute hemoglobin absorption and hence oxygen saturation.

Currently there exist multiple approaches to the use of noninvasive spectroscopy to monitor hemoglobin concentration, yet all rely upon the use of two or more wavelengths and the following equation for absorption within the medium of interest, either phantom or tissue.

$$\mu_a(\lambda_1) = \varepsilon_{HbO_2}(\lambda_1)[HbO_2] + \varepsilon_{Hb}(\lambda_1)[Hb] + \mu_{a_{back}}(\lambda_1) \quad (18a)$$

$$\mu_a(\lambda_2) = \varepsilon_{HbO_2}(\lambda_2)[HbO_2] + \varepsilon_{Hb}(\lambda_2)[Hb] + \mu_{a_{back}}(\lambda_2) \quad (18b)$$

where $\varepsilon_x(\lambda_i)$ is the specific absorption of molecule x at wavelength i.

Often the background absorption is neglected or estimated which may be valid in phantom measurements but is probably not accurate *in vivo*. Some work has been performing measurements on muscle, particularly, the forearm (Ferrari *et al.* 1992 and Ferrari *et al.* 1991). There has been much more interest in using spectroscopic methods for oxygenation monitoring in the brain (Wyatt *et al.* 1986, Ferrari *et al.* 1986a and 1986b, Hampson *et al.* 1990 and Aldrich *et al.* 1994) and there exist several instruments available for clinical use (Wickramasinghe *et al.* 1986 and Chance *et al.* 1990). Most of these systems rely upon time-resolved methods, although some investigators are using modified steady state techniques (Chance *et al.* 1988a and Cope 1991 and Liu *et al.* 1995a). The simple models originally developed for determination of tissue optical properties have been altered due to the complex structure of the brain. The brain is not a homogeneous medium. Photons penetrating into the head are likely to encounter different anatomical layers and the optical properties returned may not be of the area of interest for oxygenation measurements. In fact, the head consists of four different layers each with unique optical properties. Okada *et al.* (1997) have designed and tested models of the head with the following four layers: surface layer (skull and scalp), cerebrospinal fluid (CSF), grey matter and white matter. The CSF adds an additional problem as it clear, i.e. non scattering and greatly affects the light distribution (Firbank *et al.* 1996). Okada *et al.* (1997) also accounted for the sulci in the brain by the addition of slots in

their phantoms, which had little effect. Other research by Liu *et al.* (1995b) indicates the importance of treating the tissue as highly absorbing blood vessels surrounded by a low absorbing background and not assuming a uniform chromophore distribution under some conditions.

Many factors regarding noninvasive monitoring of tissue oxygenation are currently being studied using a variety of optical techniques. Time, frequency and spatially resolved methods, in addition to many less standard techniques are being employed (Delpy *et al.* 1988, Cope 1991, Matcher and Cooper 1994, Fantini *et al.* 1995, Liu *et al.* 1995a and Oda *et al.* 1996). Since there exist many possible solutions to the problem the advantages and disadvantages of each approach must be carefully considered. The main difficulty with spatially resolved techniques is that reflectance data accumulated at small ρ values will be indicative of superficial layers only, for example the skin, or the skin and the skull and not representative of the tissue of interest. If only large distances are used, then relative continuous wave reflectance measurements yield only μ_{eff}, which is insufficient unless further approximations are used. If absolute reflectance is measured then this technique is viable, however, absolute measurements are likely to be troublesome. Furthermore, these methods may require an auxiliary technique to measure the photon pathlength, which is essential to determine the penetration depth of the photons. These techniques also required measurements at multiple distances. Many of these problems can be overcome in the time domain. Measurements are necessary at only one ρ value to determine the reflectance and the variation of ρ produces variation in the penetration depth of the light. In this method, the

layers that are not of interest, the skin, can easily be avoided. Changes in reflectance over time can lead to direct determination of changes in absorption which can easily be related to pathlength since the time of flight is known. A further, unexplored, benefit of this tactic is time gating of the reflectance which allows for control in the depth of penetration. Although the applicability of this time gating is uncertain, it is probable that even late times contain adequate information to determine relative changes in absorption. The frequency domain methods do offer many of the advantages of the time domain system, for example, only one collection distance and some control of penetration depth. But depth control is obtained by altering the modulation frequency and hence it can only be decreased from its maximum which occurs at the dc value. Due to the numerous advantages of the time-resolved method, it is the technique employed in this investigation for the non invasive determination of tissue oxygenation.

1.6 Thesis proposal

Non invasive *in vivo* methods for studying the status of tissue through optical means have garnered much attention recently. This study will employ time-resolved methods to measure tissue oxygenation due to the inherent advantages of this technique. The time domain method relies upon the interaction of a picosecond light pulse with a turbid medium, like tissue, which broadens and attenuates the pulse due to scattering and absorption, respectively. Fitting the remitted pulse to an applicable model of light transport allows for the determination of the optical properties of the tissue. The model

of light used will be diffusion theory as it has been shown to be a good model for light propagation under these conditions. This information may be utilized to investigate the status or structure of the tissue. In particular, by taking advantage of the known differences in absorption between oxyhemoglobin and deoxyhemoglobin, it may be possible to determine the oxygen saturation of the tissue. It is the aim of this thesis to explore the feasibility of this approach through the use of two pulsed diode lasers and a miniature photomultiplier tube. The current standard for this procedure employs a mode locked solid state pumped dye laser in combination with a microchannel plate photomultiplier tube. The instrumentation proposed here would reduce the cost, complexity and size of the system which would certainly increase its clinical applicability. In order to investigate this, the system must first be characterized by the use of phantoms with known optical properties. Once accurate values for scattering and absorption can be obtained, it will then be necessary to perform *in vivo* oxygenation measurements to determine if the system is sufficiently sensitive to monitor the oxygen status of tissue.

2 EXPERIMENTAL

The initial aim of this work is to determine if time-resolved studies may be performed using a pulsed diode laser and an inexpensive photomultiplier tube (PMT) operated in single photon counting mode to determine the optical properties of a tissue simulating phantom. Monitoring of tissue oxygenation, by the method suggested in the Introduction is dependent on the ability to accurately estimate the tissue optical properties, especially the absorption coefficient.

This chapter is divided into two sections, Apparatus and Analysis. The first section will describe the time correlated photon counting system, focussing on the differences between this system and the standard approach. The Analysis portion will detail the tests of the models that were performed, the different fitting methods employed and the applicability of different boundary conditions.

2.1 Apparatus

2.1.1 Time correlated photon counting system

The methods for the determination of optical properties borrowed technology from the field of fluorescence spectroscopy. There exist three main techniques for measuring fluorescence decay times: modulation methods, pulse-sampling methods and

time-correlated single photon counting (O'Connor and Phillips 1984). Modulation methods are the basis for frequency domain measurements, the advantages and disadvantages of which are described in the Introduction. Time-correlated single photon counting, although it typically has poor resolution, has become the standard in the field of fluorescence measurements. Its resolution has proven adequate for measuring optical properties and its cost is much less than pulse-sampling techniques, an important consideration from a diagnostic or therapeutic point of view.

As previously stated, the technique of time-correlated single photon counting has its origins in the measurement of molecular lifetimes. It works under the assumption that by timing many single photons a histogram of events versus time can be produced which, if many events are recorded, becomes representative of the desired probability distribution. For each event the time delay is measured and a count is added to the channel corresponding to the measured delay. This is repeated until a large sample size has been accumulated.

This method uses a light source with a high repetition rate in order to minimize the collection time; a common light source is a mode-locked, cavity-dumped dye-laser pumped by a continuous wave Nd:YAG laser. The light from this source is optically split; a portion is sent to the sample, to produce excitation in a fluorescence measurement (or to simply travel through the sample for the measurements performed here) and focussed on a microchannel plate photomultiplier tube, which has a fast response time. The pulses are amplified and sent through a constant fraction discriminator. The logic pulses start a time to amplitude converter (TAC). The stop pulses for the TAC are

obtained from the reference portion of the laser light which has been sent to a fast photodiode and another discriminator. The TAC pulse is sent to a multi channel analyzer where each bin is representative of a time window.

Often the instrumentation is operated in "reverse mode", i.e., the trigger signal actually stops the TAC. This is because that the counting electronics would be unable to reset between successive events for high source repetition rates. By allowing the sample signal to be the start pulse, the number of start pulses is reduced providing more time for the electronics to reset.

The resolution of the system is limited by the electronics and the PMT. The distribution of distances over which the photoelectrons and secondary electrons in the PMT must travel results in a variation in arrival times of the photoelectrons at the PMT anode and a transit time spread of up to 800 ps, depending on the PMT used. Thus, the observed signal is distorted by this effect and it becomes necessary when analyzing the data to account for this temporal spreading.

The particular equipment used for the experiments which form the basis of this thesis differ in some respects from the general description given above. The instrumentation used in these experiments is shown in Figure 2.1

The diagram shows two lasers, but if simultaneous oxygenation measurements are not being performed, then one laser may be used. Both lasers are pulsed diode lasers operated at 10 MHz with a pulse width < 50 ps (Hamamatsu Picosecond Light Pulser PLP-01 Users Manual). The first laser (PLP-01, LDH075, Hamamatsu Photonics K.K., Hamamatsu, Japan) emits a train of pulses at 750 nm with a peak power of 40 mW. The

other laser (PLP-01, LDH082, Hamamatsu Photonics K.K., Hamamatsu, Japan) emits at 810 nm and has a peak power of 150 mW The laser outputs are coupled with a 400 μm fiber optic combiner (Fibersense and Signals, Concord, ON) with losses of about 0.4dB. The signal is then split into three fibers, the first fiber receives about 80% of the combined power and delivers light through a 400 μm fibre to the sample, the second 10% is used as a reference pulse while the remaining 10% of the signal is routed to the photodiode to provide a stop signal. The use of this optical trigger provided more stable operation than the electronic trigger available from the laser diode driver

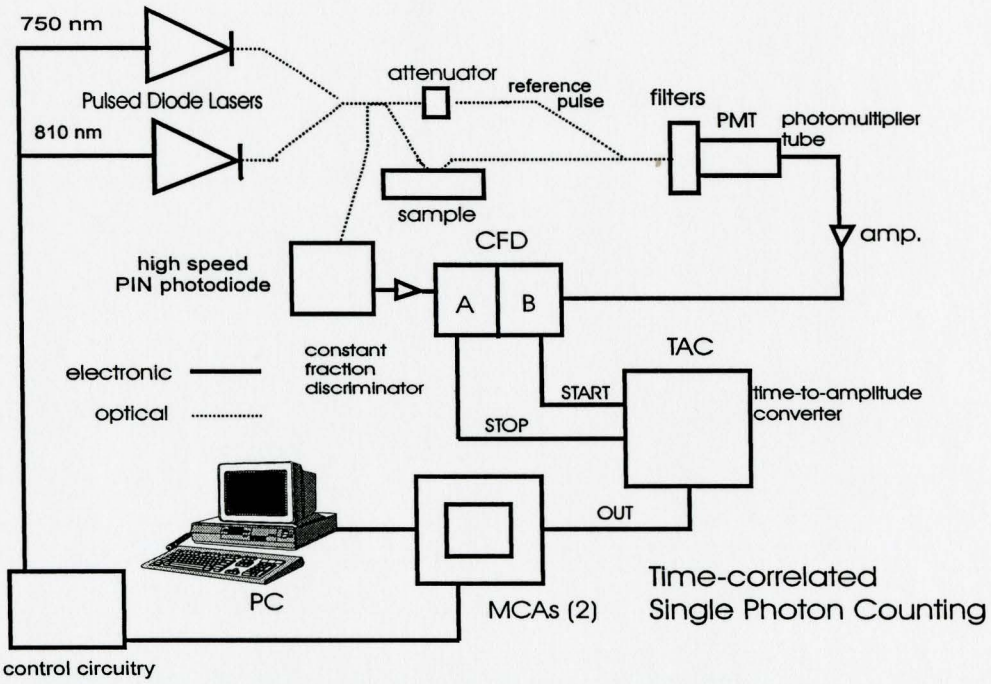

Figure 2.1 Schematic diagram of the dual wavelength time correlated photon counting system.

The light delivered to the phantom is collected with a fiber bundle and coupled to a filter wheel. The reference signal, which allows for the detection of time shifts due to drifts in the instrumentation, is sent through an attenuator (Oz Optics, Nepean, ON) and also transmitted through the filter wheel which is equipped with a range of neutral density filters. Both the attenuator and filter wheel allow for control of the amount of light to ensure the single photon counting levels, which are essential to the technique, are obtained. These signals, which are separated in time due to different fiber lengths are both incident on the photomultiplier tube (Metal Package PMT R5600U Series, Hamamatsu Photonics K.K.). The PMT was operated at 800 V and data collection time varied according to the situation but was on the order of minutes. The amplified detector output is fed through the constant fraction discriminator (CFD; TC 454, Tennelec/Nucleus, Oakridge, TN) and provides the start pulse for the time-amplitude converter (TAC; TC 864, Tennelec/Nucleus, Oakridge, TN). The third optical signal is coupled to a fast photodetector (Newport Model 875 Ultra-High Speed Photodetector, Irvine, CA) amplified, sent through the CFD, delayed (TC 412A Delay, Tennelec/Nucleus, Oakridge, TN) and acts as the stop pulse for the TAC. The TAC output, which is proportional to the temporal separation between start and stop pulses is sent to a multichannel analyzer and PCA II software (Oxford Instruments, Oakridge, TN) is used to display the time histogram.

A black plastic probe was designed to hold the source fiber in place and fix the collection fiber bundle at a given separation (10, 20, 30 or 40 mm) from the source. The probe was constructed such that the black surface would minimize reflections and so that

both fibers would be held in contact with the phantom or tissue surface. The instrument response function was measured by placing source and detector fibers face-to-face against each other. The probe also allowed for precise alignment of the source and detector fibers in this position and for the placement of additional filters so that the PMT was not saturated during the measurement of the instrument response function.

2.1.2 Pulsed diode lasers

The lasers employed in these experiments are standard semiconductor diode lasers. They are electrically pumped and emit pulses with widths of 50 ps or less up to a maximum pulse repetition rate of 10 MHz. The peak power is of the order of 100 mW, depending on the wavelength and the pulse energy is of the order of a few nJ. For any diode head only one emission wavelength is possible. The entire apparatus, including drivers is small, weighs less than 5 kg and can be run from a standard 120 V outlet. In contrast, another common laser used for these measurements, a mode locked dye laser, is pumped optically, typically by an argon ion gas laser or an Nd:YAG laser. The pulses emitted are very narrow, usually less than 10 ps and the maximum frequency is about 80 MHz. The peak power is higher than a diode laser usually on the order of W. They also offer tunability, i.e. the ability to operate at different wavelengths. However, the combined cost of the two lasers is much higher than the cost of the diode lasers used here and they are large and not easily portable. Furthermore, the lasers require a long stabilization period and cumbersome cooling and power supplies. Although in a lab setting dye lasers have advantages over diode lasers, in a clinical environment the size and portability of the diode laser makes it more feasible.

2.1.3 Photomultiplier tube

The need for compact equipment with high accuracy and sensitivity has grown with the increasing popularity of optical techniques in clinical settings. This is also true for photodetectors such as photomultiplier tubes. The most common detector used for time correlated photon counting is probably the microchannel plate photomultiplier tube (MCP-PMT) which has excellent time response, sensitivity which has low wavelength dependence over a specific range and the ability to count photons with low noise and high sensitivity. Semiconductor sensors can be used in place of MCP-PMTs but they do not have the excellent resolution nor do they have signal to noise ratios as high as MCPs. A compromise solution by Hamamatsu is the R5600U series of PMTs which employ a metal package instead of the glass envelope; they are small yet offer better sensitivity, by approximately four orders of magnitude, and resolution than semiconductor devices. They are about 1/7th the size of a standard tube and their resolution, as measured by the full width half maximum (FWHM) of the IRF, is about 275 ps compared to about 30 ps for a MCP-PMT, or about 2 ns for a standard side window PMT, under similar conditions. These miniature tubes use stacked thin electrodes (metal channel dynodes) to form an eight stage electron multiplier within a metal cylinder of 15 mm diameter and 10 mm height. These electrodes were designed using electron trajectory analysis and micromachining to make them about one-tenth the size of standard types. In addition to being compact, these tubes also cost less than ten percent of the price of an average MCP-PMT. These photomultiplier tubes have sufficient resolution to perform the time-resolved reflectance measurements and they are well suited to a clinical environment.

However, it is necessary to investigate their performance when coupled with a diode laser under practical, i.e. biologically realistic, situations.

2.1.4 Control circuitry

In order to perform simultaneous measurements with the photon counting system described above, it is necessary to implement an electronic control circuit that manages the lasers and the multi-channel analyzers. A schematic diagram of this circuit is shown below along with the appropriate timing diagrams. The 5 MHz clock provides the time basis for the circuit. The timing diagrams show the pulses sent to the time gates, G1 and G2, of the two MCAs. Hence, initially LD1 will be triggered active and G1 will activate MCA1. At some time later, LD1 will switch off and LD2 will fire and G2 will activate MCA2. Each laser is therefore pulsing, at 5 MHz, for half of the total collection time. In this way a sample can be probed with the two lasers at the same time, toggling between them at a rate of about 20 Hz. This time is short enough such that biological changes are unlikely to occur from the time one laser is on until the second laser fires. Since the measurements are performed over the same time interval, changes that occur in the optical properties of the sample, for example due to deoxygenation, are detected at two wavelengths. Hence the reflectances observed at different wavelengths are a result of the wavelength dependence of the optical properties.

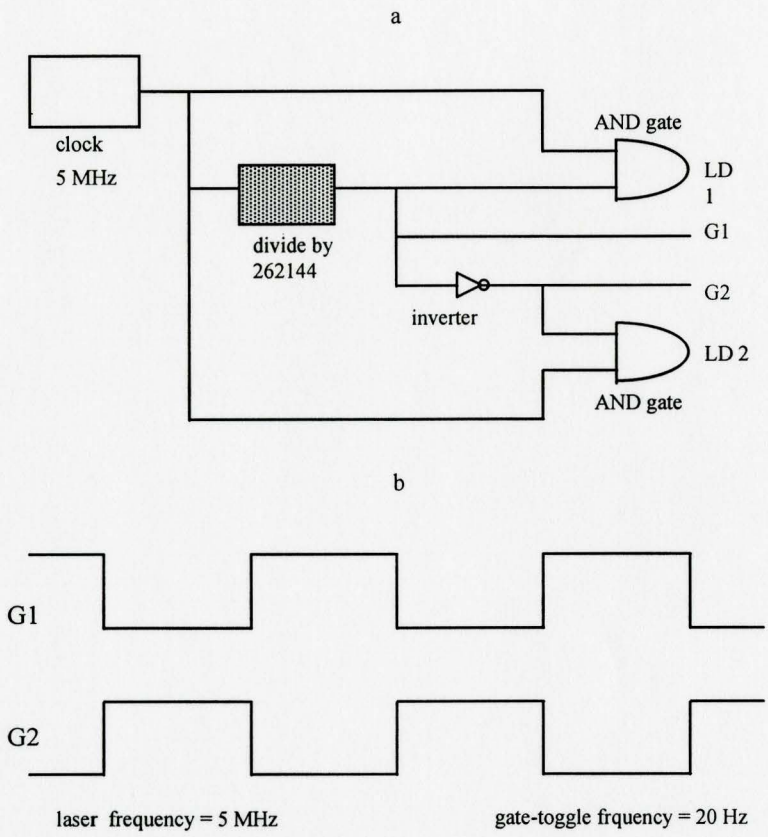

Figure 2.2. Diagram of control methods for simultaneous dual wavelength measurements (a) circuit diagram and (b) timing diagram.

2.1.5 Phantoms for measurement

Throughout the course of this project, a variety of tissue simulating phantoms were utilized, both solid and liquid. There are advantages and disadvantages to each type of phantoms. Solid phantoms offer stability over time, a solid plane to couple the probe to and the ability to measure the same phantom repeatedly The drawbacks include difficulty in predicting the absorption and scattering, fixed optical properties, an imprecise value for the refractive index and a fixed volume. Liquid phantoms are usually composed of up to three ingredients, water, a scattering substance and an absorber, if desired. Two popular scattering suspensions are Intralipid and polystyrene spheres, both

of which are turbid and have no strong absorption bands in the regions of interest. These suspensions are usually diluted with water, so if no additional absorber is added, the absorption observed is equivalent to the absorption of water at the wavelength of interest. Since water is the dominant component by concentration, the index of refraction of these phantoms is that of water, 1.33. Absorbers, such as inks or dyes, can be added to these solutions to increase the absorption coefficient. Liquid phantoms have the following advantages: a theory, or recipe to predict optical properties, the ability to change the optical properties and the volume of the phantom and a known value for the refractive index. These phantoms have disadvantages which include, the possibility of settling over time, a limited shelf life, an indefinite surface to couple against and the possible presence of bubbles in the suspension which affect the coupling of the fibers to the phantom and can, in turn, alter the optical properties.

2.2 Analysis

The pulse profiles obtained from the time correlated photon counting system contain information regarding the scattering and absorption properties of the sample probed. However, a pulse which does not pass through a turbid medium is temporally broadened due to the electronics, the PMT and the fiber optics involved in signal collection. This pulse, known as the instrument response function (IRF) is an intrinsic part of any data collected through a sample and must be taken into account. The experimental pulse observed, E(t), is a convolution of the true signal $R_{exp}(t)$ due to the

turbid medium and the impulse response, I(t). Diffusion theory can be used to predict the shape of the reflectance profile, $R_{theory}(t)$. There are two options for eliminating the effect of the IRF: one could perform the deconvolution of E(t) or could convolve the theoretical reflectance with the IRF and compare this to the observed reflectance. Due to the difficulty of the deconvolution process, the latter approach has been shown to be superior in this application.

The fitting algorithm is shown in Figure 2.3. An initial estimate of the optical properties, μ_a and μ_s' is used to calculate the theoretical reflectance $R_{theory}(t)$ based on diffusion theory. This function is convolved with the measured experimental IRF, I(t) and the experimental reflectance, E(t) is then compared to $R_{theory}(t)*I(t)$. The chi-squared (χ^2) value for the fit is calculated and if the difference between two successive values is not within a preset tolerance, the values of μ_a and μ_s' are changed such that the χ^2 decreases and the process is repeated until the χ^2 value is at a minimum. The χ^2 is calculated by assuming that the variance of each data point is equal to the number of counts in that bin. At this point it is assumed that the best estimates of the optical properties have been determined and the final results are stored. A Fortran routine was written to find the optimum values of μ_a and μ_s' by a grid search, as outlined in Bevington (1992). This program outputs the final values of μ_a and μ_s', the calculated fit, the experimental data and the χ^2 value obtained.

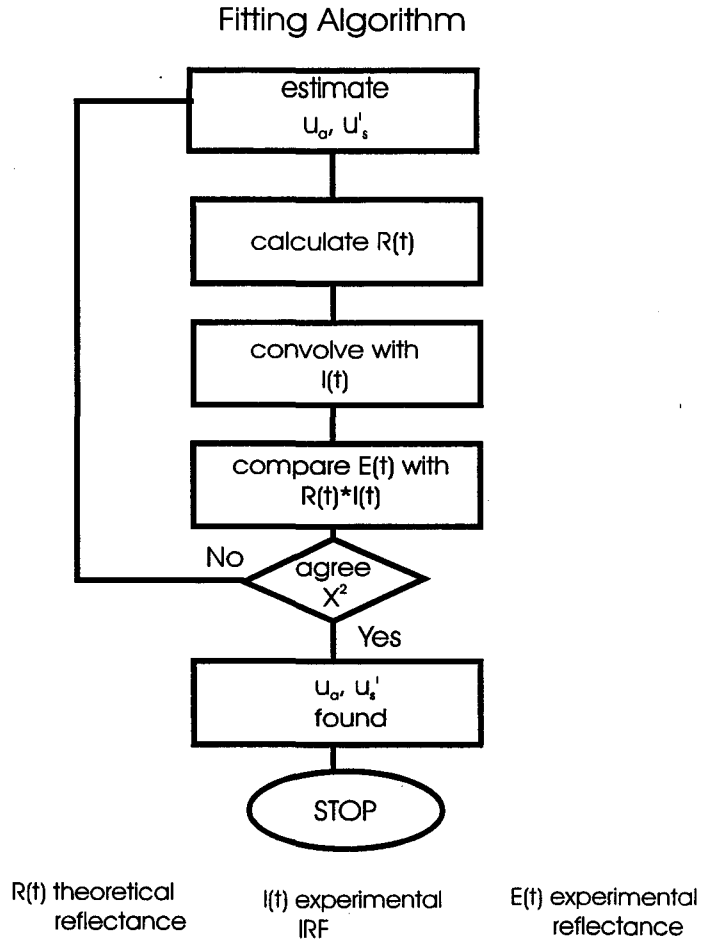

Figure 2.3: Non linear least squares fitting algorithm used to estimate μ_a and μ_s' from time-resolved reflectance and experimental IRF.

In this section, four main topics will be investigated regarding the analysis of time-resolved data. The first issue is how accurately the grid search method can fit diffusion theory data. By simply fitting model-generated diffusion data and diffusion data with added noise with the non linear least squares fitting routine, it is possible to test the performance of the computer program itself. Another topic that has seen much previous attention (Cubeddu *et al.* 1996, Patterson *et al.* 1991b and Haskell *et al.* 1994) is the accuracy with which the diffusion theory models light propagation in a turbid

medium. This is tested by fitting Monte Carlo generated data with a model based on diffusion theory. It is essential to determine the accuracy of the model at smaller ρ values, e.g. 10 mm, as these will be used in experiments on phantoms. The third area of interest, which was discussed in the Introduction, is how to account most economically for the effect of boundaries on the measured reflectance. Hence, the advantages of the different boundary conditions will be investigated. The final question which will be addressed is the advantages of fitting in the frequency domain. Because the lasers and the photomultiplier tube used in these investigation have significantly worse temporal resolution than other systems, it is necessary to determine how to best account for this fact. It is believed that fitting the time-resolved data in the frequency domain i.e., phase and modulation versus frequency, may help minimize the significant effect of the instrumentation on the reflectance measured.

2.2.1 Non linear least squares fitting in time domain

(A) *Fitting Diffusion Theory Data*

The first step in the test procedure was simply fitting data generated by diffusion theory with diffusion theory. Of course, there should not be any difficulty associated with this process, but it provided confirmation of the correctness of the fitting procedure. Theoretical diffusion data were generated using equation (10) and were fit under various conditions. Since this is only to test the fitting program, the particular model used is irrelevant and hence the most simple model was used. The first factor that was varied was the tolerance value for changes in the value of χ^2, i.e. once the changes were within the tolerance, they were considered to be insignificant. For a high tolerance value (1),

values of the properties differed from their true values by as much as 7%. At this point it must be noted that three parameters were actually fit, the absorption, the scattering and a normalization value which is necessary to compare signals of varying magnitude. An optimum value for the tolerance was found to be much lower, on the order of 0.001; errors in this case were around 2%. By varying the fraction by which the parameters were adjusted after each iteration little improvement was observed in the fits, however, the speed of the fit was affected by the step size. If too large a step was used it was possible to miss the correct solution completely, but little difference was observed for step sizes less than 10%. Changing the parameters by 1% each iteration gave best results in terms of a compromise between speed and accuracy. Data were also generated at different source detector separations with insignificant variations in the estimated properties. There were no difficulties associated with fitting theoretically generated data. The next step was to test the convolution portion of the routine. The theoretical data were convolved with a delta function and fit using the optimum tolerance and step size values previously determined. The results obtained were similar to before, small errors of about 2% were observed in the optical properties returned. Finally, the data were convolved with a Gaussian and fit with results similar to above, errors observed were about 2-3%. In both cases, the errors were not systematic, values returned were both higher and lower than the true values. These tests were able to show that the non linear least squares fitting program and the convolution subroutine were functional.

(B) *Fitting Diffusion Theory Data with Added Noise*

A test which provides more information regarding the performance of the fitting routines under realistic experimental conditions is the fitting of diffusion theory data to which noise is added. Once more, the simple expression for the diffusion theory is employed to generate theoretical data under various conditions; in this case, Poisson noise is added to the data. Since there are large numbers of counts involved in an experiment, it can be assumed that the noise is distributed according to the Poisson distribution with variance N where N is the number of counts in a particular time bin. The noise was added by random sampling of a Normal distribution with a standard deviation equal to $\sqrt{N}$.

Three different factors, the source detector separation (ρ), the absorption and scattering coefficients, were varied to determine their influence on the fits obtained. The fitting range for these data were two orders of magnitude, i.e. the data were fit two logs down from the peak value on either side. The fitting parameters used were similar to those in the preceding section. The data generated for different ρ values were produced such that the number of counts in the peak of any profile would be about the same and typical of an experiment, approximately $3\text{-}4 \times 10^3$ counts; the optical properties were typical as well, μ_s' was set to 1.0 mm^{-1} and the absorption fixed at 0.01 mm^{-1}. Figure 2.4 shows the data for ρ=15 mm along with the fit and the residuals. The fitted function and the experimental reflectance appear to be in excellent agreement. Furthermore, the weighted residuals are small and appear to be distributed like white noise, as expected. The fits for the other distances show similar behavior.

a

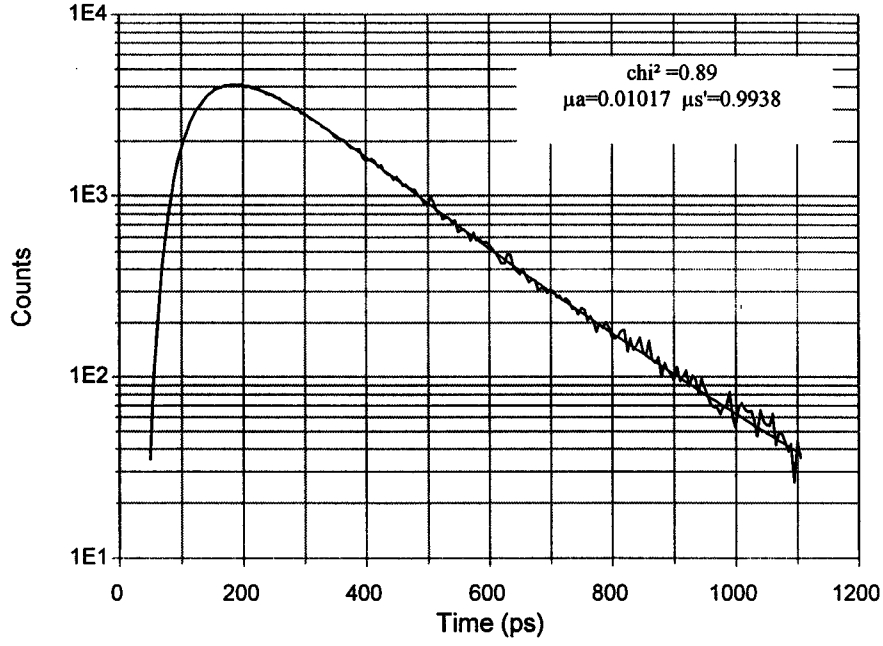

b

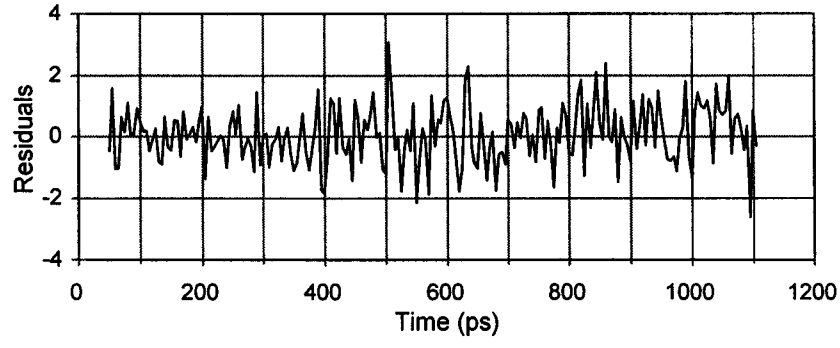

Figure 2.4: Results of fitting diffusion data with noise (a) fit (b) residuals for μ_a=0.01, μ_s'=1.0mm^{-1}and ρ = 15 mm.

A summary of the optical properties returned and the χ^2 values is shown in Table 2.1 below.

ρ (mm)	χ^2	μ_a	μ_s'
10	0.96	0.01029	0.9797
15	0.89	0.01017	0.9938
20	1.03	0.01030	1.007

Table 2.1: Optical properties returned from diffusion fitting routine with varying ρ. Expected values are μ_a=0.01 mm^{-1}, μ_s'=1.0mm^{-1}.

Despite noise added to the data, the fitted values returned are always within 3% of the theoretical values. The reduced chi-squared values are always close to unity, as expected and the differences between values at the three ρ values are insignificant.

Since the diffusion theory is most applicable for larger values of ρ, subsequent studies were performed at 20 mm. The optical properties used to generate the data were varied over a wide range to determine if this would affect the fits. In this case, the peak count value was allowed to vary according to changes in reflectance as predicted by diffusion theory. Table 2.2 displays the results of this investigation.

χ^2	μ_a theoretical (mm^{-1})	μ_a fit (mm^{-1})	μ_s' theoretical (mm^{-1})	μ_s' fit (mm^{-1})
1.07	0.01	0.01021	0.5	0.4899
1.08	0.01	0.01012	1.0	0.9936
1.10	0.01	0.01004	1.5	1.4951
1.07	0.01	0.01003	2.0	1.9917
1.01	0.0	9.449×10^{-6}	1.0	0.9945
1.46	0.02	0.02038	1.0	0.9855
1.44	0.03	0.03059	1.0	0.9825
1.04	0.04	0.04172	1.0	0.9587

Table 2.2: Variation of estimated results of fits with varying theoretical optical properties for ρ=20 mm.

When the value for the absorption coefficient is held constant at 0.01 mm^{-1} and the scattering is varied, the values for the absorption are excellent, within 2% The scattering errors are even smaller at approximately 1% and the χ^2 value remains close to one. However, when the absorption is varied over the range of 0 to 0.04 mm^{-1}, the quality of the fits and the accuracy of the returned values do change. As absorption increases the relative error in the absorption coefficient increases, up to a maximum of 4%, while the error in the scattering coefficient also increases up to 4%. The chi-squared value also increases but no trend is evident. The fits and the residuals for this set of tests

show good agreement between the fits and the data and no trends are visible in the residuals.

The fit and the residuals for μ_a=0.01 mm^{-1} and μ_s'=1.5 mm^{-1} are shown in Figure 2.5; once more, there is good agreement between the fit and the experimental data and the residuals seem to be randomly distributed. The variation in the scattering coefficient has less effect on the peak count values than the variation in absorption. Thus for the highest absorption, there are only about 100 counts in the peak and the pulse appears noisy. This seems to account for the variation in the optical properties returned, the noisier the data become, the less precise the optical properties. The noise should not affect the accuracy of the estimated properties but may lead to increased variation, which is probably what was observed in this instance. This was investigated by generating data with μ_s'=1.0 mm^{-1} and μ_a=0.04 mm^{-1}, but with 4000 counts in the peak. The optical properties returned were μ_s'=0.9846 mm^{-1} and μ_a=0.04082 mm^{-1}, the errors are similar to those resulting from fits with lower absorption coefficients. From these results it can be seen that although noise does affect the quality of the fits and the values returned, reasonable results can be obtained under a wide variety of conditions using the non linear least squares fitting routine.

a

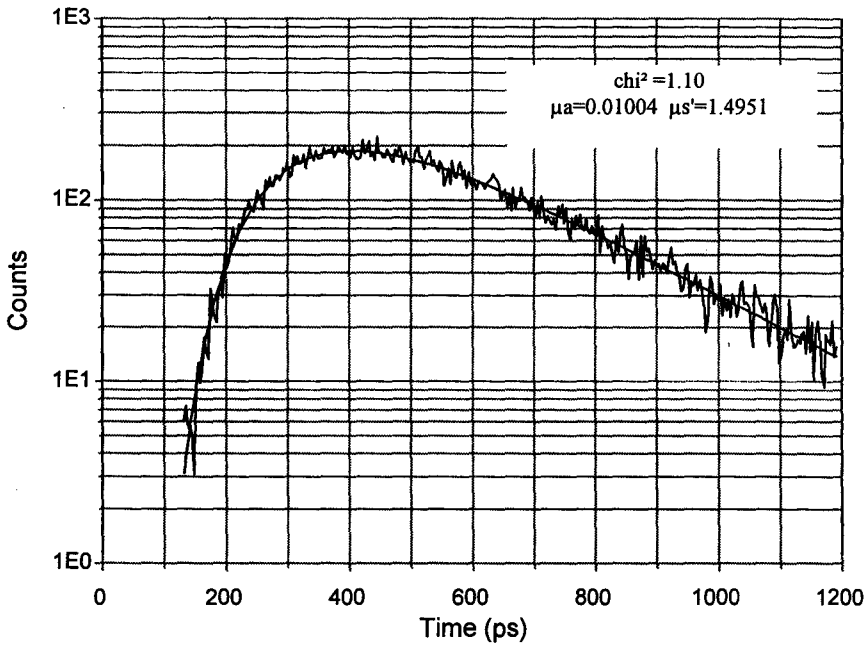

b

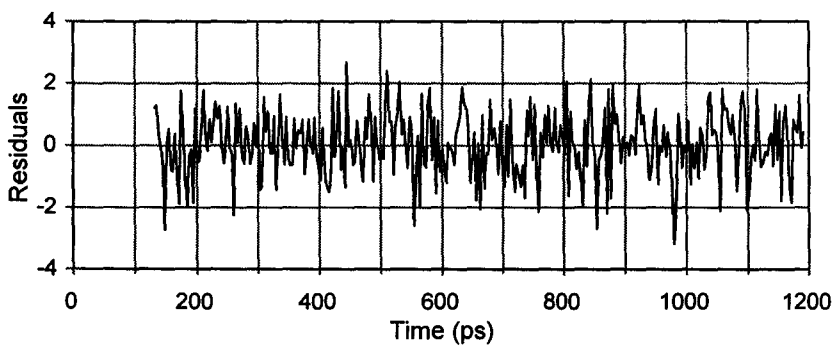

Figure 2.5: Results of fitting diffusion data with noise at ρ = 20 mm, μ_a=0.01 mm^{-1} and μ_s'=1.5 mm^{-1}. Figure 2.5(a) shows the data and the fit and (b) shows the residuals.

(C) *Fitting Monte Carlo Data with Diffusion Theory*

As discussed previously, the most accurate of the practical methods to model light transport in a turbid medium is the Monte Carlo method. In this method individual photon histories are traced under specific conditions by sampling the relevant quantities from appropriate probability distributions. In order to test the validity of the diffusion model under experimental conditions, Monte Carlo data were generated and fit using the non linear least squares routine described above. This was essential to provide an idea of the accuracy with which the model could be expected to predict optical properties during an experiment. In addition, it should be noted that the diffusion model, especially for early times, with ρ=10 mm is probably approaching its limits of validity. Therefore, a study similar to that performed for the diffusion theory data was performed. Since the Monte Carlo data more accurately represents experimental conditions three changes were made. The more accurate diffusion model, equation (16) was used to fit the Monte Carlo data. The boundary conditions used for generating and fitting the data assumed no mismatch in the indices of refraction. The Monte Carlo data were also convolved with an experimentally collected instrument response function to determine its influence on the ability to model the data accurately in section D. Finally, since the model was questionable for early times, the range of times over which the data were fit was varied to determine how the fits and values returned varied as a function of the start time of the fitting range.

Identical optical properties were employed in the Monte Carlo simulations as in the diffusion theory, μ_a=0.01 mm^{-1} and μ_s'=1.0 mm^{-1} and the data were collected for ρ=10 and 20 mm.

The results are shown in Figures 2.6 and 2.7; Figure 2.6(a) shows the data for 10 mm, the χ^2 is large at 6.16, the absorption is about 40% too large and the scattering coefficient 27% too high. After the peak the fit and the residuals (Figure 2.6(b)) appear acceptable, however, the model overestimates the rising edge and underestimates the peak; this is clearly reflected in both the fit and the residuals. At 20 mm, Figure 2.7, the χ^2 is much closer to one and the absorption and scattering errors are much more reasonable at 7 % and 6% respectively. A small overestimation of the rising edge is visible in this graph as well.

a

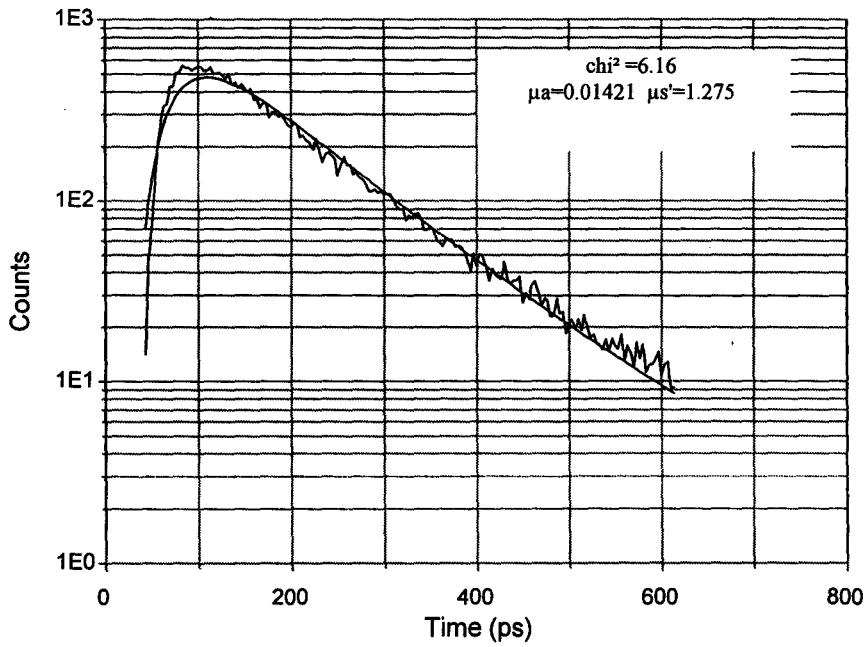

b

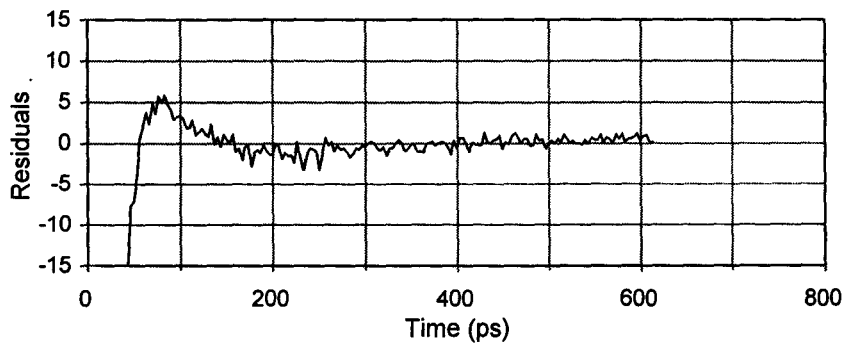

Figure 2.6: Fit (a) and residuals (b) for Monte Carlo data at 10 mm for μ_a = 0.01 mm^{-1} and μ_s' = 1.0 mm^{-1}.

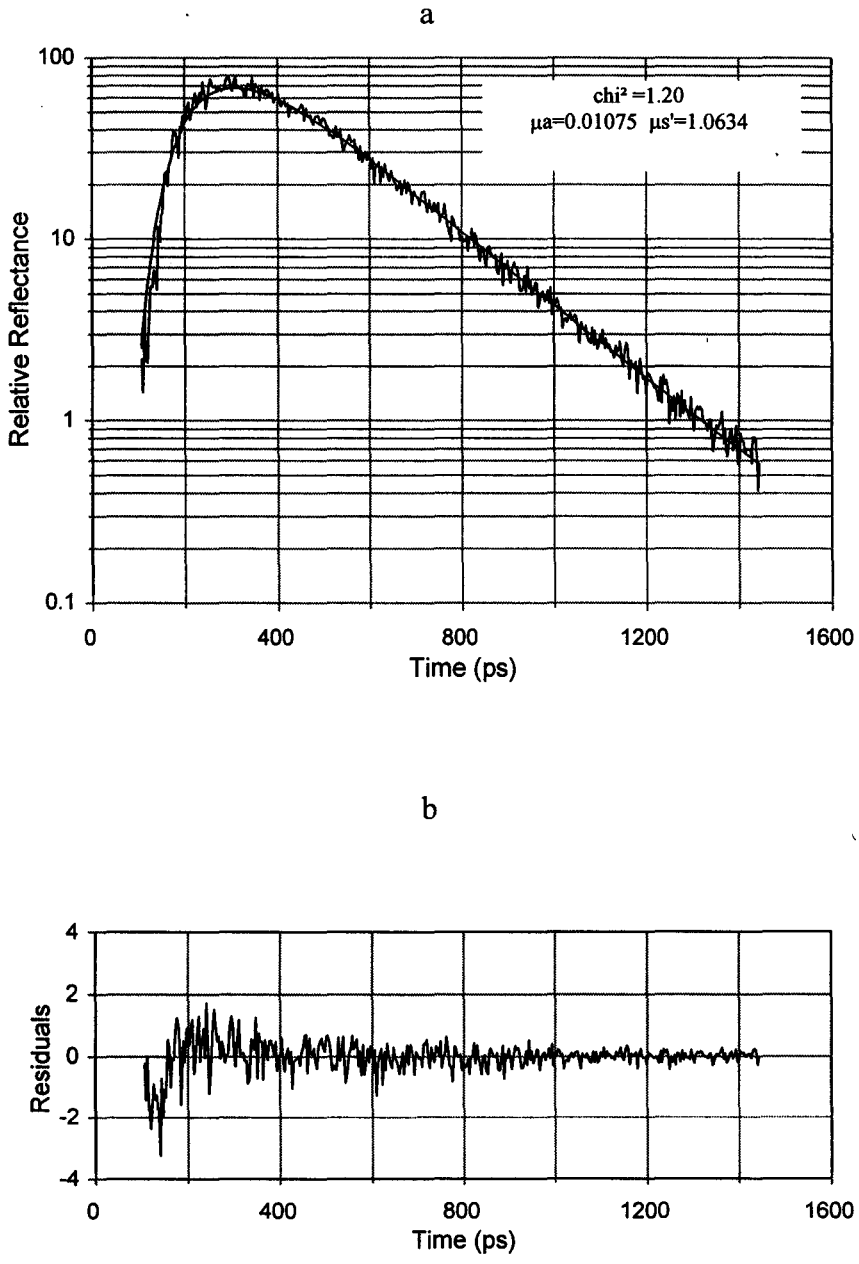

Figure 2.7: Fit (a) and residuals (b) for Monte Carlo data at 20 mm for μ_a = 0.01 mm^{-1} and μ_s' = 1.0 mm^{-1}.

The diffusion theory does not model the data very well , especially for early times and for a source detector separation of 10 mm. The radiance this close to anisotropic source may not be close to isotropic and the early arriving photons are approaching the ballistic limit; both of these factors contribute to the poor fits shown.

In order to investigate the full effects of the rising edge on the ability of the model to predict the reflectance, the range over which the data were fit was varied. In the above Monte Carlo fits the data were fit over two logs as in the previous section. Figure 2.8 shows the variation of optical properties with the start time of the fit. The final start time was determined by the position of the peak, which for the 20 mm data was 300 ps and for the 10 mm reflectance was 100 ps. For the data collected at 10 mm, it was possible to improve the fits considerably by fitting less of the rising edge of the reflectance spectrum. Errors of only 1-2 % for both the scattering and absorption are shown in 2.8b for fits starting within 30 ps of the peak of the reflectance. Similar results are shown in 2.8a for the 20 mm data, however, the improvements are less dramatic. By varying the start of the fitting range, the scattering coefficient can be estimated to about 1% of the actual value and the absorption within about 2.5%. For both ρ values, it is possible to decrease the estimated value of the scattering coefficient below the true value. The absorption coefficient can be decreased from its initial high estimate, however, it is not driven below the true value in either case. When fitting Monte Carlo data, it is advisable to eliminate the early times, where the model validity is doubtful, from the fitting range to improve the accuracy of the optical properties calculated.

a

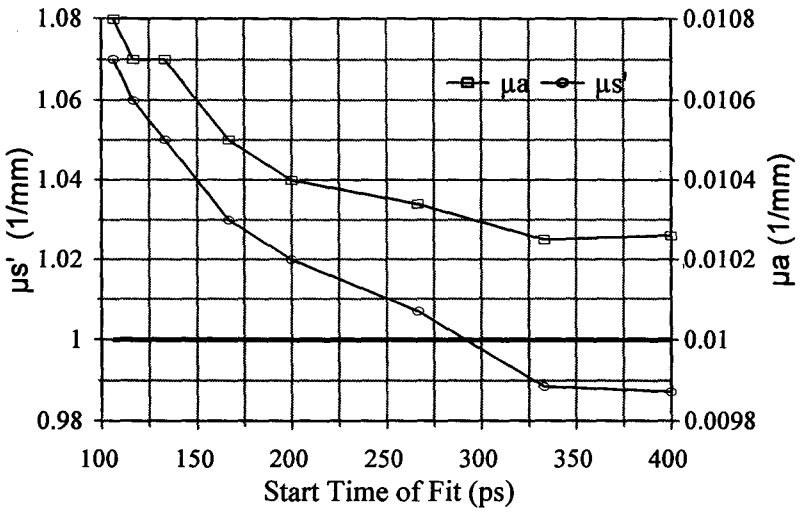

b

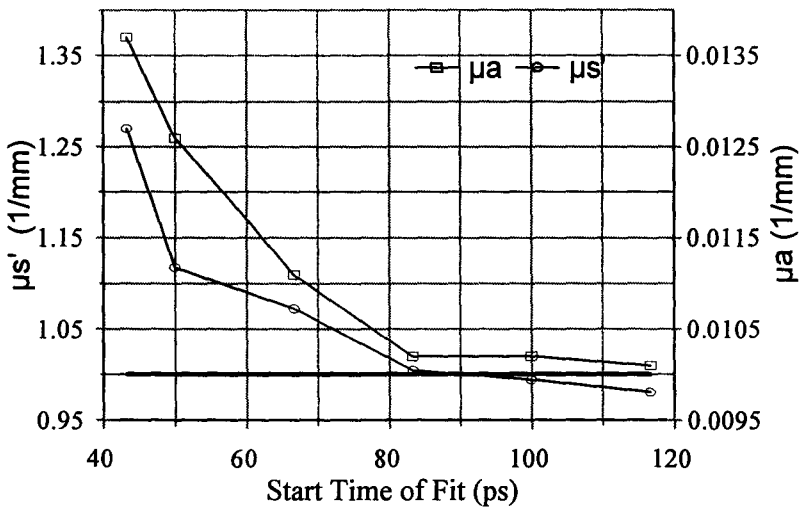

Figure 2.8: Variation of optical properties with start time of fit for Monte Carlo data (a) 20 mm (b) 10 mm. Reference line shows true values.

The effect of the optical properties used in the Monte Carlo simulations on the quality of the fits was also examined. The values of absorption and scattering were varied but the source detector separation was held constant at 20 mm as in the diffusion data study. In accordance with the results of the investigation of the start time, the fitting range was decreased such that it extended one log before the peak and two logs after the peak in order to eliminate the data at early times. The results are shown in Table 2.3 below.

μ_a **theoretical** (mm^{-1})	μ_a **fit** (mm^{-1})	μ_s' **theoretical** (mm^{-1})	μ_s' **fit** (mm^{-1})
0.01	0.0106	0.5	0.5038
0.01	0.0104	1.0	1.034
0.01	0.0103	1.5	1.566
0.01	0.0104	2.0	2.124
0.0	1.8×10^{-4}	1.0	1.023
0.02	0.0209	1.0	1.045
0.03	0.0314	1.0	1.056
0.04	0.0422	1.0	1.070

Table 2.3: Results from fitting Monte Carlo data with different optical properties at a fixed ρ value of 20 mm.

An example of a fit to the data and the residuals is displayed in Figures 2.9 (a) and (b), for μ_a=0.02 mm^{-1} and μ_s'=1.0 mm^{-1}. After the peak the fit and the residuals appear acceptable, however, for early times there are large discrepancies between the Monte Carlo data and the diffusion theory fits, as expected. This is less obvious in the fit than it is in the residuals where large differences are evident up to about 200 ps. The error in the absorption coefficient was about 4%, while the error in μ_s' was 4.5%. The χ^2 value is fairly high at 18.75, however, this could be improved by fitting less of the rising edge of the reflectance spectra. This was attempted and did not vary the optical properties returned significantly, although it did improve the χ^2.

From the results presented in this section, it is clear that errors are present when fitting Monte Carlo data with diffusion theory. Better results are possible at a source detector separation of 20 mm than at 10 mm. Results also depend on the optical properties used and the fitting range. A more accurate comparison to an experimental situation is performed in the next section where Monte Carlo data is convolved with an experimental IRF and fit with diffusion theory.

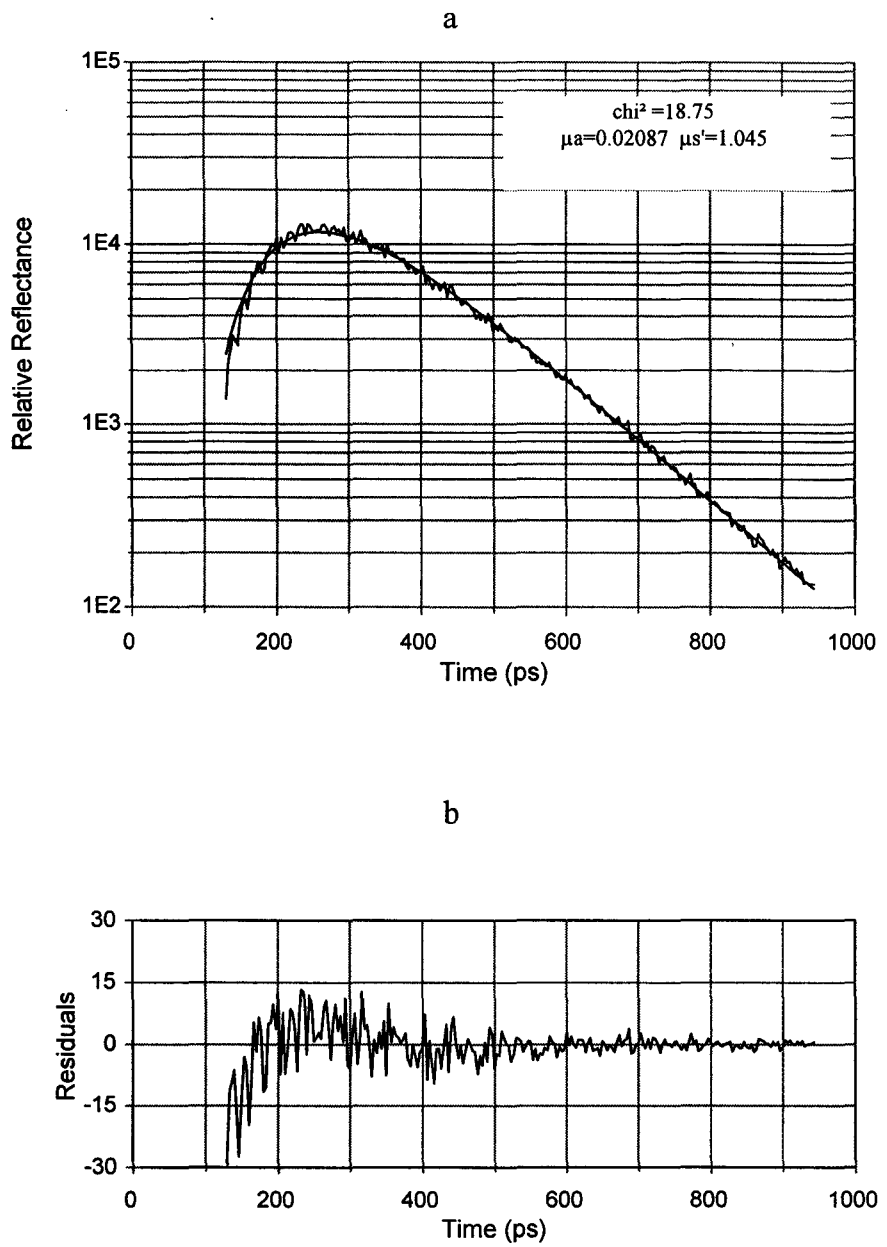

Figure 2.9: (a) Diffusion theory fit to Monte Carlo data at ρ = 20 mm. The expected optical properties are μ_a=0.02mm^{-1}and μ_s'=1.0 mm^{-1} and (b) residuals from the fit.

(D) *Fitting Monte Carlo Data Convolved with an IRF with Diffusion Theory*

To investigate the effect of the instrument response function, the data from section C were convolved with an experimentally collected impulse response and fitted using diffusion theory. The fits for the two ρ values are shown in Figures 2.10 and 2.11. The fits shown were performed over two logs and again the optical properties used in the Monte Carlo simulation were μ_a=0.01 mm^{-1} and μ_s'=1.0 mm^{-1}. The values returned for the 10 mm source detector separation, seen in Figure 2.10 are within 4 % for absorption and 11% for scattering. The fit and the data appear to be indistinguishable even for early times, but there are systematic errors visible in the residuals. Similarly at ρ=20 mm, the fit and the data are in excellent agreement but the residuals are non random. In both instances, the residuals are less than 2 in magnitude; although it must be noted that the best method of weighting for the residuals was unclear as this data involved real experimental results and computer generated results. The error in the absorption is large at 14% while the scattering coefficient has an error of about 8%. The results, after convolution with an IRF, are hence better at 10 mm and less accurate at 20 mm, especially for the absorption. In both cases, there is better agreement between the model and the data for early times. The convolution process removed some of the high frequency components present which are responsible for the difficulties in fitting over early times. The data are smoothed by the convolution and the noise is no longer visible.

a

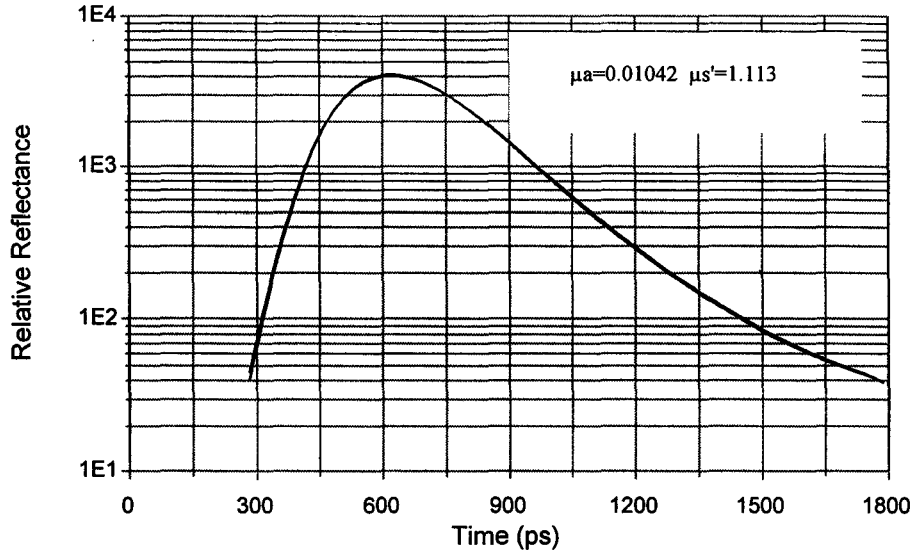

b

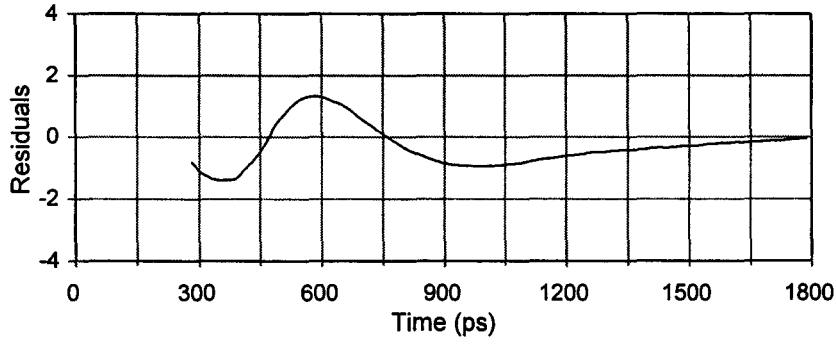

Figure 2.10: Fit (a) and residuals (b) for Monte Carlo data convolved with an IRF at 10 mm. Expected optical properties are $\mu_a = 0.01$ mm^{-1} and $\mu_s' = 1.0$ mm^{-1}.

a

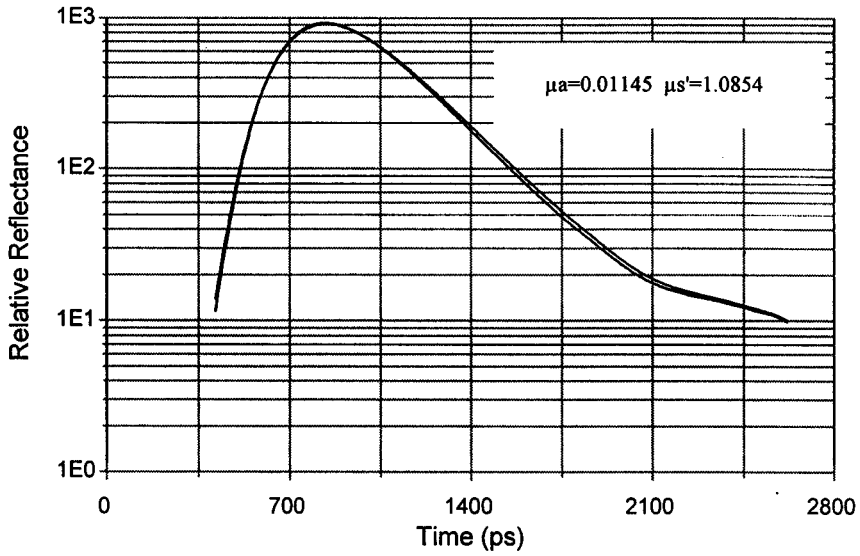

b

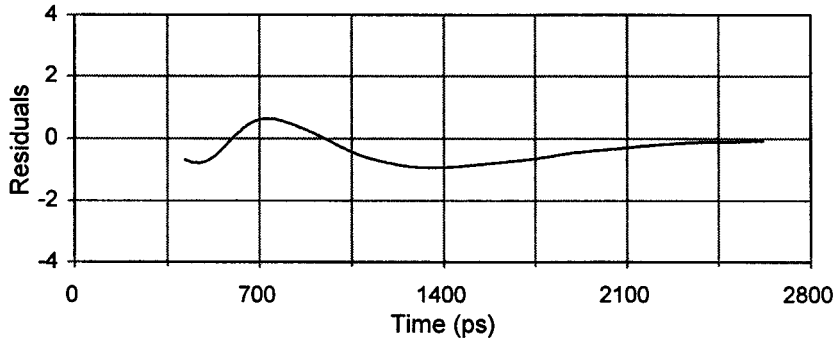

Figure 2.11: Fit (a) and residuals (b) for Monte Carlo data convolved with an IRF at 20 mm. Expected optical properties are $\mu_a = 0.01$ mm^{-1} and $\mu_s' = 1.0$ mm^{-1}.

To investigate the effect of the variation in the start of the fitting range, the data for both distances were fit over a variable range. For the Monte Carlo data, it was observed that improvements in the accuracy of the results could be obtained by not fitting the data at early times. The results of varying the start time of the fitting range for the Monte Carlo data that has been convolved with an IRF are shown in Figure 2.12. For the data at 20 mm, it is possible to improve the accuracy of the scattering coefficient returned by about 5%. The absorption value seems unaffected by the variation in the start time of the fit. At 10 mm, the error in the scattering coefficient can be decreased by about 5% while no significant change is observed in the absorption coefficient. In both cases, it is possible to estimate the scattering coefficient to within 10% and the absorption coefficient to about 5%. Both coefficients are found to be higher than their true values. While for the Monte Carlo data alone it was possible to drive the coefficients below their actual values by changing the start time of the fit, this trend was not observed for these data sets.

a

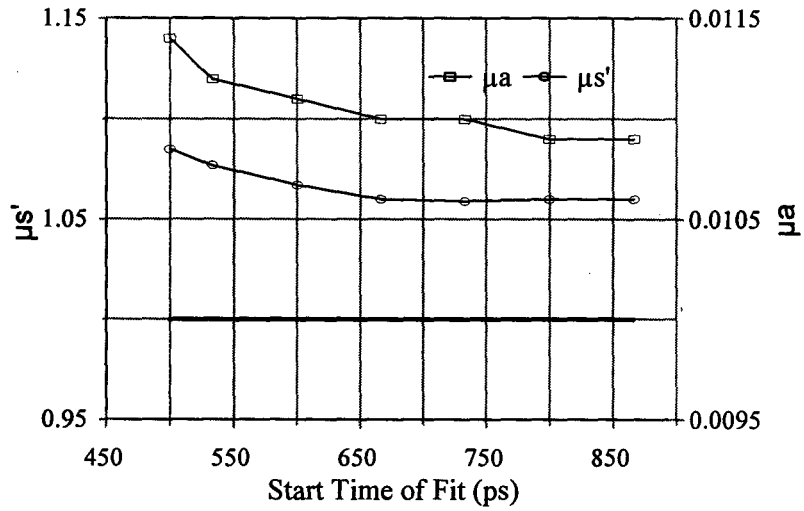

b

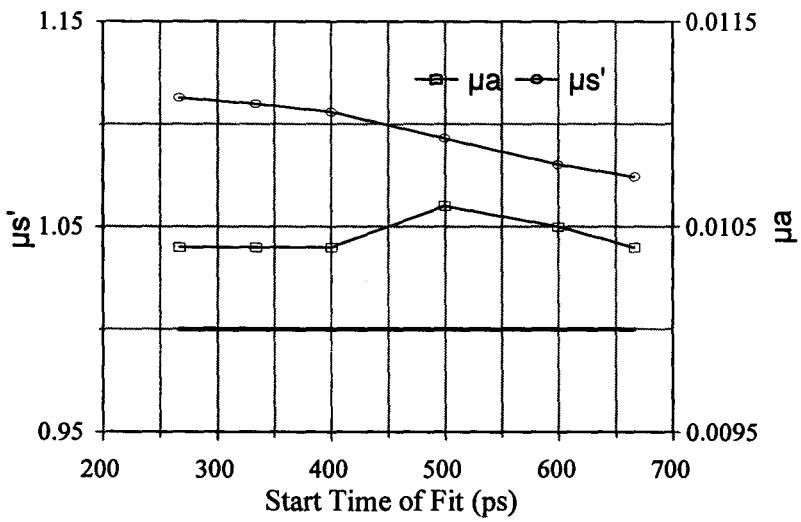

Figure 2.12: Variation of optical properties with start time of fit (a) 20 mm (b) 10 mm for MC data convolved with an IRF. Units for both coefficients are mm^{-1}. Reference line shows true values.

2.2.2 Boundary Conditions

The theories which form the basis for each of the three boundary conditions were presented in the Introduction. Each of the three boundary conditions has advantages and disadvantages. The zero boundary condition is simple but less accurate, does not take into account index of refraction mismatches and has little physical basis. The EBC and the PCBC are both physically sound but the PCBC requires time consuming fits and the EBC leads to an expression which depends on the numerical aperture of the fibre (Haskell *et al.* 1994). In testing the fitting routines, the ZBC and the EBC were employed but the PCBC was not used due to its computational expense. As stated previously, the most significant changes in the accuracy of the model occur when the EBC is used instead of the ZBC; little is gained from the costly incorporation of the partial currents with the PCBC. This is due to the fact that the best single point image representation of the PCBC is the extrapolated boundary and they differ only in octupole and higher moments (Haskell *et al.*, 1994). However, the differences between the two simpler theories were examined.

From the previous work in fitting Monte Carlo data, it is known that diffusion theory and Monte Carlo data are not in agreement, especially for early times and smaller ρ values. This is further substantiated by Figure 2.13 which compares diffusion theory using two boundary conditions, the EBC and the ZBC with Monte Carlo data. The

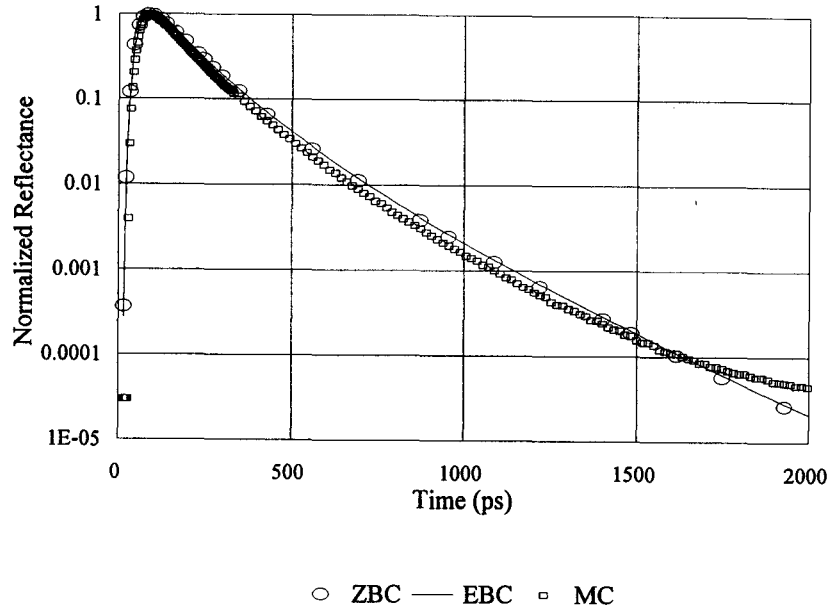

Figure 2.13: Comparison of reflectance from diffusion model using EBC and ZBC with Monte Carlo reflectance at 10 mm. Optical properties were μ_a=0.01 mm^{-1} and μ_s'=1.0 mm^{-1}.

optical properties used were μ_a=0.01 mm^{-1} and μ_s'=1.0 mm^{-1}; the sources detector separation was 10 mm. The similarities between the two boundary conditions are evident. Although the curves are separable after the peak, their slopes appear identical. For early times the two boundary conditions predict the same reflectances. It should be noted that the data have been normalized at their respective peaks and that no mismatch in the indices of refraction was assumed. With a mismatch in refractive indices, the curves would not be so similar. The reflectance obtained from the Monte Carlo simulations appears to fall off at the same rate as the reflectance predicted by the

diffusion model. However, for early times there is a deviation between the Monte Carlo data and the theoretical reflectance, as expected.

In order to more clearly demonstrate the agreement between the two boundary conditions, under the assumption of no index of refraction mismatch, Figure 2.14 shows the theoretical reflectances calculated by both boundary conditions at two different ρ values. There are no visible differences between these curves at either distance, although, when fitting data, it was found that the optical coefficients returned depended on the model used. Typically the extrapolated boundary condition gave values for μ_a that were about 1% more accurate Although the EBC does not give significantly different results from the ZBC, it has been utilized for the rest of the modeling in this investigation. This is due to the fact that the extrapolated boundary is more physically plausible than the ZBC and that this formulation takes into account mismatches in indices of refraction, a point that will become important later. Furthermore, the accuracy gained by using the extrapolated boundary is not costly; it is no more difficult to model with the extrapolated boundary condition than it is with the zero boundary condition.

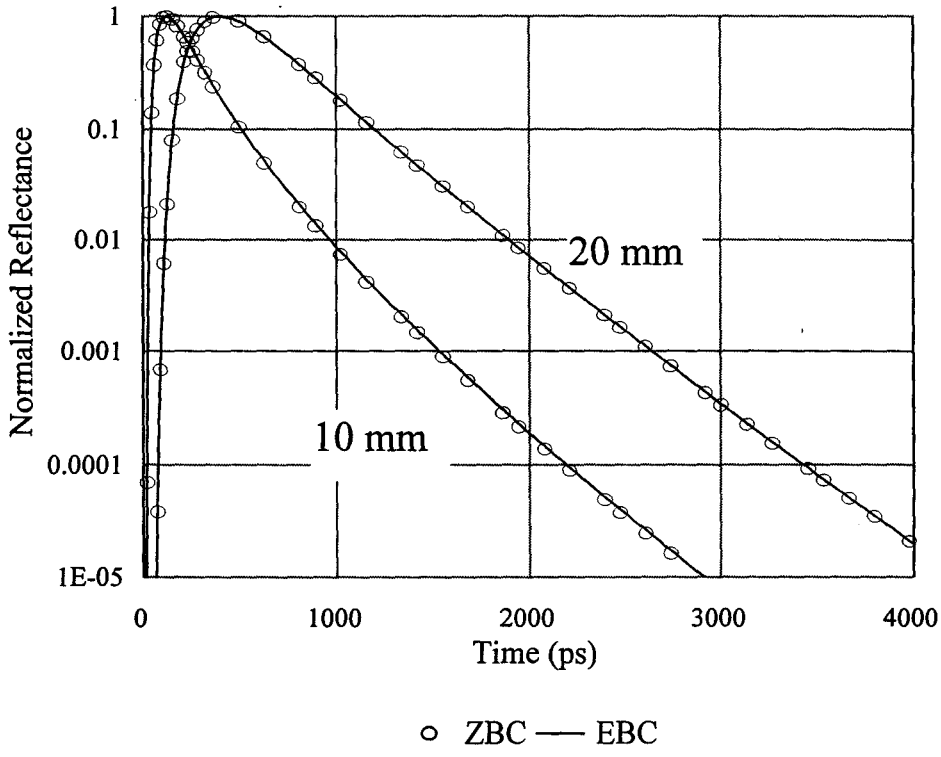

Figure 2.14: Comparison of EBC and ZBC for source detector separations of 10 mm and 20 mm. Optical properties were μ_a=0.01 mm^{-1} and μ_s'=1.0 mm^{-1}.

2.2.3 Fitting phase and amplitude in frequency space

The nonlinear least squares fit in the time domain is time consuming due to the convolution with an instrument response which must be performed with each iteration. An alternative is to perform the fitting of the data in the frequency domain. Although frequency domain measurements typically use a modulated source to measure demodulation and phase difference, it is possible to obtain the same information from a temporal reflectance pulse. The data are collected in the same manner as in the time-resolved measurements, but the resulting reflectance and/or instrument response are transformed. One method to analyze the data is to Fourier transform two reflectance pulses at different distances and determine how their relative modulation and their phase differences vary with increasing frequency. In this case, it is not necessary to measure an IRF. It is also feasible to use a reflectance measurement and an instrument response function and determine the modulation and phase differences relative to the IRF. The advantage of this approach is that the IRF is effectively eliminated from the measurement by simple division and no deconvolution is necessary. As well, the fit is performed over fewer points in the frequency domain than in the time domain, due to the limited frequency range over which the data is fit. These factors increase the speed with which data can be analyzed and may improve the results obtained.

Once the phase and modulation information has been extracted from the time-resolved data, it is simply a matter of fitting these two parameters in the frequency domain. As previously stated, the expressions for time-resolved reflectance $R(\rho,t)$ are linked to the frequency domain expressions $R(\rho,\omega)$ through the Fourier transform. The

quantities observed in the frequency domain are the phase angle θ between the source and the detected signal and the modulation (Kienle and Patterson 1997b):

$$\theta = \tan^{-1}\frac{\mathrm{Im}[R(\rho,\omega)]}{\mathrm{Re}[R(\rho,\omega)]} \tag{19}$$

$$\mathrm{MOD} = \sqrt{\frac{[\mathrm{Im}\,R(\rho,\omega)]^2 + [\mathrm{Re}\,R(\rho,\omega)]^2}{[R(\rho,\omega=0)]^2}} \tag{20}$$

where $\omega = 2\pi f$. The same boundary condition problems that exist in the time domain exist in the frequency domain. Haskell (Haskell *et al.*, 1994) found the zero boundary condition produced the largest errors of any of the boundary conditions and suggested a unification between the EBC and the PCBC. Kienle (Kienle and Patterson, 1997b) utilized the frequency domain analogue of equation (16) in which the reflectance is calculated as the integral of the radiance over the backward hemisphere to fit Monte Carlo generated reflectances with greater accuracy at small ρ values. The frequency domain expression is (Kienle and Patterson, 1997):

$$R(\rho,\omega) = \frac{m_1}{4\pi D}\left[\frac{\exp(-kr_1)}{r_1} - \frac{\exp(-kr_2)}{r_2}\right]\exp(i\omega t) + m_2 R_f(\rho,\omega) \tag{21}$$

where m_1, m_2, r_1, r_2, D are as previously defined, $i=\sqrt{-1}$ and

$$k = k_{real} + ik_{imag} = [(\mu_a c + i\omega)/Dc]^{1/2} \tag{22}$$

Also, the flux $R_f(\rho,\omega)$ is given by:

$$R_f(\rho,\omega) = \frac{1}{4\pi}\left[z_o(k+\frac{1}{r_1})\frac{\exp(-kr_1)}{r_1^2}+(z_o + 2z_b)(k + \frac{1}{r_2})\frac{\exp(-kr_2)}{r_2^2}\right]\exp(i\omega t) \quad (23)$$

The imaginary part of k can also be defined here as:

$$k_{imag} = \sqrt{\frac{3\mu_a\mu_s'}{2}}\left[\sqrt{1 + (\frac{\omega}{\mu_a c})^2}-1\right]^{1/2} \quad (24)$$

At this time, k_{real} should also be defined:

$$k_{real} = \sqrt{\frac{3\mu_a\mu_s'}{2}}\left[\sqrt{1 + (\frac{\omega}{\mu_a c})^2}+1\right]^{1/2} \quad (25)$$

It is this expression (21) for the frequency dependent reflectance that will be used in this investigation; it is the most accurate expression and is the exact analogue of the time domain expression employed in the previous section. In order to fit the observable quantities, the phase lag and the modulation, it is necessary to assume that the detector fiber is oriented normal to the boundary

Finally, the cumbersome expressions for the real and imaginary parts of the reflectance are given by the weighted contributions from the fluence rate (scaled by the constant m_1) and the flux (scaled by m_2).

$$REAL = m_1\left[exp\_r_1 - \cos(k_{imag}r_3)exp\_r_2\right] + m_2\left[\left(k_{real}+\frac{1}{r_1}\right)\frac{z_o^2}{r_1}exp\_r_1 + \left(k_{real}+\frac{1}{r_2}\right)\frac{(2z_b+z_o)z_o}{r_2}\cos(k_{imag}r_3)\right.$$

$$\left.\times exp\_r_2 + k_{imag}\frac{(2z_b+z_o)z_o}{r_2}\sin(k_{imag}r_3)exp\_r_2\right]$$

$$IMAG = m_1\sin(k_{imag}r_3)exp\_r_2 + m_2\left[k_{imag}\frac{z_o^2}{r_1}exp\_r_1 + k_{imag}\frac{(2z_b+z_o)z_o}{r_2}\cos(k_{imag}r_3)exp\_r_2 - \right.$$

$$\left.\left(k_{real}+\frac{1}{r_2}\right)\frac{(2z_b+z_o)z_o}{r_2}\sin(k_{imag}r_3)exp\_r_2\right] \qquad (26)$$

where $r_3 = r_2 - r_1$, $exp\_r_1 = \exp(-k_{real}r_1)/r_1$ and $exp\_r_2 = \exp(-k_{real}r_2)/r_2$.

From the experimentally measured phase and modulation, real and imaginary parts of the reflectance are calculated. Theoretical real and imaginary parts of the reflectance are calculated using equation (26) along with estimates for the optical properties of the sample. The sum of the squares of the residuals of the real and the imaginary parts of the reflectance is minimized by varying the μ_a and μ_s' values. It would also be possible to minimize phase and modulation differences, but to ensure proper weighting of the fitting, it is better to use the real and imaginary parts of the reflectance. Using the best estimates of the optical properties obtained from the minimization procedure, the corresponding phase and modulation are determined and plotted with the experimental results. Prior to fitting experimental data with this approach, it was necessary to test this method by fitting diffusion theory data with noise and Monte Carlo data under various conditions.

(A) *Fitting Diffusion Theory Data with Added Noise*

The simplest testing procedure for the frequency domain fitting method is to generate diffusion theory data and add Poisson noise as in section 2.2.1(A). In fact, the same data from that section were Fourier transformed and fit in frequency space using the procedure detailed above. The best estimates of the optical properties were obtained by minimizing the differences between the real and imaginary components of the generated data and the fitted data. Data were generated at three different source detector separations (10, 15, 20 mm) with about 4000 counts in the peak, which is typical of an experiment. The same optical properties which were used in the time domain fits were used in this investigation: μ_a=0.01 mm^{-1} and μ_s'=1.0 mm^{-1}. The data were analyzed at one distance, where a simple Fourier transform with no division was necessary and at two distances. In the two distance approach, the two reflectance pulses are Fourier transformed and the data at the larger ρ value is divided by that obtained at the smaller value. From this, the relative phase and modulation are calculated and the data are in the correct form to be fit using equations (19) and (20).

The results from the fitting the data in the frequency domain are shown in Table 2.4 below. In all cases, the errors observed are small, usually less than 2% in both the scattering coefficient and the absorption coefficient. Fitting at one or two distances does not affect the accuracy of the results obtained. Nor are the results significantly different from those obtained in the time domain (see Table 2.1). An example of a fit is shown in Figure 2.15; the source detector separation used was 15 mm. The data sets were fit to a maximum frequency of 7 GHz at which point the data become very noisy.

Distance (mm)	μ_a (mm^{-1})	μ_s' (mm^{-1})
20/10	0.01001	1.021
20/15	0.01009	1.016
15/10	0.01071	1.048
10	0.009873	0.9811
15	0.01009	1.001
20	0.009979	1.003

Table 2.4: Results of frequency domain fits of diffusion data with μ_a=0.01 mm^{-1} and μ_s'=1.0 mm^{-1}. Using one distance and relative distance approaches.

However, up to 5 GHz there is excellent agreement between the fitted line and the data for both phase and modulation. Results at 15 mm (Figure 2.15) show excellent agreement at lower frequencies and noise becomes evident at the higher frequencies. Actually, all fits performed show the same trends as those displayed here. The presence of low frequency oscillations in the phase and modulation at high frequencies (8 GHz) will be discussed later. The frequency domain approach is as accurate as the time domain fitting procedure but has the advantage of being considerably faster. Time domain fits typically take 10 to 20 minutes, but may take longer before accurate initial estimates for μ_a and μ_s' are available. Fitting in the frequency domain, in contrast, takes less than a few minutes.

a

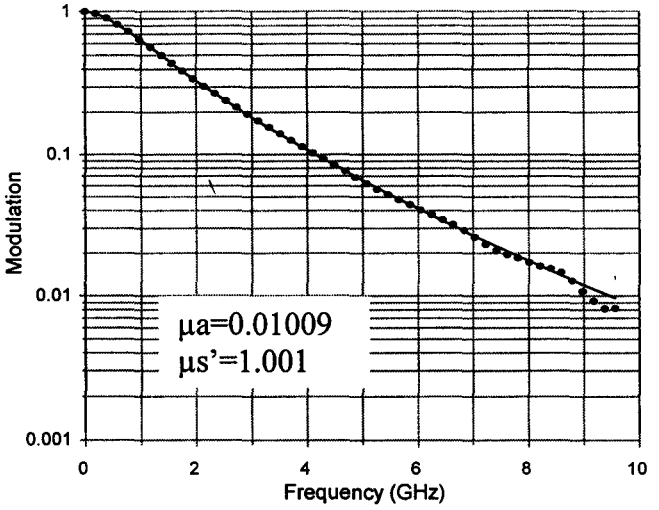

b

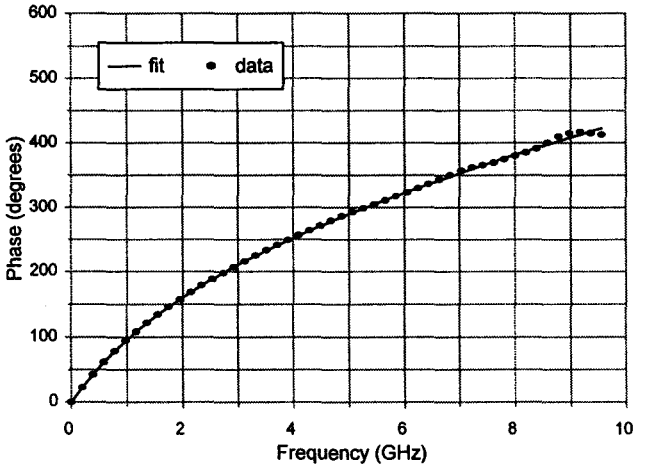

Figure 2.15: Fitting diffusion theory data in the frequency domain at 15 mm (a) modulation and (b) phase. Theoretical optical properties are μ_a = 0.01 mm^{-1} and μ_s' = 1.0 mm^{-1}.

(B) *Fitting Monte Carlo Data with Diffusion Theory*

Monte Carlo data were generated at three different source detector separations and Fourier transformed. The phase and modulation were computed as described above and the same diffusion theory fitting procedure applied to the data in section A was applied to the Monte Carlo data. Initially, the data were analyzed using the relative distance approach such that three combinations were possible. Another factor to be considered was the range of frequencies over which the data were fit. By eliminating high frequency components from the fitting range, it should be possible to improve the fits and the optical properties returned. This is analogous to fitting less of the rising edge in the time domain. The simulated data start to become noisy at about 7 GHz; this is the maximum frequency of the fitting range. A typical fit is shown in Figure 2.16 for 15 mm relative to 10 mm results; at low frequencies the phase and modulation are modeled very well, while at the end of the fitting range the some noise in the data is evident. It appears that the same low frequency oscillations observed in Figure 2.15 are also seen in this plot, although they are not as obvious. The error in the absorption coefficient was about 25%, while the scattering error was about 7%. For the 20 mm relative to 15 mm results, the errors were 8% in either coefficient. The errors were comparable for the 20 mm relative to 10 mm results; the error in μ_a was 9% and the error in μ_s' was 5%.

In order to improve the results obtained, the fitting range was varied. The maximum frequency was varied from 500 MHz to 7.3 GHz and the optical properties returned were recorded. Figure 2.17 (b) shows the variation in the scattering coefficient versus the maximum frequency fit for the three combinations of distances available. The

results obtained were somewhat dependent on the range of the fit. There was some variation in the scattering coefficient returned, it decreased towards the theoretical value as high frequency information was removed. The estimated absorption coefficient, shown in Figure 2.17(a) also improved as only lower frequencies were included in the fit. This trend was more obvious in μ_a than it was in μ_s'. Also, the largest improvements were seen in the 15 relative to 10 mm results. This is probably not surprising since the influence of the rising edge, (high frequency) component of the data is most evident at small source detector separations. As expected, the optical coefficients returned can be affected by the amount of high frequency information available in the data.

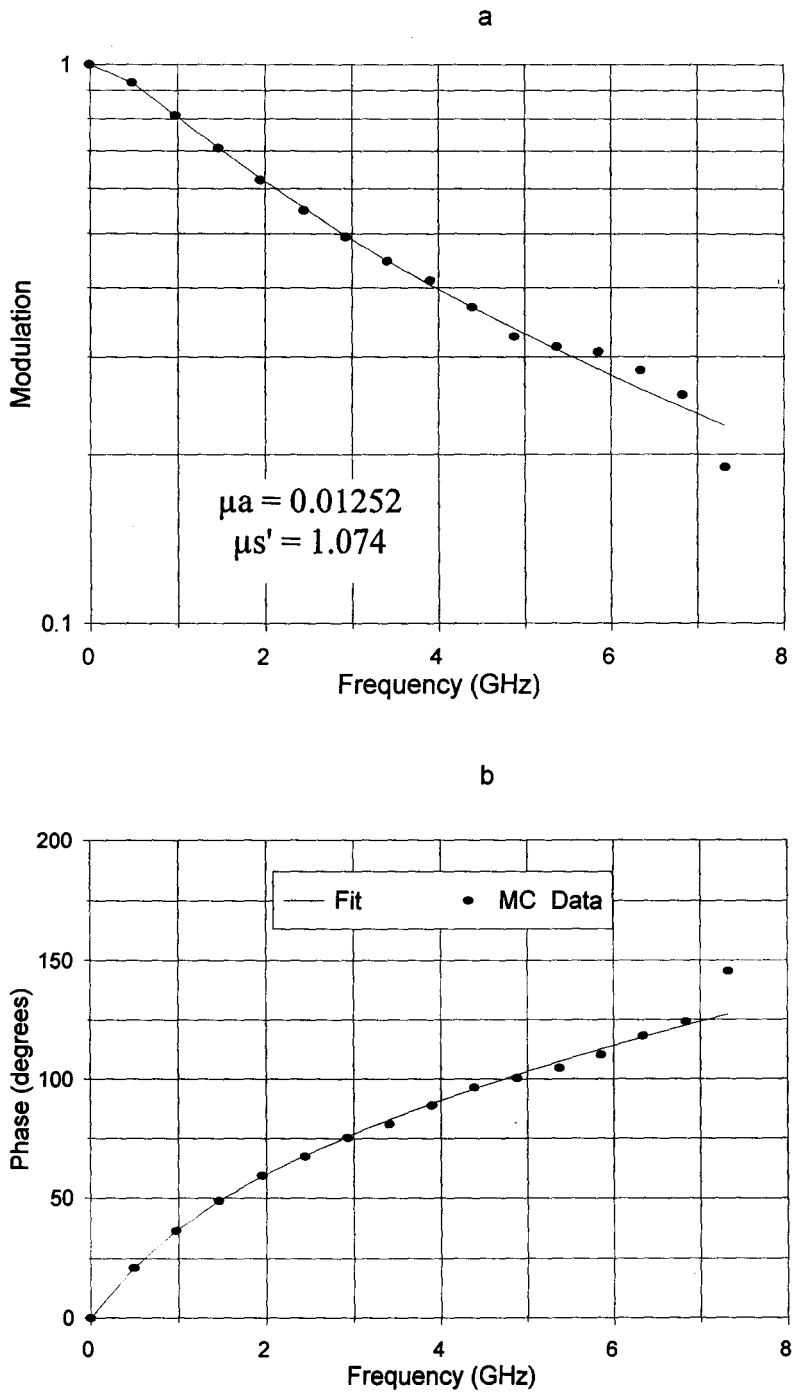

Figure 2.16: Fit for phase (a) and modulation (b) Monte Carlo data for 15 mm relative to 10mm results. Theoretical optical properties are $\mu_a = 0.01$ mm^{-1} and $\mu_s' = 1.0$ mm^{-1}.

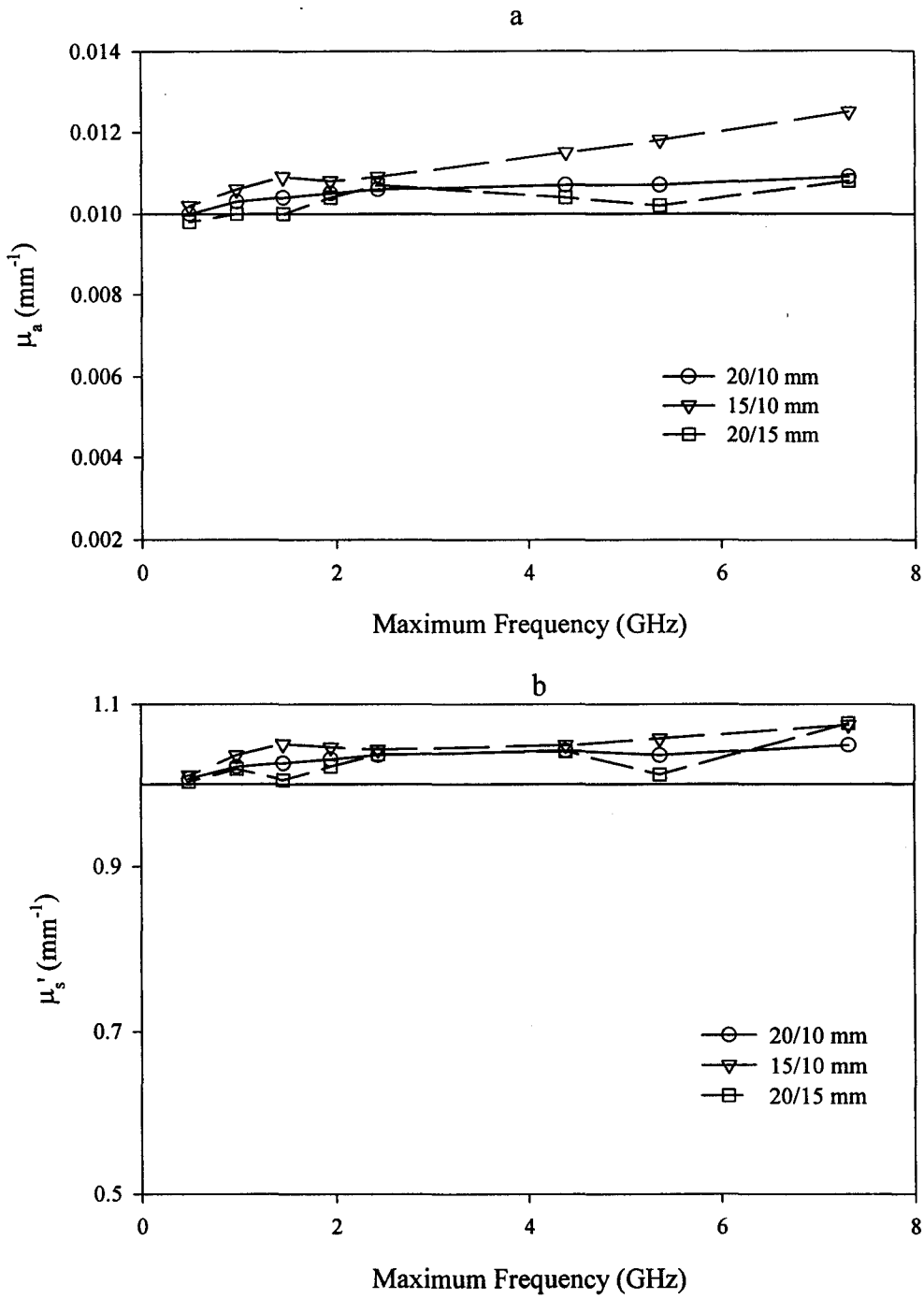

Figure 2.17: Variation of optical properties, (a) μ_a and (b) μ_s', with maximum frequency fit for Monte Carlo data 2 using relative distance approach.

The data were also analyzed using the one distance approach. For fitting up to 4 GHz, the results depended on the ρ value. The largest errors were observed at 10 mm, the scattering was overestimated by 13% and the absorption was overestimated by about 13%, as well. At 20 mm, the optical coefficients were both overestimated, the scattering by about 3% and the absorption by 7%. The results for the data collected at 10 mm are shown in Figure 2.18. The phase appears to be in excellent agreement with the theory for all but the highest frequencies, while the modulation is fit with much less success, showing the low frequency oscillations that were observed previously and some deviation at high frequency. In general, the phase is the easier parameter to fit as it is related to the first moment of the distribution, while the modulation depends on the second moment and is harder to model with accuracy. Although these low frequency oscillations have little effect on the results, it was necessary to investigate the source of this phenomenon. Since these oscillations were present in both the Monte Carlo data and the diffusion data with added noise, it seemed likely that they were related to the noise in the data. The oscillations were present at the same frequency regardless of the length of the array sent to the Fourier transform routine or the step size of the data set. However, when diffusion data were fit without noise, there were no oscillations observed. By sending only the noise record through the Fourier transform routine it was determined that the noise manifested itself in the form of low frequency oscillations.

Once more, the maximum frequency to which the data sets were fit was varied. The results for absorption and scattering are summarized in Figures 2.19 (a) and (b) respectively for both distances. This graphs appear similar to Figures 2.17 (a) and (b).

Both optical properties are overestimated at either distance and it is again possible to improve the results by fitting only the lower frequencies. At 10 mm, both values were initially overestimated but could be decreased to be closer to their true values by decreasing the maximum fitting frequency. This was also observed at 20 mm, although the improvements are less significant. As seen previously, removal of the high frequency components of the data leads to improved accuracy in the estimates of the optical properties obtained.

Fitting Monte Carlo data in the frequency domain leads to results that are variable, depending on the fitting range. Although the accuracy observed was only improved by a few percent from the time domain fits, the speed of the fitting procedure was increased. The accuracy improvements are only observed if the correct fitting range is utilized. The other advantage of this method, the removal of the IRF convolution, is investigated in the next section.

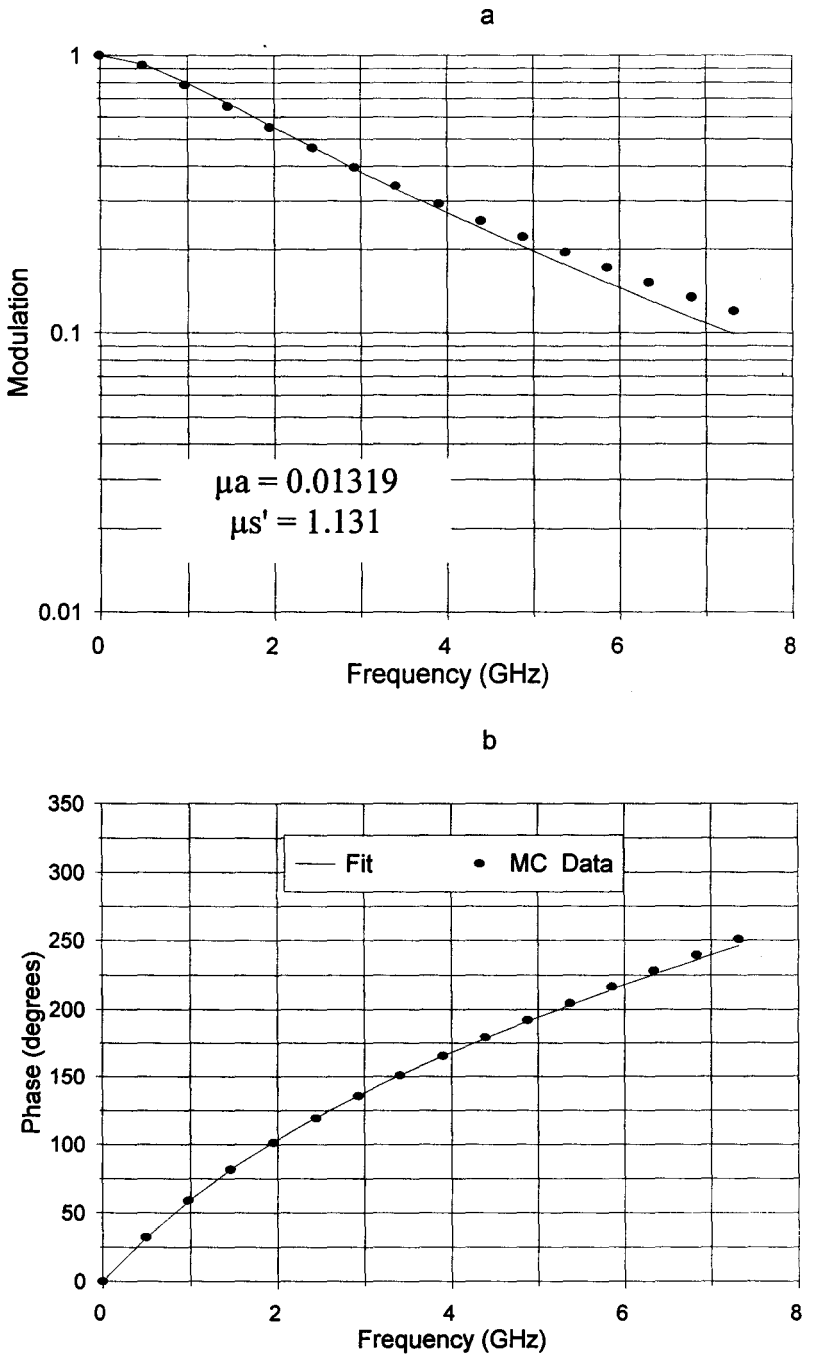

Figure 2.18: Frequency domain fit of (a) modulation and (b) phase for MC data 10 mm. Theoretical optical properties are $\mu_a = 0.01$ mm^{-1} and $\mu_s' = 1.0$ mm^{-1}.

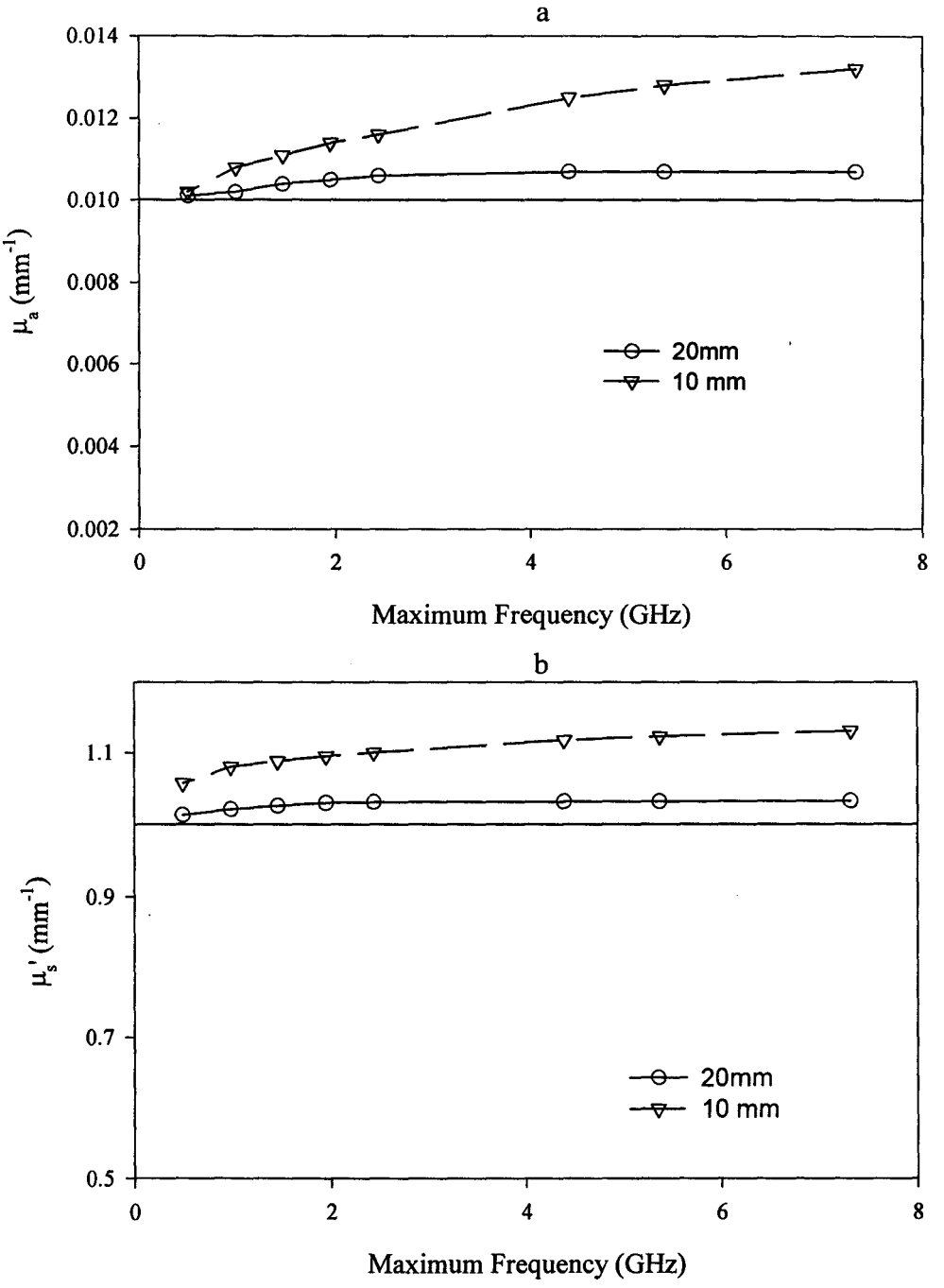

Figure 2.19: Variation of optical properties with maximum frequency fit for Monte Carlo data at a single distance (a) μ_a and (b) μ_s'. Theoretical optical properties are μ_a = 0.01 mm^{-1} and μ_s' = 1.0 mm^{-1}.

(C) *Fitting Monte Carlo Data Convolved with an IRF with Diffusion Theory*

The final stage in the investigation into the feasibility of fitting the time-resolved data in the frequency domain is fitting Monte Carlo data convolved with an experimental IRF. The previously generated pulses, which consisted of an instrument response convolved with Monte Carlo data, were Fourier transformed and fit with diffusion theory using the real and imaginary parts of the reflectance. The data were analyzed by dividing the reflectance by the IRF in the frequency domain. The two distance approach was not used in this instance as it gave the same results as Monte Carlo data alone due to the fact that the instrument responses cancel out in the numerator and denominator.

$$\frac{R(20,\omega)\times FT(IRF)}{R(10,\omega)\times FT(IRF)} = \frac{R(20,\omega)}{R(10,\omega)}$$

where $R(\rho,\omega)$ is the reflectance in frequency space and FT(IRF) is the Fourier transform of the instrument response function. The variation of the optical properties with the maximum frequency fit was also determined, as in previous sections.

An example of a fit at 20 mm is shown in Figure 2.20. The data appear to show some noise above about 4GHz. Both optical properties are overestimated, the scattering by 6% and the absorption by 9%. In general, there is good agreement between the fit and the data for both phase and modulation over the entire fitting range. Results are very similar to results obtained with the same data without convolution with an IRF (see section B).

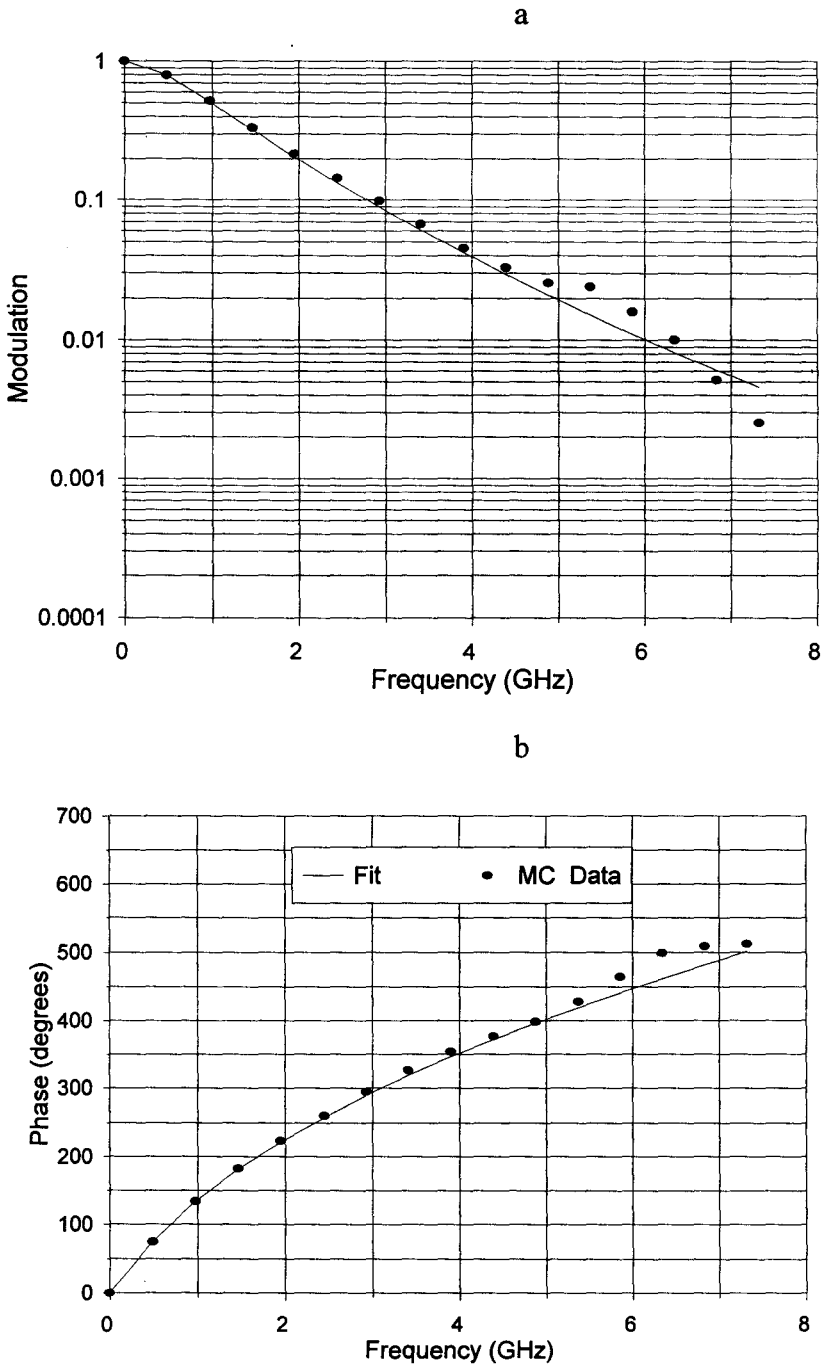

Figure 2.20: Fit to (a) modulation and (b) phase for Monte Carlo data convolved with an IRF at 20 mm. Theoretical optical properties are $\mu_a = 0.01$ mm^{-1} and $\mu_s' = 1.0$ mm^{-1}.

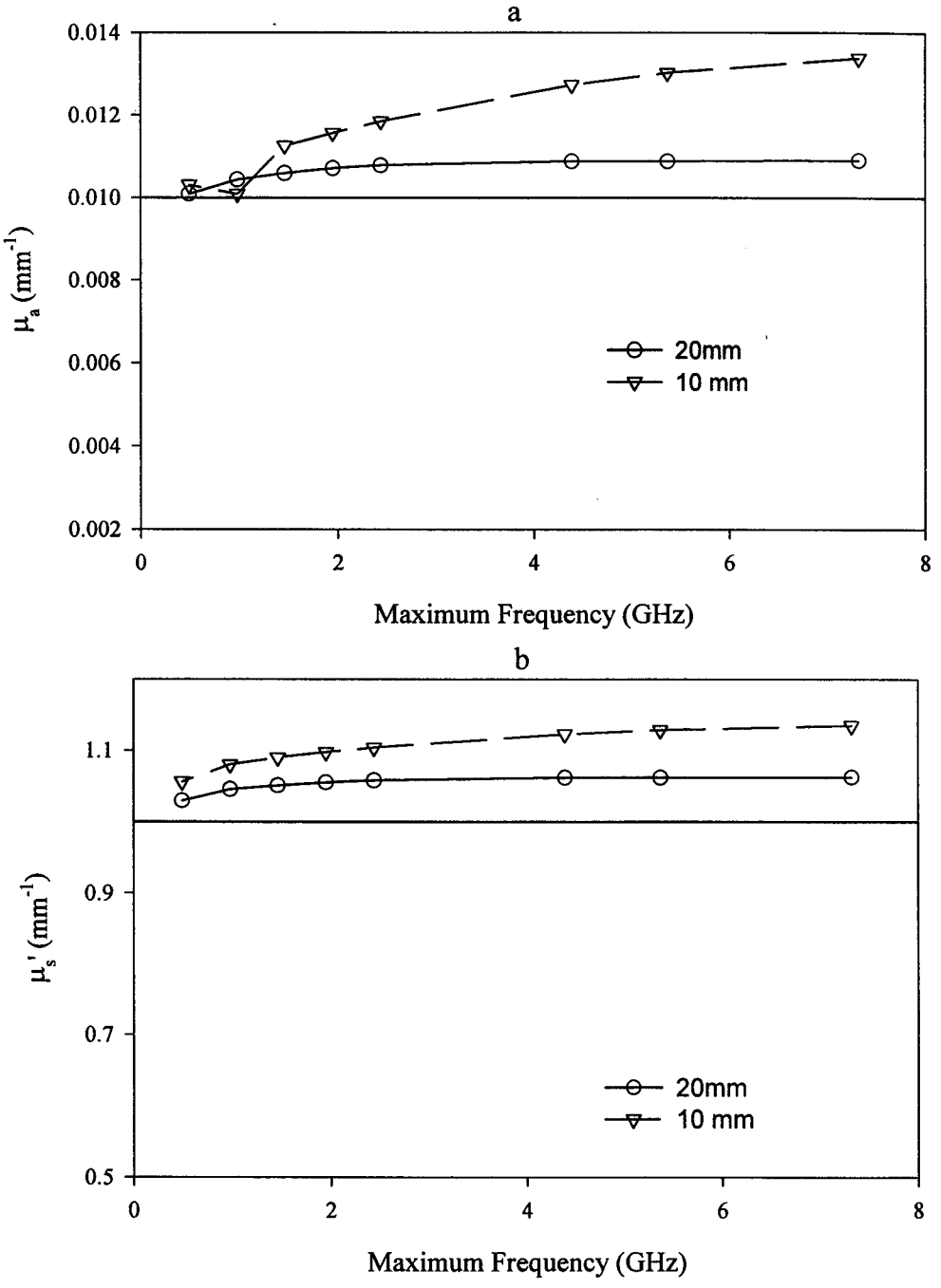

Figure 2.21: Variation of optical properties with maximum frequency fit Monte Carlo data convolved with an IRF (a) μ_a and (b) μ_s'. Theoretical optical properties are $\mu_a = 0.01$ mm^{-1} and $\mu_s' = 1.0$ mm^{-1}.

The same trends seen in Figure 2.19 are observed in Figure 2.21 which shows the variation in the absorption and scattering coefficients with the maximum frequency to which the data were fit. Figure 2.21 (a) shows variation in the absorption coefficient. The absorption coefficient was overestimated at both distances, especially at 10 mm. Results could be improved by limiting the high frequency components of the data as previously observed. This is more evident at 10 mm than at 20 mm, again as expected. Figure 2.21 (b) displays the variation in μ_s' with the maximum frequency fit. The trends in $\mu s'$ were similar to those seen in μ_a, poorer results at 10 mm and improvements when only lower frequencies were fit.

In general, the results obtained for the scattering and absorption coefficients in the frequency domain when fitting Monte Carlo data that has been convolved with an instrument response are slightly better for both ρ values in comparison to the time domain fits (see section 2.2.1 (D)) if only low frequency components are fit. As seen in the time domain, the range over which the data is fit has an effect on the values obtained for the optical properties. By choosing the best fitting range, it is possible to obtain very accurate results using this method; errors of less than 5% in either coefficient are possible at 20 mm, while errors of less than 10% are possible at 10 mm. In addition, this method is less time consuming than the time domain approach. Although for Monte Carlo data alone, the frequency domain method of analysis showed little difference from the time domain technique, the presence of an IRF convolved with the reflectance alters this, making the frequency domain method superior. However, experimental data does not always behave exactly like simulated data and therefore, experimental results were

usually analyzed using both methods, over various fitting ranges to ensure the best possible method of analysis was employed. It is also essential to note that regardless of the conditions, there is not perfect agreement between the Monte Carlo data and diffusion theory, errors from 5-15% are observed. Hence, errors of similar magnitude should be expected when fitting experimental data with the diffusion theory model.

These investigations have shown that the computer routine itself produces only small inaccuracies when fitting diffusion theory data with or without noise. When fitting Monte Carlo generated reflectance data with the diffusion model, errors in the optical properties of up to 15% are possible, depending on the source detector separation and the range of data fit. For early times and small ρ values, the discrepancies between diffusion theory and Monte Carlo data are the largest. In addition, the extrapolated boundary condition provides an accurate description of the effect of boundaries on the reflectance, with a minimum of computer time invested. It is also evident that the fitting in the frequency domain should be performed out to a maximum of two or three MHz depending on the noise present in the data. Finally, fitting in the frequency domain is faster than performing the time domain fits, due to the simplification of the convolution procedure, and seems to improve the accuracy of the results under certain conditions. This provides incentive to investigate if improvements in fitting experimental data are possible by employing the frequency domain approach.

3 RESULTS

After identification of the limitations of the diffusion model, it was necessary to optimize the instrument response function. It is essential that this profile be made as narrow as possible to limit its effect on the measurement. The IRF is extremely sensitive to a variety of factors and it was important to determine systematically the conditions which minimized the FWHM of the IRF. Once this was accomplished, the next step was to determine the accuracy of the system in measuring optical properties of tissue simulating phantoms. The performance of the single wavelength system was investigated by measuring various types of phantoms under a range of conditions. In addition, different methods of data analysis were tested by varying the fitting techniques used. Once the system was characterized, measurements on tissue simulating phantoms were performed simultaneously at two wavelengths. The final experiments were two wavelength measurements performed *in vivo* on the hand using a blood pressure cuff to alter the oxygenation of the tissue.

3.1 System Characterization

Since the PMT used in these studies does not have the temporal resolution of more expensive MCP-PMTs, it was essential that the electronics were adjusted to minimize the FWHM of the IRF. Firstly, the PMT high voltage bias control was adjusted

to ensure that single photon counting levels were obtained. As a general rule, this is done by limiting the CFD count rate to be 10% of the exciting laser pulse repetition frequency, in practice, an even lower rate is used. The most stable laser pulse was obtained with the laser operated at 10 MHz in the lock mode. The three adjustments on the CFD which could be varied to alter the FWHM of the IRF were the threshold, pulse width and zero crossing monitor. These factors proved to have the largest effect on the temporal resolution of the system. The first IRFs collected had widths of about 500 ps, while after optimization the width was approximately 250 ps. It was also found that careful alignment of the fibres at the junction of the source and the collection fibers was important in maintaining a narrow width.

A typical IRF measured on the system is shown in Figure 3.1a, while Figure 3.1b displays the IRF as published by the manufacturer for this type of PMT. Both PMTs were operated at 800 V although the sources were different. The light source used in Figure 3.1a was an 810 nm pulsed diode laser with a pulse width of about 50 ps. The Hamamatsu results were obtained using a 410 nm source with a width of 30 ps. Although the IRFs have similar widths (250 ps versus 275 ps) and the same general shape, distinct differences are evident. The rising edge of the pulse measured by our system is much cleaner than that measured by the manufacturer. The Hamamatsu result appears to have a secondary peak similar to the one observed in Figure 3.1a, but it is much less obvious and occurs at a different time. It was not possible to remove this feature from the pulse and it is not clear what caused it. Fortunately, this peak appears in

a

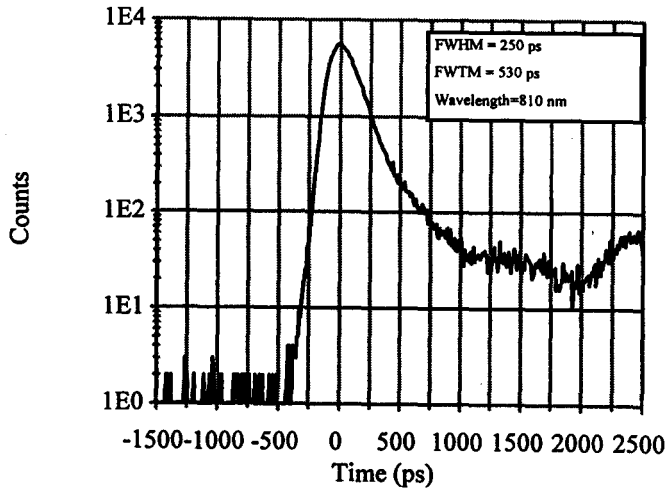

b

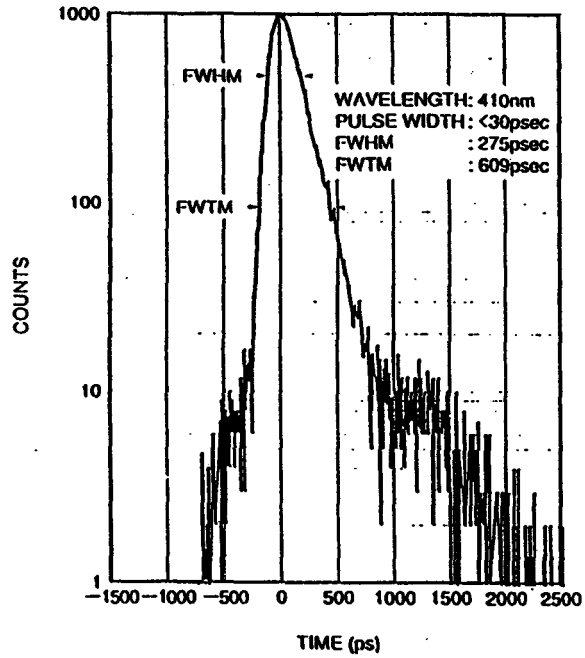

Figure 3.1: Instrument response function of R5600U PMT (a) as measured with pulsed diode laser in our lab and (b) as measured by Hamamatsu Photonics K.K.

a portion of the pulse that is not usually included in the fitting range and hence it is assumed that this feature does not affect the results.

Another concern that existed with respect to the performance of the system was the temporal stability of the IRF. Although the reference pulse allowed for the correction of time drifts during an experiment, it was still essential to maximize the stability of the system. Drifts that occur during an experiment could have a profound effect on the shape of the reflectance pulse collected. The optical trigger described in the Experimental section was used because the electronic trigger provided by the laser driver caused results to be less stable. Following optimization of the electronics, ten IRFs were collected, with collection times of 60 seconds and the values of the centroid and FWHM of each pulse were recorded. It was found that the standard deviation in the centroid was 0.2 channels or about 2 ps, while the FWHM had a standard deviation of 0.4 channels or about 3.5 ps. Although these variations and the effects of drifts during an experiment were insignificant, the stability of the system when performing measurements of optical properties of phantoms was also investigated. The results from these studies are discussed in section 3.3.

3.2 Preliminary Phantom Measurements using Intralipid

The initial experiments performed that are described in this section used dilute solutions of Intralipid as a scatterer. Intralipid is assumed to have the same index of refraction as water at 810 nm, 1.33 and the same absorption coefficient, 0.002 mm^{-1} (Hale

and Querry 1973). The use of Intralipid as a tissue-simulating phantom is common and many characterization studies have been performed (van Staveren *et al.* 1991). An empirical formula which is used to estimate the relationship between the scattering coefficient and the Intralipid concentration is: 1% Intralipid results in a scattering coefficient of 1 mm^{-1} at 800 nm (Pogue 1996). This was used to provide an estimate of the scattering coefficient in these investigations. It must be noted that the Intralipid stock solution is quoted as ten or twenty percent, yet since it is not produced for research purposes, it is unlikely that these values are precise. There could exist variations between different batches of solutions and hence some uncertainty in the final Intralipid concentration is expected. It was also assumed that there was no mismatch in the indices of refraction between the black plastic probe and the liquid. Finally, all the experiments performed in this chapter used the 810 nm diode laser unless otherwise specified. The wavelength of the laser used should not have any effect on the results, outside of those factors that are known to be wavelength dependent, for example the optical properties and the refractive index of the medium.

3.2.1 Characterization

Initial experiments did not produce results which were accurate, but these investigations were necessary and useful in characterizing the system and determining the performance of the fitting routines under realistic situations. Typically, results produced reasonable estimates of the absorption coefficient but overestimated the scattering coefficient by as much as 50 %. Although no specific results will be presented here, the relevance of these experiments to later work will be discussed. From an experimental

point of view, these investigations were useful in providing estimates for collection times that were necessary to obtain adequate counts. They also indicated the need for limiting the light incident on the PMT with filters of varying optical densities. With respect to the fitting program, the primary investigations revealed many factors which could affect the quality and the accuracy of the fits obtained. It was evident that a reference pulse was necessary to account for temporal drifts between the instrument response function and the experimental pulse. This was ascertained by observing that time shifts applied during the fitting procedure were found to have a dramatic effect on the results obtained, especially the scattering coefficient estimated. Shifts as small as 8 ps between the IRF and the reflectance pulse could alter the estimated scattering coefficient by as much as 15%. It should also be noted that the fitting program used in these early experiments used the zero boundary condition and fitting was performed in the time domain only. It was, however, the difficulty in obtaining accurate optical properties in these initial trials that prompted an investigation into applying different boundary conditions and alternate fitting approaches. The fitting was performed over two logs on the falling side of the peak and down one log on the rising edge of the pulse. It was found that varying the start time of the fitting range did not produce the dramatic changes in the optical properties seen with the Monte Carlo data. The explanation for this is probably the same as for the Monte Carlo data which was convolved with an experimental IRF (section 2.2.1 (D)).

3.2.2 Intralipid Dilutions

Although the time domain system had little success in obtaining values which were in agreement with the expected values for the optical properties of Intrapilid, the

ability of the system to detect relative changes was investigated. An Intralipid phantom with a concentration of 1% was prepared. No absorber was added to the solution, therefore the expected values for the optical properties were μ_a=0.002 mm^{-1} and μ_s'=1 mm^{-1} at 810 nm. This phantom was then measured on the time domain system at source-detector separations of 10 and 20 mm and on a continuous wave system. The continuous wave apparatus is similar to that described in the Introduction and this specific system has been described elsewhere (Bruulsema *et al.* 1997). The phantom was then diluted with water by a factor of 2/3 such that the new scattering coefficient was expected to be 0.67 mm^{-1}. Results from this experiment are shown in Table 3.1 below.

Method	**μ_a (mm^{-1})**	**μ_s' (mm^{-1})**	**ratio of μ_s'**
Initial Phantom	0.0020	1.0	NA
Spatial (cw)	0.0015	0.80	NA
Time (ρ=10 mm)	0.0044	1.72	NA
Time (ρ=20 mm)	0.0034	1.26	NA
Final Phantom	0.0020	0.67	0.67
Spatial (cw)	0.0007	0.61	0.76
Time (ρ=10 mm)	0.0048	1.09	0.64
Time (ρ=20 mm)	0.0037	0.95	0.75

Table 3.1: Variation of estimated scattering and absorption coefficients with Intralipid concentration, from different measurement methods and different ρ values.

Neither system was able to provide accurate estimates for either optical property, but both methods did detect the change in the scattering coefficient. The spatially-resolved technique underestimated the scattering and the absorption in both cases with errors ranging from 4 to 65%. In contrast, the time domain method systematically overestimated the optical properties. Errors in the absorption coefficient were as large as 140% while the scattering errors ranged up to 72%. It can also be seen that the time-resolved measurements performed at 20 mm produced more accurate values for both optical coefficients. In addition, the reduced χ^2 values for the 20 mm fits were approximately 1.7, while the 10 mm fits produced χ^2 values around 4. The results obtained from the 10 mm data, although they were the least accurate, did show the best agreement in terms of the relative change in the scattering coefficient. Regardless of the lack of accuracy in the results obtained in this experiment, the ability of the different systems to reflect relative changes in the scattering coefficient was illustrated.

3.2.3 Increasing Concentration of Melanin Ink

In order to investigate the response of the system to variations in absorption, increasing concentrations of Melanin Ink were added to an Intralipid phantom. The phantom was prepared to have a scattering coefficient of 1 mm^{-1} and an initial absorption coefficient of 0.002 mm^{-1}, as above. Once more, the phantom was measured using the spatially-resolved system and in the time domain system at two distances. The ink concentration was then increased by steps of 0.01% up to 0.05% at which point the signal was limited by too much absorption. The scattering should have remained constant and the absorption should have increased linearly with concentration. No attempts were

made to quantify the relationship between ink concentration and absorption coefficient; it is assumed that the relationship is linear and hence only relative absorption changes were examined. Figure 3.2a shows the variation of the measured scattering coefficient with increasing ink concentration and Figure 3.2b shows the variation of absorption with ink concentration.

The continuous wave technique and the time-resolved data collected at 20 mm appeared to have produced similar estimates of μ_a. The results for the scattering coefficient, averaged over all six ink concentrations, for the time domain data at 10 mm were 1.29 ± 0.10 mm^{-1} and for 20 mm, 1.16 ± 0.06 mm^{-1} compared to an expected value of 1.0 mm^{-1}. These differences are evident in Figure 3.2a. A typical fit is shown in Figure 3.3 which displays the experimental data, the fit and the residuals for the measurement performed at 20 mm on the phantom with an ink concentration of 0.02%.

There is good agreement between the fit and the experimental data over most of the fitting range. The residuals, however, show a systematic variation similar to that observed in the Monte Carlo data fits seen previously. Since there are no theoretical values for the absorption coefficient, this cannot be compared. However, to further compare the three sets of results, linear regression of absorption coefficient versus ink concentration, can be performed. The slope of the best fit line for the 10 mm data is 0.63 $\pm$ 0.04 mm^{-1}/% and the R^2 value is 0.981. The 20 mm and the spatial data have slopes of 1.05 ± 0.06 mm^{-1}/% and 1.13 ± 0.09 mm^{-1}/% respectively and R^2 values of 0.989 and 0.976. The similarity between the spatially-resolved data and the time-resolved results is evident. The deviations in the scattering coefficients for the time domain results are

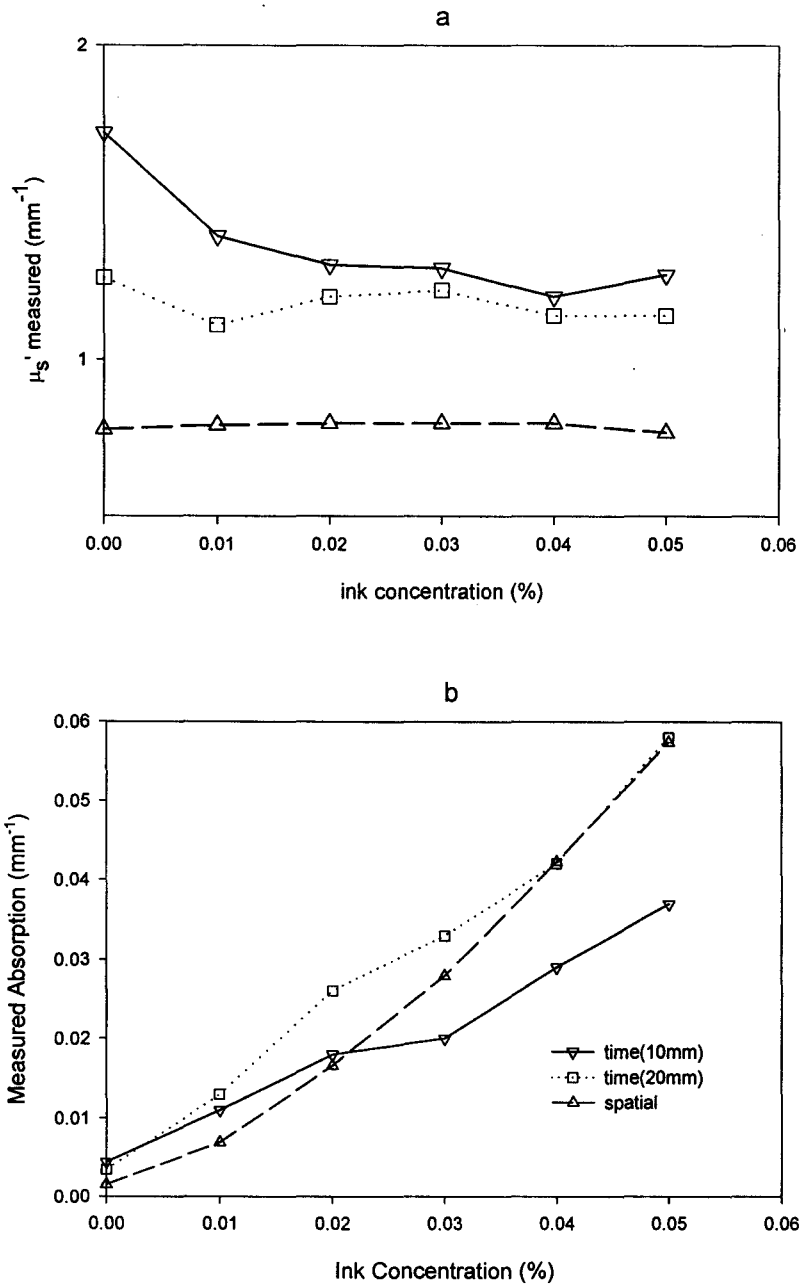

Figure 3.2: Variation of measured scattering coefficient (a) and absorption coefficient (b) with concentration of Melanin ink in 1% Intralipid for three different measurements methods.

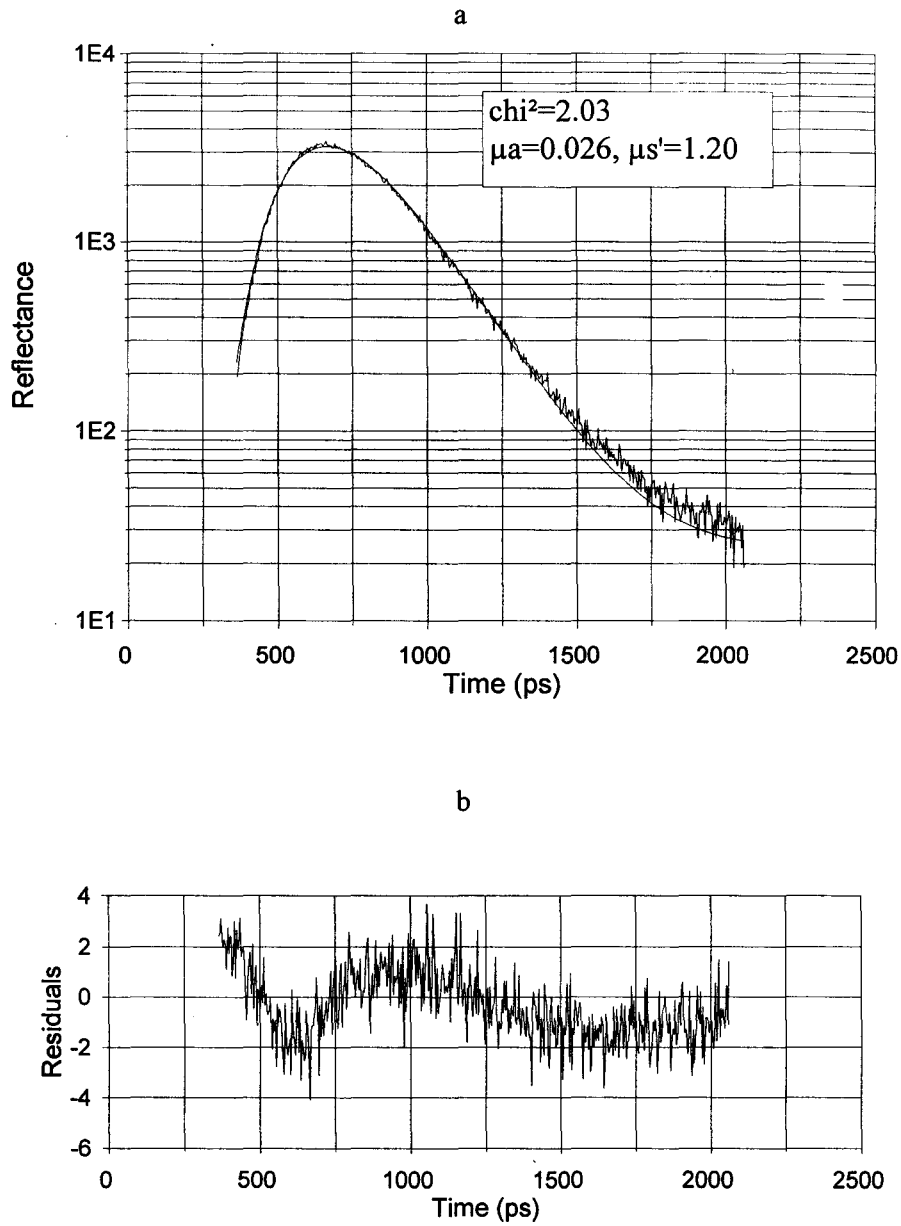

Figure 3.3: Fit (a) and residuals (b) for Intralipid with 0.02% ink. The source-detector separation was 20 mm.

similar to those observed in the previous experiment, i.e. overestimates at both distances with 10 mm results being less accurate. However, the addition of an absorber has increased the accuracy with which the scattering coefficient can be estimated. For the results at 20 mm the errors have decreased from 26% to about 16%, while the change was more dramatic at 10 mm where the error dropped from 72% to 29%. The addition of ink not only verified the ability of the systems to detect relative changes in absorption but also increased their ability to predict the scattering coefficient accurately.

3.3 Phantom Measurements using Solid Phantoms

Since liquid phantoms have potential for settling resulting in temporal variation in optical properties, solid phantoms are useful in studies which require repeated measurements. The experiments performed in this section used solid phantoms made from an epoxy resin with dye added as an absorber. The theoretical optical properties of these phantoms are not known, but the index of refraction has been measured to be about 1.6 for these phantoms. Measurements were performed with the time domain apparatus on three different phantoms, referred to as Marley 8, Marley 8d and Marley 3A. The phantoms were designed to have similar absorptive properties, but Marley 8 has the highest scattering coefficient and Marley 3A the lowest. In this section, there are no theoretical values available for the optical properties of the phantoms, although comparisons are made with measurements performed on other systems. This is not

essential, as the primary objective here is to determine the effect of various factors on the optical properties returned by the time domain fitting program.

3.3.1 Short Term Stability

This section refers to a series of 10 measurements performed on the phantom known as Marley 8. The data were collected for 105 seconds and 2 000 counts were obtained in the peak channel. Results were then fit in the time domain using the simplest diffusion model, i.e. the zero boundary condition. Since the black plastic probe has a similar index of refraction to the solid phantom and since optical coupling gel was used to minimize any mismatches, it was assumed that the boundary was matched. For all experiments the source-detector separation was equal to 10 mm. Results shown in Table 3.2 are averages and standard deviations. A typical example of a fit and its residuals is shown in Figure 3.4 for one of the reflectance measurements.

Series (N=10)	**Peak Counts ($\times 10^3$)**	**Collection Time (s)**	**Mean χ^2**	**Mean μ_a (mm^{-1})**	**Mean μ_s' (mm^{-1})**
Marley 8	2	105	2.0	0.0189 (0.0002)	2.14 (0.03)

Table 3.2: Summary of 10 measurements on Marley 8. Standard deviations are shown in parentheses.

The variations observed here indicate the short term stability of the system and reproducibility, i.e. the variation in the optical properties returned if the same phantom is measured numerous times. The results show little variation between the ten separate measurements. The standard deviations for both optical properties were small and the fits were quite good as indicated by the low χ^2.

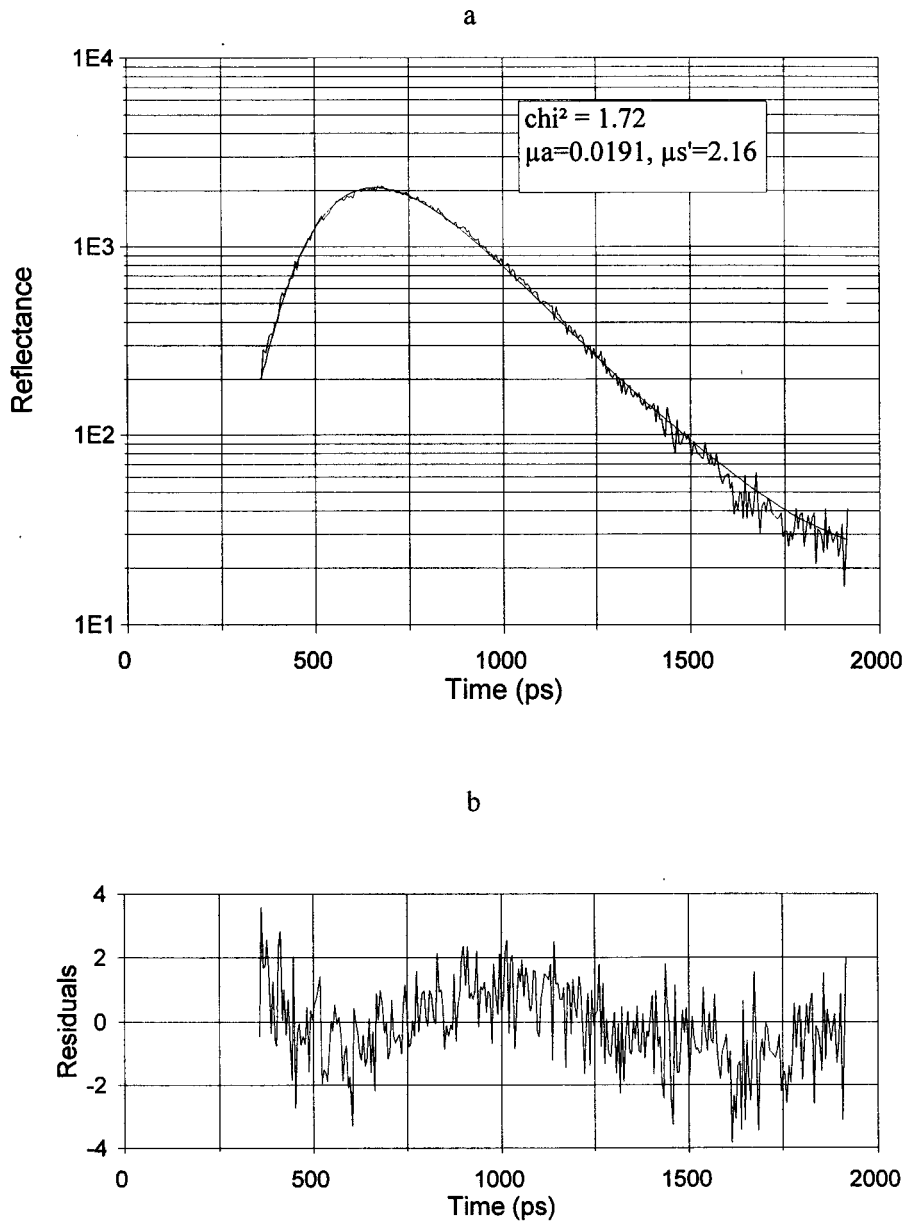

Figure 3.4: Fit (a) and residuals (b) for Marley 8 phantom measurement. Collection time was 105 s and ρ = 10 mm.

3.3.2 Effect of Statistics on Optical Properties

In order to determine the effect of statistics on the optical properties estimated, the Marley 8d phantom was measured using six different collection times. The longest collection time was two minutes and the shortest time was 2 seconds; these corresponded to four thousand counts and eighty counts, respectively, in the peak channel of the reflectance spectrum. As in the previous section, coupling gel was used, the boundary was assumed to be matched and the source detector separation used was 10 mm. Five measurements were performed at each count time. The results were analyzed in the time domain and summarized as averages and standard deviations in Table 3.3. The same information is shown graphically in Figure 3.5; Figure 3.5a shows the absorption and (b) shows the scattering variation.

Peak Counts	**Count Time (seconds)**	**Mean μ_a and standard deviation**	**Mean μ_s' and standard deviation**
80	2	0.0188 (0.0014)	1.77 (0.07)
25	6	0.0172 (0.0006)	1.69 (0.03)
500	15	0.0172 (0.0004)	1.68 (0.03)
1000	30	0.0166 (0.0003)	1.67 (0.02)
2000	60	0.0168 (0.0005)	1.69 (0.06)
4000	120	0.0169 (0.0003)	1.71 (0.04)

Table 3.3: Variation of μ_a and standard deviation in μ_a and μ_s' and standard deviation in μ_s' with collection time and number of counts in peak channel.

a

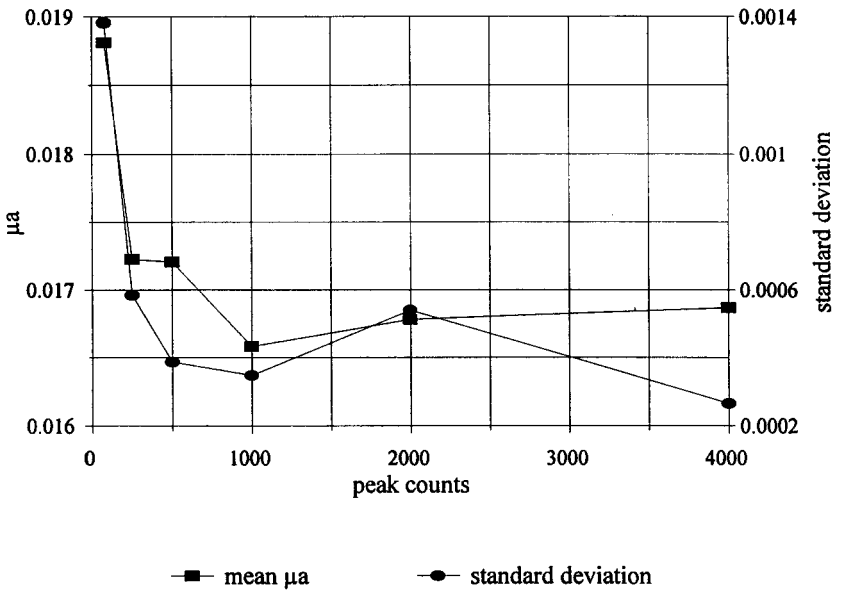

b

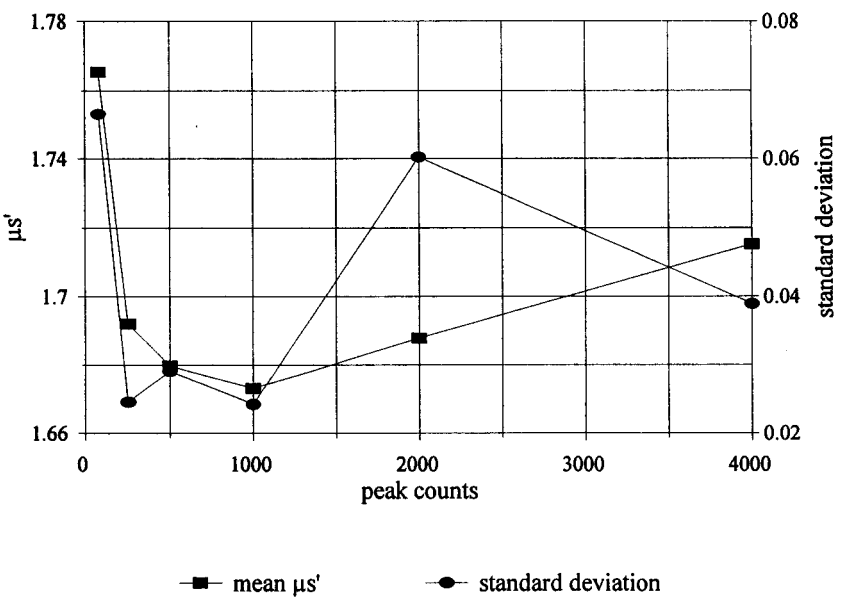

Figure 3.5: Variation of (a) μ_a and standard deviation in μ_a and (b) μ_s' and standard deviation in μ_s' with number of counts in peak. Units are mm^{-1} for both coefficients.

For short collection times and poorer statistics, less than about 500 peak counts, the value and the standard deviation for both optical properties increased dramatically. There did not appear to be an advantage to longer collection times. The standard deviations for the 15 and 30 second measurements were similar to those for the two minute measurements. It would appear that the data collected for 60 seconds showed variations which were larger than expected. However, unlike the results from short collection times, the values of optical properties returned are similar to all other measurements. These results would indicate that counting statistics are not the limiting source of uncertainty when more than 500 counts are obtained in the peak channel and that longer data acquisition times are not worthwhile.

Two other experiments were performed using the same phantom to determine other possible sources of error. The first experiment investigated if coupling to the phantom was an error source. The phantom was measured five consecutive times, with a collection time of thirty seconds. Between each measurement, the probe was lifted off the phantom and placed back on the phantom in the same location. The standard deviations for these five measurements were larger than that observed in the control experiment above where the probe remained on the phantom. The standard deviations for absorption and scattering were 0.009 mm^{-1} and 0.07 mm^{-1}. The second experiment involved five measurements on different, but central locations on the probe. The standard deviations for absorption and scattering were 0.005 mm^{-1} and 0.08 mm^{-1}. Again, these results showed more variation than the previous experiment.

3.3.3 Boundary Conditions

Measurements were performed using the spatially-resolved method on Marley 8 and on Marley 3A for comparison. The probe used was made of black plastic and the extrapolated boundary condition was used, assuming no mismatch in the indices of refraction between the probe and the phantom existed. Time-resolved measurements were performed on Marley 8 and Marley 3A at a source detector separation of 10 mm. The Marley 8 data were fit using the ZBC and the extrapolated boundary condition, EBC, assuming no mismatch, i.e. the same conditions used in the cw measurements. The differences between the results obtained were small. The ZBC returned estimates of 0.0195 mm^{-1} and 2.12 mm^{-1} for the absorption and the scattering respectively, while the EBC estimated 0.0193 mm^{-1} and 2.03 mm^{-1} respectively. To maintain consistency with the cw approach, the values from the EBC were used for comparison. The results from these measurements are shown in Table 3.4. Since large differences were observed initially, the cw results were also fit using a relative mismatch of 1.4 and the cw measurements were repeated using a coupling gel. These results are also shown in Table 3.4. The cw results which are most logical, those assuming matched boundary with the use of a gel and those assuming a mismatch when no gel was used are shown in italics. It can be seen that the results obtained from the spatially-resolved measurements are strongly dependent on the boundary condition used, while this was not the case for the time domain measurements. However, since the mismatch in refractive indices is difficult to estimate, it is unclear which results are most accurate. It can be seen that the results from the cw system in italics show better agreement among one another and to the

time domain than do the non-italicized results. Actually, the optical properties from the time-resolved and cw techniques, obtained by measurements using a coupling gel and assuming a matched boundary are very similar (shown in bold italics).

Phantom	System	Boundary	Gel	μ_a (mm^{-1})	μ_s' (mm^{-1})
Marley 8	time domain	EBC (n=1)	yes	***0.0193***	***2.03***
	spatial	EBC (n=1)	yes	***0.0180***	***2.07***
	spatial	EBC (n=1)	no	0.0263	1.23
	spatial	EBC (n=1.4)	yes	0.0130	3.33
	spatial	EBC (n=1.4)	no	*0.0236*	*1.76*
Marley 3A	time	EBC (n=1)	yes	***0.0199***	***0.985***
	spatial	EBC (n=1)	yes	***0.0231***	***0.879***
	spatial	EBC (n=1)	no	0.0158	0.738
	spatial	EBC (n=1.4)	yes	0.0280	1.15
	spatial	EBC (n=1.4)	no	*0.0305*	*0.827*

Table 3.4: Variation of optical properties of solid phantoms with different measurement techniques and boundary conditions.

The time domain fits produced values for the scattering coefficient which were much higher than those estimated by the cw method prior to studying boundary effects. In order to determine if the time-resolved results were different due to some problem with the time domain fitting approach, the results were also analyzed in the frequency domain using the method described in the Analysis section. Because data were available at only

one distance, the Fourier transform of the reflectance was divided by the transformed IRF and the real and imaginary parts of the reflectance were fit. The maximum frequency of the fitting range was varied from 2.6 GHz to 430 MHz. There was no relationship evident between the value of the absorption coefficient estimated and the maximum frequency fit; results ranged from 0.0174 to 0.0193 mm^{-1}. The scattering coefficient decreased from 2.10 to 1.91 mm^{-1} as the maximum frequency decreased. Although the optical properties returned varied, they remained similar to the time domain results and the spatial results with the optimum boundary conditions.

Since it is difficult to know the value of the relative mismatch, it was necessary to attempt to minimize the boundary problems. This was done by performing measurements on liquid phantoms. However, due to problems in quantification of the scattering in Intralipid, a suspension of polystyrene spheres in water was used instead. The optical properties of a polystyrene sphere suspension can be calculated with more accuracy and precision because the size and concentrations of the particles are better known than for Intralipid. These experiments are described in section 3.4.

3.3.4 Source Detector Separation

In order to determine the effect of the source-detector separation, ρ on the optical properties estimated, measurements at 10 and 20 mm were performed on Marley 3A. Due to a low signal at 20 mm from Marley 8, it could not be used. In fitting theoretical and Monte Carlo data, variations were seen depending on the ρ value used. Typically, the scattering coefficient was overestimated by about 6-8% at 20 mm and 8-12% at 10 mm for Monte Carlo data; the absorption coefficient was overestimated by about 3-6%

for the 10 mm data and about 9-15% for the 20 mm Monte Carlo results. Six measurements were made at each distance to test the dependence of the optical properties on ρ. The 10 mm results had a collection time of 90 seconds and the 20 mm data had a collection time of 120 seconds. The results were fit using the EBC and assuming no mismatch in the index of refraction. The results from this experiment were: at 10 mm, $\mu_a = 0.0199 \pm 0.0002$ mm^{-1} and $\mu_s' = 0.985 \pm 0.008$ mm^{-1} and at 20 mm, $\mu_a = 0.0259 \pm 0.0008$ mm^{-1} and $\mu_s' = 0.931 \pm 0.010$ mm^{-1}. The source detector separation used clearly affected the results obtained. The trends observed are similar to those seen when fitting Monte Carlo data, the absorption is about 5% higher at 20 mm and the scattering is approximately 5% lower at 20 mm. These trends were also observed on measurements performed using a suspension of polystyrene spheres in water as described in section 3.4.

3.3.5 Measurements using 750 nm Diode Laser

To ensure that the 750 nm diode laser was able to measure optical properties as well as the 810 nm laser, measurements were performed on Marley 8 and Marley 3A using the same experimental set up as before, with the 750 nm laser. Spatially-resolved measurements were also compared at the two wavelengths. It was found that for Marley 8 using the cw system, at 750 nm, the scattering and absorption decreased by about 1% and 26% respectively, compared to results at 810 nm. For Marley 3A, the scattering increased (3%) but the absorption decreased, 40%. The time domain results showed the same trends; a summary of all of the measurements is shown in Table 3.5. Although the percent changes are not identical to those observed with the cw method, their relative magnitudes are similar in all cases. Although this is not a thorough test of the

performance of the 750 nm laser, it does indicate that its behavior is similar to that observed at 810 nm. Also, the IRFs collected with either laser appeared similar in shape.

Phantom	Wavelength (nm)	ρ (mm)	μ_a (mm^{-1})	μ_s' (mm^{-1})
Marley 8	810	10	0.0193	2.03
time domain	750	10	0.0135	2.01
% change			**-29**	**-1**
Marley 8	810	NA	0.0173	1.337
spatial	750	NA	0.0128	1.333
% change			**-26**	**-1**
Marley 3A	810	10	0.0199	0.985
time domain	750	10	0.0136	1.07
% change			**-32**	**8**
Marley 3A	810	20	0.0259	0.931
time domain	750	20	0.0178	1.02
% change			**-31**	**9**
Marley 3A	810	NA	0.0388	0.628
spatial	750	NA	0.0222	0.645
% change			**-40**	**3**

Table 3.5: Variation of optical properties with wavelength, 750 nm versus 810 nm for Marley 8 and Marley 3A. In all cases, the reflectance was fit using the same routines and boundary conditions. Since no true values for μ_s' and μ_a are known only relative changes between the two wavelengths were examined.

3.4 Polystyrene Spheres

The phantoms used in the previous experiments had limitations which could not be overcome. The Intralipid phantoms, although they allowed for variation in scattering coefficient, were difficult to characterize due to uncertainties in the stock concentrations. Therefore any calculation of theoretical scattering coefficient could not be precise. The solid phantoms suffered from similar problems; there did not exist theoretical values for the optical properties, including the index of refraction. As well, it was not possible to vary the scattering or absorption of these phantoms and it was unclear how to best account for mismatches in refractive indices. Another option, widely used in optical studies, is a suspension of polystyrene spheres (Duke Scientific, Pao Alto, CA) in deionized water. These spheres are available in various well defined diameters and in precise concentrations. If the diameter and the index of refraction of these spheres is known, Mie theory can be used to predict the scattering coefficient, μ_s and anisotropy parameter, g. Two diameters of polystyrene spheres were used, 0.653 ± 0.0048 μm and 1.53 ± 0.018 μm. A program obtained from Ed Hull (University of Rochester) was used to determine the variation of scattering coefficient with wavelength. This provided a phantom with known optical properties; the scattering was calculated with Mie theory, the absorption and the index of refraction were assumed to be that of water at the wavelength of interest. Variation in the scattering coefficient was achieved simply by varying the concentration of spheres used. As well, since the phantoms were liquid, the problems associated with coupling at boundaries that existed for the solid phantoms were

negligible; the index of refraction of the liquid was that of water, 1.33 at the wavelength of interest and the probe material has a refractive index of about 1.4

3.4.1 Variation with Concentration

Seven different concentrations were used for each particle size and measurements were performed on the time-resolved system and the continuous wave system, both of which have been discussed previously. The wavelength used for this study was 810 nm and the source detector separation for the time domain measurements was 10 mm. The index of refraction was assumed to be 1.33 and the absorption was that of water, 0.002 mm^{-1}. Both methods fit the data with diffusion theory using the extrapolated boundary condition (equation 16) and assuming no mismatch in the indices of refraction.

In the time domain, collection times were less than two minutes and each measurement was performed twice. The data were fit over one log on the rising edge and down two logs on the falling edge. Typically, the data and the fit showed good agreement from the peak onward, but an underestimation of the data was evident for early times i.e. the rising edge of the reflectance. This was also seen previously in the Monte Carlo fits, for example, Figure 2.6 in the Experimental section. There was little difference in the quality of the fits between the two different sphere sizes. An example of a typical fit is shown in Figure 3.6. This shows reflectance and the fitted line for the sixth phantom with small diameter spheres (s6). The deviations between the fit and the data at early times are evident in both the fit and in the residuals. The optical properties estimated in this example are typical as well; the absorption is off by about 10% and the

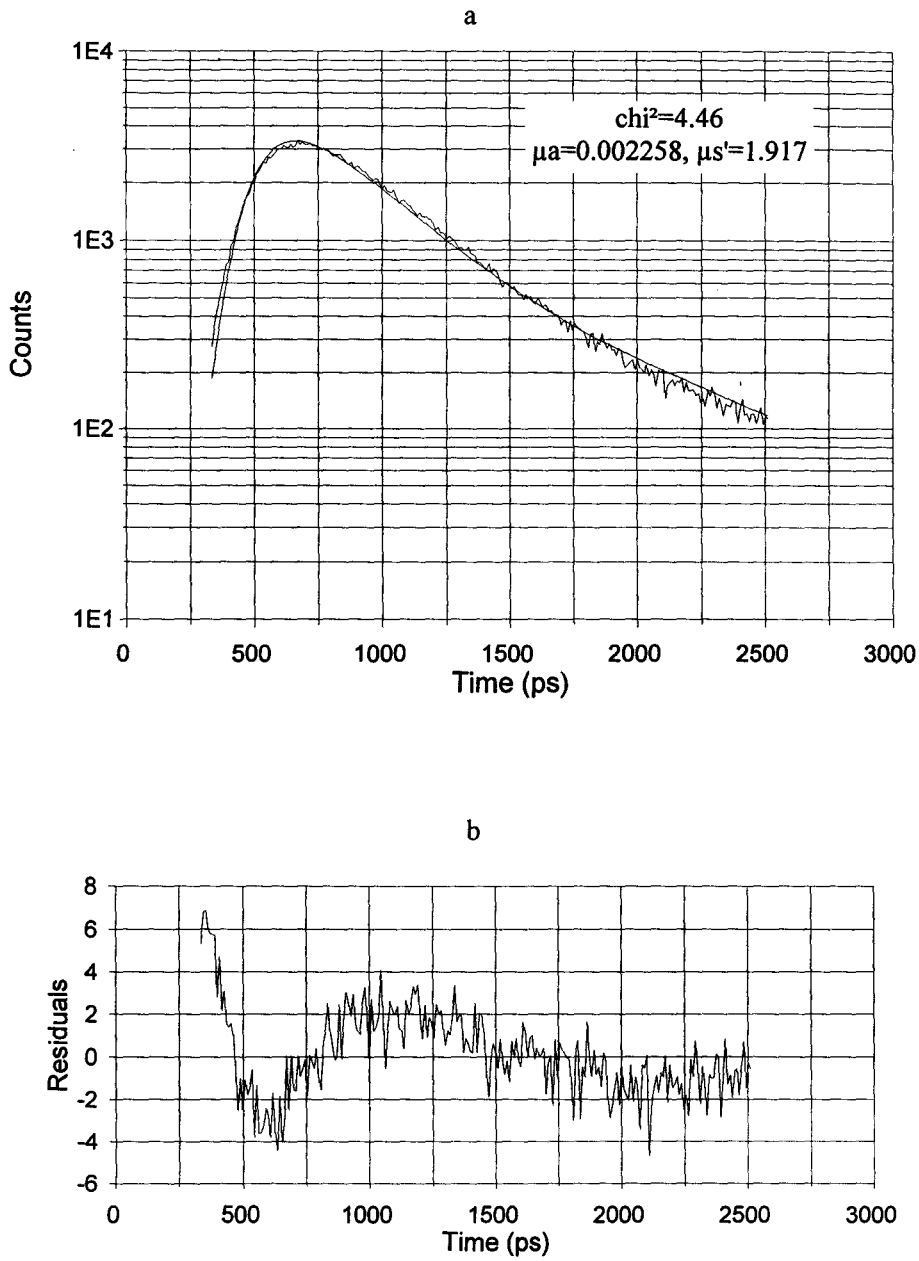

Figure 3.6: A typical result from a measurement using polystyrene spheres. This is from the sixth phantom using spheres with d=0.653 μm. Theoretical optical properties are μ_a = 0.002 mm^{-1} and μ_s' = 1.393 mm^{-1}. The fitting range has been limited at later times to remove the secondary peak evident in the IRF from the fitting range.

scattering is about 35% too high. A summary of the results from these experiments is shown in Table 3.6.

Phantom Number	Particle Diameter (μm)	Expected (mm^{-1})		Time-resolved (mm^{-1})		Spatially-resolved (mm^{-1})	
		μ_a	μ_s'	μ_a	μ_s'	μ_a	μ_s'
s1	0.653	0.00200	0.511	0.00089	0.658	0.00496	0.417
s2	0.653	0.00200	0.699	0.00117	0.869	0.00357	0.593
s3	0.653	0.00200	0.887	0.00193	1.172	0.00465	0.684
s4	0.653	0.00200	1.031	0.00261	1.502	0.00218	0.884
s5	0.653	0.00200	1.211	0.00196	1.516	0.00230	1.077
s6	0.653	0.00200	1.393	0.00226	1.905	0.00226	1.196
s7	0.653	0.00200	1.575	0.00218	2.000	0.00260	1.346
b1	1.53	0.00200	0.490	0.00089	0.666	0.00406	0.377
b2	1.53	0.00200	0.679	0.00184	0.952	0.00586	0.511
b3	1.53	0.00200	0.870	0.00226	1.226	0.00419	0.679
b4	1.53	0.00200	1.065	0.00225	1.450	0.00334	0.839
b5	1.53	0.00200	1.247	0.00262	1.785	0.00286	0.986
b6	1.53	0.00200	1.431	0.00271	2.001	0.00264	1.150
b7	1.53	0.00200	1.615	0.00221	2.200	0.00193	1.343

Table 3.6: Optical properties estimated from time and spatially-resolved reflectance measurements on varying concentrations of polystyrene spheres in water. Results in the time domain are for $\rho = 10$ mm and are the average of two measurements.

It is more convenient to examine the data graphically as in Figure 3.7 (a-d). Figure 3.7a shows the measured versus expected values of the scattering coefficient estimated by the two different methods using the small diameter spheres. Although both systems showed a linear relationship between the scattering and the concentrations of polystyrene spheres, there are large differences between the scattering coefficients predicted. The time domain results systematically overestimated the scattering by about 25%, while the continuous wave system underestimated the scattering by about 15%. In order to quantify these results, linear regression was performed on the data using the expected μ_s' value as the independent variable and the measured scattering as the dependent variable. These results are summarized in Table 3.7. Both systems have R^2 values close to unity and intercepts near zero.

Measurement Method	**Diameter of Spheres (μm)**	**Slope (theory=1)**	**Intercept (theory=0)**	**R^2**
time	0.653	1.246 ± 0.092	-0.004 ± 0.091	0.972
spatial	0.653	0.848 ± 0.036	-0.049 ± 0.036	0.991
time	1.53	1.316 ± 0.021	-0.003 ± 0.018	0.999
spatial	1.53	0.816 ± 0.016	-0.059 ± 0.016	0.998

Table 3.7: Results from linear regression of measured versus expected scattering coefficients for the two techniques and two different sphere sizes.

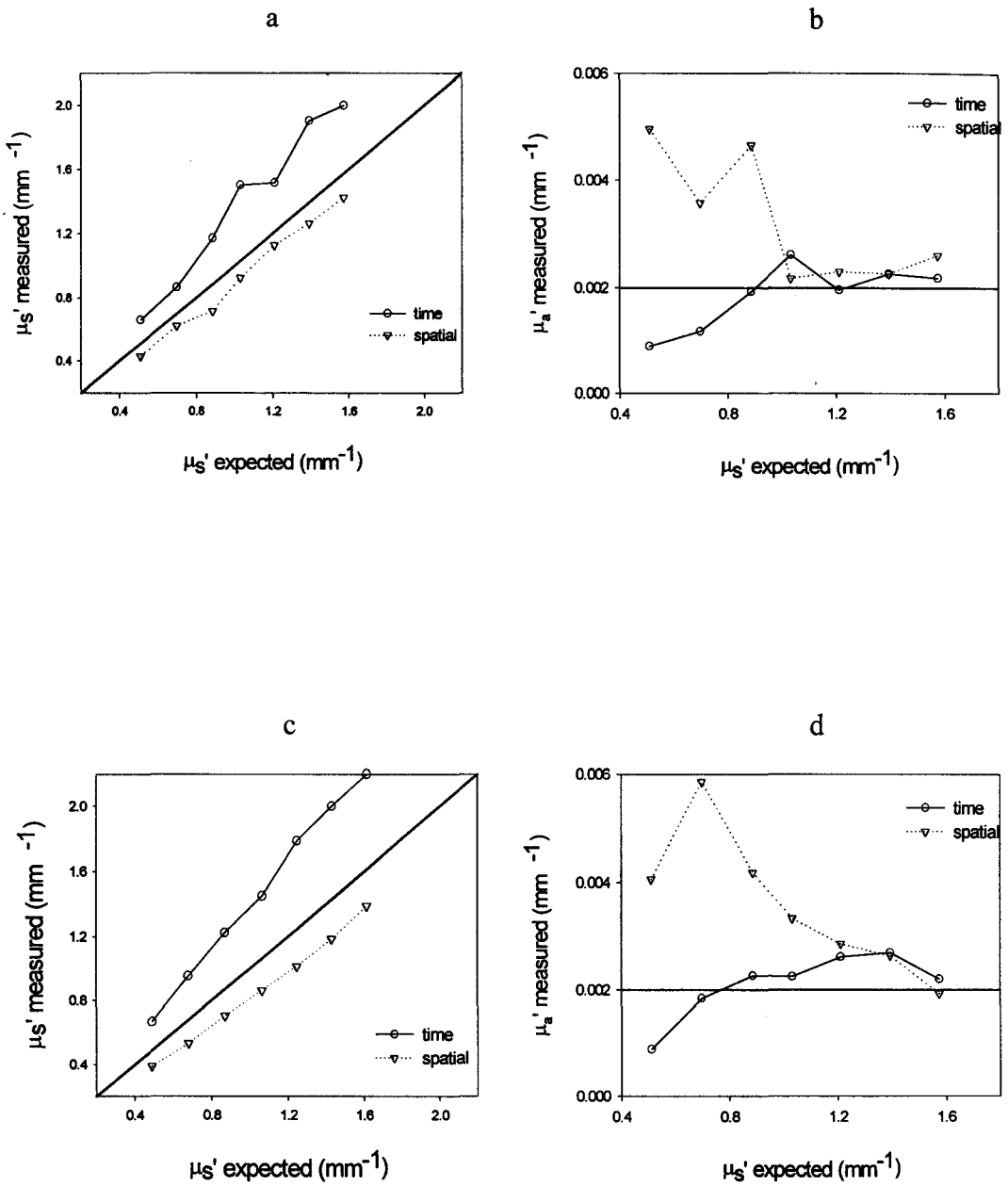

Figure 3.7: Results from polystyrene sphere measurements using spatial and time domain methods.

(a) variation of scattering for small spheres (d=0.653 μm) (b) variation of absorption for the same spheres. (c) variation of scattering for large (d=1.53 μm) (d) variation of absorption for large spheres.

Figure 3.7b shows the variation of absorption with the seven measurements performed on the same spheres. The absorption should remain constant at 0.0020 mm^{-1} which is the absorption of water at 810 nm. For low values of the scattering coefficient, the absorption is underestimated by the time domain system and overestimated by the spatial system. However, for larger values of the scattering, both systems have good estimates of the absorption and do not show any systematic variation.

The results from the series of measurements performed on the large spheres are shown in Figures 3.7c and 3.7d. Figure 3.7c shows the measured versus expected values of the scattering coefficient as estimated by both systems. The trends observed with the smaller spheres are evident here. From Table 3.7, the excellent linearity of both systems is evident due to the good R^2 values. The intercepts are both close to zero as well. The errors in the slopes of the lines obtained from linear regression are larger in this experiment. The time-resolved method predicts scattering coefficients that are about 32% too high and the cw system produces results that are about 18% too low. Therefore, although the linearity of the measurements was better in the second series, the accuracy of the results was poorer than the first set of experiments. The trends seen in the estimation of the absorption coefficient are the same for either size of spheres. The differences observed between the two sizes of spheres are, however, insignificant compared to the large differences from the Mie theory predictions.

3.4.2 Phantom Size and Boundary Effects

One of the initial concerns with the measurements performed on the polystyrene spheres was the physical size of the phantom used. The phantom volume was 300 mL which was poured into a black plastic box with approximate dimensions of 7 cm × 7 cm × 6 cm deep. Due to the size of the phantom, time domain measurements were performed at 10 mm only. This was not a factor for the cw measurements, as the largest ρ value used was 10 mm. For larger source-detector separations, which are possible in the time domain, there was a possibility of light that would otherwise be scattered back being absorbed on the sides or bottom of the phantom; this would distort the reflectance collected. However, to ensure that this was not a factor for the measurements performed at 10 mm, another polystyrene phantom with a volume of 500 mL was prepared. No absorber was added to the phantom and the scattering coefficient was calculated by Mie theory to be about 0.910 mm^{-1}. This phantom was measured in the same container in which the previous measurements where performed and in another, larger container with dimensions of 8 cm × 8 cm × 8 cm. This phantom was also measured at two different ρ values, 10 and 20 mm in the larger container, to investigate if boundary effects were a problem at either distance.

Results obtained for the two different phantom sizes from the spatially-resolved technique did not show significant differences; the scattering coefficient only varied by about 1%. As in the previous experiment, the estimated value for the scattering coefficient was less than predicted by theory; the theoretical value was 0.765 mm^{-1}. The time domain measurements at 10 mm did not show any variation of optical properties

with the size of the phantom. The absorption coefficient varied by a few percent, but variation of that magnitude was observed in the previous measurements as well. There was no significant difference in the scattering coefficients estimated from the two phantoms of different volumes either. However, optical properties estimated were found to be dependent on the source detector separation used. Results from the 10 mm measurement were μ_s'=1.274 mm^{-1}, μ_a=0.00265 mm^{-1} and χ^2=2.1. For comparison, the 20 mm results were μ_s'=1.182 mm^{-1}, μ_a=0.00239 mm^{-1} and χ^2=1.4. The optical properties obtained at 20 mm are more accurate than those estimated at 10 mm and the quality of the fit is better. These differences were also seen in both Monte Carlo and diffusion theory studies. From this, the following is evident: phantom size does not affect the optical properties estimated, even for larger source-detector separations (at least to the extent investigated here) and optical properties obtained from measurements performed at 20 mm are more accurate than those at 10 mm.

3.4.3 Variation of Results with ρ

The improvement in accuracy obtained by measuring the large volume phantom at 20 mm, suggested that time domain results performed at 20 mm provide better estimates of the scattering coefficient. This is probably due to the fact that the applicability of the diffusion theory is becoming questionable at 10 mm. Unfortunately, since the initial polystyrene experiment was performed by adding additional polystyrene to the previous phantom to increase its scattering coefficient, it was not possible to repeat the experiment at 20 mm. Also, due to the high cost of the spheres it was not practical to repeat the entire experiment. The two final phantoms (s7 and b7) could be remeasured at

20 mm however. The theoretical absorption for each phantom was 0.002 mm^{-1}. The phantom with the small diameter spheres (s7) had a theoretical scattering of 1.575 mm^{-1}, while the phantom with the larger spheres (b7) had a scattering coefficient of 1.615 mm^{-1}. A summary of this investigation is shown in Table 3.8.

ρ (mm)	**Phantom**	χ^2	μ_a	**% error**	μ_s'	**%error**
10	s7	2.7	0.00218	9	2.000	27
20	s7	1.8	0.00216	8	1.818	15
10	b7	2.6	0.00221	11	2.200	36
20	b7	1.7	0.00224	12	1.844	14

Table 3.8: Variation of results for two polystyrene phantoms with source-detector separation. Theoretical scattering coefficients are 1.575 mm^{-1} and 1.615 mm^{-1} for the small and large diameter spheres respectively.

The errors in estimating absorption are about 10% and are independent of the ρ value used. Although time domain results at 20 mm still overestimate the scattering coefficient by about 15%, they do provide a better estimate than measurements performed at 10 mm which show errors of up to 36%.

3.4.4 Investigation of Performance of 750 nm Diode Laser

The performance of the 750 nm laser had been investigated on the Marley phantoms, as mentioned above. However, theoretical values of the optical properties were not available for those phantoms. To investigate the accuracy of the results obtained from this laser, the large volume polystyrene phantom used in section 3.4.2 was also measured at 750 nm using both the time domain and the continuous wave systems,

for comparison. The results, which proved similar to the results obtained at 810 nm, are shown in Table 3.9. Once more, the scattering coefficient is underestimated by the spatial system and overestimated by the time-resolved method. More accurate results were obtained at 20 mm than at 10 mm, as noted at the longer wavelength.

Method	μ_a (mm^{-1})	% error	μ_s' (mm^{-1})	%error
theory	0.0026	0	0.984	0
spatial	0.00263	1	0.831	-16
time(10 mm)	0.00232	-11	1.295	32
time (20 mm)	0.00239	-8	1.125	14

Table 3.9: Results on polystyrene phantom measured at 750 nm using both measurement systems and two different source detector separations.

The errors in estimating both the scattering and the absorption at either distance are similar to those observed in the preceding section. As expected, system performance is independent of wavelength.

3.5 Variation of absorption

In section 3.4, the ability of the time-resolved system to predict the scattering coefficient was studied. The following two experiments were performed to investigate the accuracy of the system in estimating the absorption coefficient. The suspensions of polystyrene spheres gave control over the value of the scattering, but the absorption was fixed to be that of water at the wavelength of interest. It was necessary to introduce a

known absorber, which could be quantified in the suspension to allow for variation in the absorption coefficient. Two different absorbers were used, Melanin Ink (MeL-Co, Orland, CA) and indocyanine green (Becton Dickinson, Cockeysville, MD) in combination with a suspension of polystyrene spheres.

3.5.1 Variation of Absorption with Ink Concentration

Ink provides a convenient method for increasing the absorption of a liquid phantom; it mixes easily in water and is readily available. The use of India Ink as an absorber has been well documented (Madsen 1992b) but has the primary difficulty that the ink also acts as a scatterer. In addition, there does not exist a theoretical means of determining the absorption coefficient for a given ink concentration. Therefore, to determine the relationship between the absorption coefficient and the ink concentration, it was necessary to perform an absorbance measurement on the ink solution. This involved measuring the changes in intensity observed when light passes through a dilute solution of ink and water. The experiment was performed in a cuvette with a pathlength of 5 mm using a white light source and Ocean Optics software. The stock solution of ink was a 9% aqueous suspension; ink concentrations discussed in this investigation refer to a given percent of the stock solution in water. By relating the changes observed in transmission to an absorbance and with a knowledge of the ink concentration and the pathlength, it is simple to obtain a value of the absorption coefficient for each ink concentration used. Linear regression is then performed to determine the best relationship between the absorption coefficient and the ink concentration. This provides an empirical method for determining the absorption coefficient with the only assumption

being that no scattering occurs within the ink. However, from previous studies it is known that the ink probably scatters and the absorption coefficient determined by this technique will probably be higher than the true value.

For this experiment, a suspension of large diameter (d=1.53 μm) polystyrene spheres with a predicted μ_s' value fixed at 1.22 mm^{-1} was prepared. Five different ink concentrations were added ranging from 0 to 0.04%. Measurements were performed on the continuous wave system, the time domain system (at 10 and 20 mm) and a frequency domain system. The frequency domain system used an 810 nm laser; the details of the system have been described elsewhere (Patterson 1995). The frequency domain data were collected for distances from 5 to 21 mm in steps of 2 mm and the frequency domain reflectance was fit using a non-linear least squares fitting routine.

The results from this study are shown graphically in Figure 3.8 as measured absorption coefficient versus concentration of ink. All systems reflect the linear increase in absorption, as expected. The accuracy of each method can be better quantified by performing linear regression with ink concentration as the dependent variable. This is shown in Table 3.10 as well as the mean scattering coefficient and standard deviation obtained by each method for the four different ink concentrations. All methods show good linearity but the slopes of the best fit lines vary from 0.57 ± 0.04 to 0.98 ± 0.04.

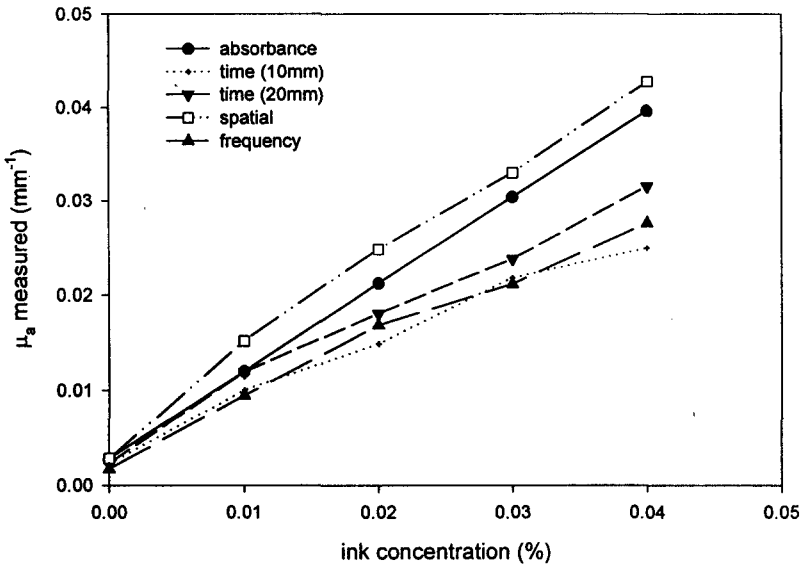

Figure 3.8: Variation of measured absorption versus ink concentration, at 810 nm, for a suspension of polystyrene spheres in water.

Measurement Method	Mean $\mu s'$ (mm^{-1})	Slope $(mm\ \%)^{-1}$	Intercept (mm^{-1})	R^2
absorbance	NA	0.92 ± 0.04	0.003 ± 0	1
spatial	0.960 (0.020)	0.98 ± 0.04	0.004 ± 0.001	0.995
frequency	1.246 (0.036)	0.63 ± 0.04	0.003 ± 0.001	0.990
time (20 mm)	1.524 (0.090)	0.70 ± 0.04	0.003 ± 0.001	0.991
time (10 mm)	1.577 (0.103)	0.57 ± 0.04	0.003 ± 0.001	0.984

Table 3.10: Results from linear regression of measured versus expected μ_a values from three measurement systems.

Standard deviations for μ_s' values are shown in parentheses.

As in previous experiments, the scattering coefficient was overestimated by the time-resolved method. The spatially-resolved results show the same underestimation as previously observed. However, the frequency domain system shows excellent agreement in estimating μ_s'; the error in the scattering is only about 2%. On the contrary, the frequency system is the least accurate method to determine the absorption (assuming that the best results are obtained from the absorbance measurements). Although every system shows a linear response and good stability in predicting the scattering coefficient, as reflected by the standard deviations, the cw method produces the results most similar to the absorption predicted by the transmission measurement. However, although these values are most similar, they are almost certainly wrong as the absorbance method probably overestimates μ_a. Without a knowledge of the amount of overestimation it is not possible to say which method makes the most accurate predictions. Hence, the main disadvantage of using ink in this experiment is the fact that it also contributes to scattering. It would be advantageous to perform this experiment with a substance that did not scatter and had a predictable absorption coefficient. The use of a dye instead of ink would result in a experiment with less uncertainties, since dyes do not scatter.

3.5.2 Variation of Absorption with Indocyanine Green Concentration

To reduce the effects of scattering on the calculation of the absorption coefficient from absorbance measurements, it is necessary to use a dye, such as indocyanine green (ICG). This is a water soluble dye with a peak spectral absorption at 800 to 810 nm, which is ideal for the system using the 810 nm laser. There do exist disadvantages to using this particular absorber: the dye fluoresces and the fluorescence signal could

interfere with the reflectance, it dissociates within hours and the calibration curve that accompanies the product is for the dye in normal blood serum, not water. It is a simple task to eliminate the fluorescence signal through the use of an 800 nm band pass filter inserted into the measurement apparatus. Although the absorption differences between the dye in blood or in water may be small, the absorption can be measured using the absorbance method described in the previous section. This should produce an accurate result as ICG absorbs light but does not act as a strong scatterer.

A stock solution of ICG with a concentration of 5 mg/mL was prepared. A portion of this was used in three absorbance measurements to determine the absorption coefficient of the dye. At 810 nm, the predicted absorption for the stock concentration from these measurements was 0.26 mm^{-1}, while the corresponding value for ICG in serum was 0.32 mm^{-1} (Becton Dickinson, Cockeysville, MD). These values are different by about 20%, somewhat larger than expected. However, since this experiment was performed using water with polystyrene spheres, the absorption as measured by the absorbance measurement was taken as the standard value, i.e. 0.26 mm^{-1} for the stock solution. A phantom was prepared using the large diameter polystyrene spheres; the value of μ_s' predicted by Mie theory for the sphere concentration used was 1.093mm^{-1} at 810 nm. Three different ICG concentrations were measured on all three systems: time, spatial and frequency domain. The improvements observed by increasing the source-detector separation in the time domain suggested that the ρ value could have a large effect on the optical properties estimated. Therefore, time domain measurements were performed at four distances from 10 to 40 mm. It should be noted that in order to

perform all these measurements it was necessary to limit the number of different concentrations used.

A typical fit from this experiment is displayed in Figure 3.9. This shows the fit, the data and the residuals for the reflectance collected at 30 mm for the phantom with the highest concentration of ICG. The agreement is good over the entire fitting range and the residuals do not show any observable pattern. All of the fits performed at larger ρ values i.e. greater than 10 mm, appear similar to this, good agreement between the fit and the data and chi-squared values below 2. The fits for the 10 mm data show the same deviations for early times as previously observed and have higher χ^2 values, typically around 4. The accuracy of the results obtained from the various approaches can be seen in Figure 3.10 (a-d). Figure 3.10a shows the measured μ_a values versus the concentration of ICG for the absorbance method and the time domain results for four distances. The results from the measurements performed at 20, 30, or 40 mm appear very similar to one another and to the standard, the absorbance method. However, the results from the 10 mm data are not in good agreement with any of the other results. Figure 3.10b shows the same data for the absorbance method and the other two indirect methods, the spatial and frequency domain systems. The spatially-resolved results are in agreement with the absorbance method but the frequency domain results are not. In general, these results are similar to those observed when phantoms with different ink concentrations were measured: good agreement between all of the methods expect the frequency domain system and the time domain measurements at 10 mm. Figure 3.10c shows the variation

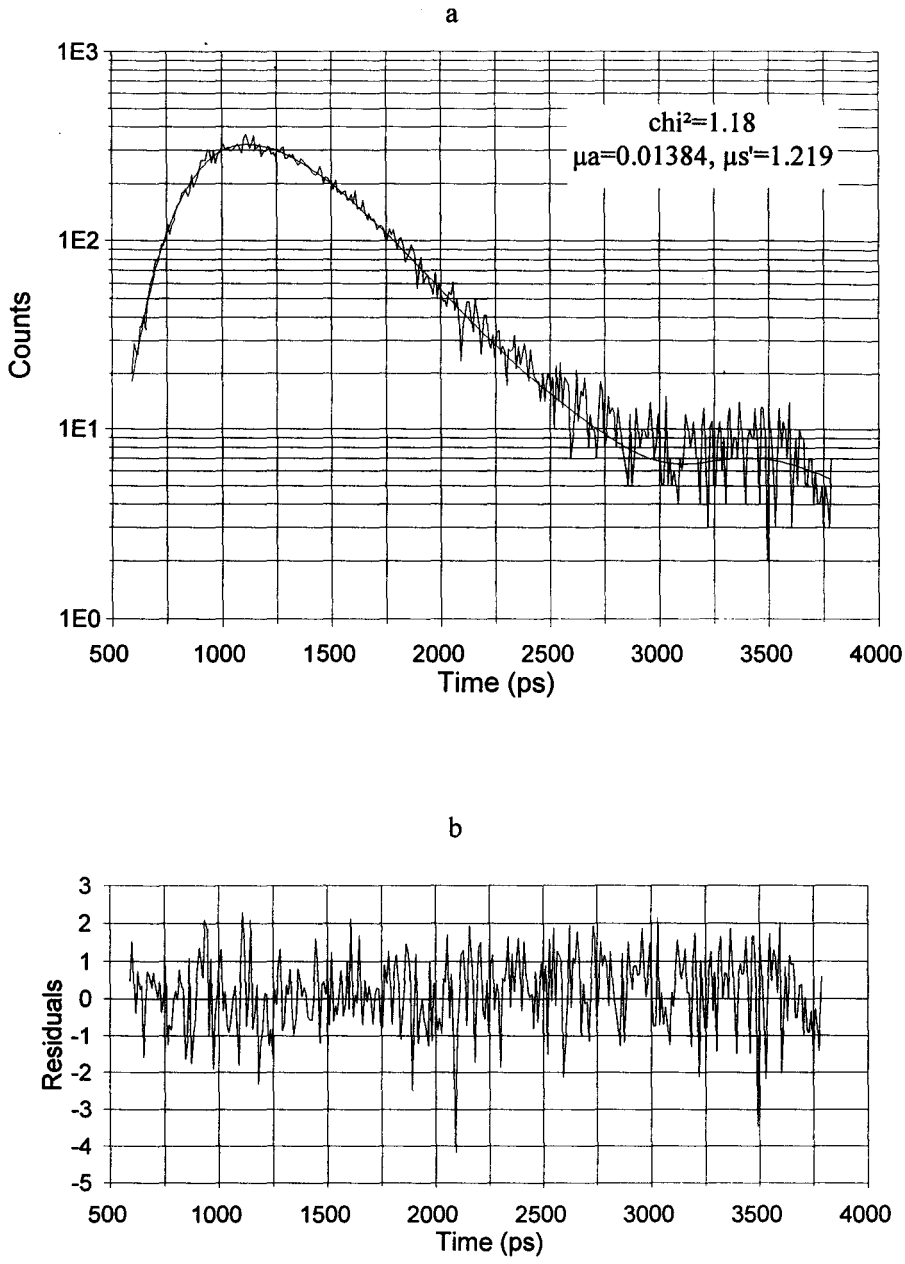

Figure 3.9: An example of a fit for polystyrene spheres with ICG. Collected at 30 mm for the highest concentration of ICG. Theoretical results are: μ_s'=1.093 mm^{-1} and μ_a=0.0140 mm^{-1}.

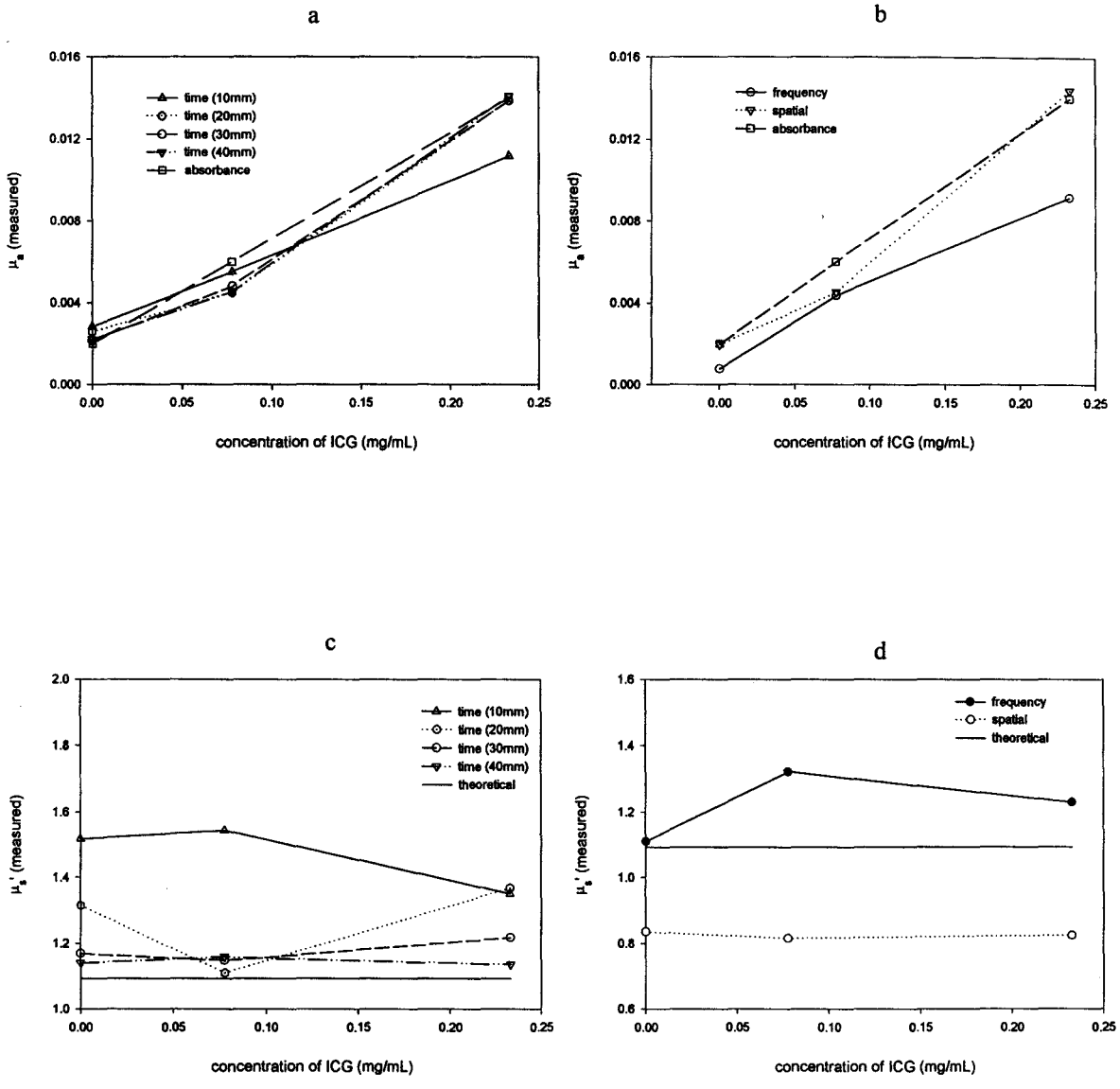

Figure 3.10: Variation of absorption for polystyrene and ICG (a and b) and scattering (c and d) for different measurements. (a) μ_a from time domain and absorbance (b) μa from spatial, frequency and absorbance (c) μ_s' from time domain and (d) μ_s' spatial and frequency.

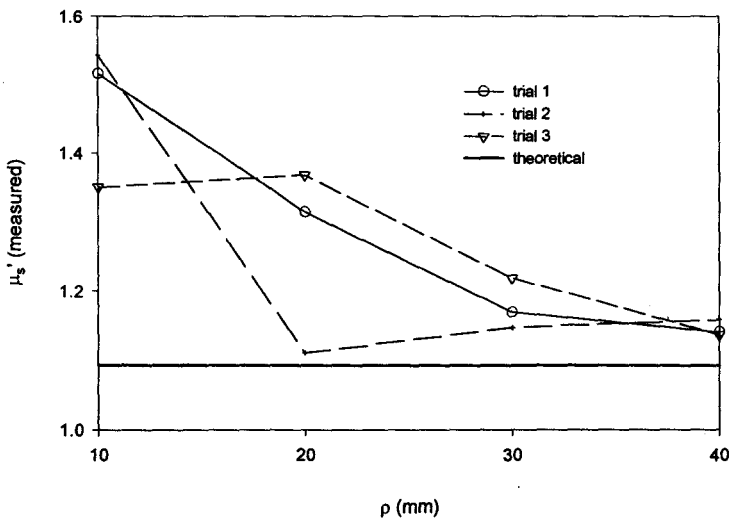

Figure 3.11: Variation of optical properties with source detector separation for measurements on polystyrene phantom with added ICG. Different trial numbers indicate increasing concentrations of ICG.

of the μ_s' value estimated by the time domain technique with the ICG concentration. Again the 10 and 20 mm results are similar to before, with large overestimates of the scattering coefficient at both distances. However, the results for the larger ρ values, 30 and 40 mm, are within 10% of the theoretical value. The final Figure 3.10d shows μ_s' values estimated by the other two methods. The cw system underestimated the scattering by about 20% but the frequency system showed wide variation in the scattering. The poor results in the frequency domain were unexpected, as this method had excellent accuracy when predicting the scattering with no absorption present (section 3.4). The other unexpected result was the variation of the estimated scattering with ρ in the time domain; it was thought that the differences between 10 and 20 mm were due to

limitations of the diffusion model for small ρ values, however, it was surprising that this trend continued with distances larger than 20 mm. This variation can be more clearly seen in Figure 3.11 which displays the variation in scattering with distance for the three measurements performed with different absorption coefficients.

To better quantify the performance of each system, linear regression was performed using ICG concentration as the independent variable and the predicted μ_a value as the dependent variable. These results are shown in Table 3.11. Again, all methods show good linearity, accurate predictions of the intercept (which is the μ_a value for water alone at 810 nm) but widely varying slopes. The best agreement, with respect

Method	Slope $\times 10^{-2}$ (mm %)$^{-1}$	Intercept (mm^{-1})	R^2
absorbance	5.2	0.0020	1
frequency	3.4 ± 0.9	0.0016 ± 0.0015	0.940
spatial	5.5 ± 0.6	0.0014 ± 0.0010	0.989
time (10 mm)	3.6 ± 0.2	0.0027 ± 0.0003	0.998
time (20 mm)	5.1 ± 0.9	0.0018 ± 0.0015	0.968
time (30 mm)	5.1 ± 0.4	0.0018 ± 0.0007	0.994
time (40 mm)	5.3 ± 0.6	0.0015 ± 0.0014	0.977

Table 3.11: Results of linear regression of μ_a measured against concentration of ICG (%) for the different techniques used and the different ρ values measured.

to the absorbance method, is observed for the spatial system and the time domain measurements performed at ρ values greater than 10 mm. This experiment demonstrated that the time domain technique for predicting changes in absorption is dependent on the source-detector separation used. For larger ρ values, the time-resolved technique can predict the scattering coefficient to about 10% and the absorption within 2% for larger values of μ_a. The relative errors in estimating small μ_a values are large, about 25%, but the absolute errors are small, about 0.0015 mm^{-1}. Although there were large errors present in the experiment in which the scattering of a polystyrene solution was varied, it is probable that a large fraction of those errors were due to the ρ value used. This experiment showed the success of the time domain method in measuring changes in absorption accurately.

3.6 Results from Dual Wavelength System

All the measurements described thus far have been performed at a single wavelength. The aim of those measurements was to study the ability of the system to estimate optical properties of tissue simulating phantoms. In this section, the simultaneous dual wavelength system, as described in the Experimental section, was used to measure optical properties. Since either diode laser worked independently, this section will determine if the control circuitry and the dual MCAs affect the performance of the system. Prior to performing *in vivo* measurements, simultaneous dual wavelength measurements were made on two different phantoms.

3.6.1 Dual Wavelength Measurements on Tissue Simulating Phantoms

The first phantom that was used was Marley 3A; this had been previously measured in section 3.3.5 using both wavelengths, 750 and 810 nm. The other phantom measured was the large volume polystyrene phantom measured at both wavelengths in sections 3.4.2 and 3.4.4. A summary of the results, including previous results, is shown in Table 3.12 for both phantoms at both wavelengths. Both phantoms were measured only at ρ=10 mm using the dual wavelength set up. Theoretical results for the polystyrene phantom were μ_a = 0.0026 $mm^{-1}$and μ_s' = 0.984 mm^{-1} at 750 nm and μ_a=0.002 mm^{-1} and μ_s' = 0.910 mm^{-1} at 810 nm.

	750 nm		**810 nm**	
Marley 3A	μ_a **(mm^{-1})**	μ_s' **(mm^{-1})**	μ_a **(mm^{-1})**	μ_s' **(mm^{-1})**
single λ	0.0136	1.068	0.0199	0.985
dual λ	0.0164	1.191	0.0160	1.072
Polystyrene				
single λ	0.00232	1.295	0.00265	1.274
dual λ	0.00194	1.103	0.00243	1.1731

Table 3.12: Phantom measurements performed at two wavelengths independently and simultaneously on Marley 3A and a suspension of polystyrene spheres in water.

Some differences are evident in the measurements performed using the simultaneous dual wavelength system. However, there are no trends evident for all the

measurements. In addition, similar variations in optical properties estimated from different measurements was observed on many previous occasions. The coefficients estimated are quite similar to those measured previously, as expected. Therefore, the final investigations, measuring *in vivo,* were undertaken.

3.6.2 Dual Wavelength Measurements Performed *in vivo*

In order to determine if the time domain system was sensitive enough to detect changes in absorption due to variations in the oxygenation status of the tissue, *in vivo* measurements were made on the palm of the left hand of a volunteer. The probe was placed on the lateral surface of the palm, below the thumb. The source detector separation used was 10 mm and the collection time was two minutes. The index of refraction of the tissue was assumed to be 1.4 and the boundary was assumed to be matched. Initially, a measurement was made under normal conditions followed by a measurement performed during arterial occlusion. A blood pressure cuff at a pressure of about 240 mm Hg was used to occlude blood flow to the hand. The pressure was applied for about 30 seconds before measurements were performed, in order to allow some time for the tissue to deoxygenate. This should result in deoxygenation of the tissue below the cuff, including the tissue being measured and should produce different absorption properties for the tissue volume of interest. Once the four different absorption coefficients at two different wavelengths are known, it is possible to estimate the hemoglobin saturation, SO_2, of the tissue using equations (18 a and b), followed by equation (1). The values for the extinction coefficients of each molecule at each wavelength can be found in Cope's thesis (Cope 1991) and can be calculated in units of

$mM^{-1}mm^{-1}$. The background absorption was assumed to result from a water concentration in the tissue of 70%. Substituting these constants and the appropriate wavelengths into equations (18 a and b) gives the following equations:

$$\mu_a(750) = 0.1494[HbO_2] + 0.4202[Hb] + 0.0018 \quad [mm^{-1}] \qquad (27a)$$

$$\mu_a(810) = 0.2526[HbO_2] + 0.2171[Hb] + 0.0014 \quad [mm^{-1}] \qquad (27b)$$

Once total absorption was measured at each wavelength, it was a simple task to solve this system of equations for [Hb] and [HbO_2] and hence calculate SO_2.

The results from these four measurements are shown in Table 3.13 and the fit for the second measurement is displayed in Figure 3.12. Previous measurements done in our lab using the cw system showed typical optical properties for the hand to be about μ_a = 0.014 ± 0.005 mm^{-1} and μ_s' = 0.92 ± 0.20 mm^{-1} at 750 nm. It must be noted that large

Wavelength (nm)	**Oxygenated or Deoxygenated**	χ^2	μ_a **(mm^{-1})**	μ_s' **(mm^{-1})**
810	oxy	2.85	0.01686	1.4591
750	oxy	1.62	0.01450	1.4788
810	deoxy	1.97	0.02018	1.4864
750	deoxy	1.95	0.02396	1.5623

Table 3.13: Optical properties estimated from *in vivo* measurements on the hand at two wavelengths under normal conditions (oxy) and arterial occlusion (deoxy).

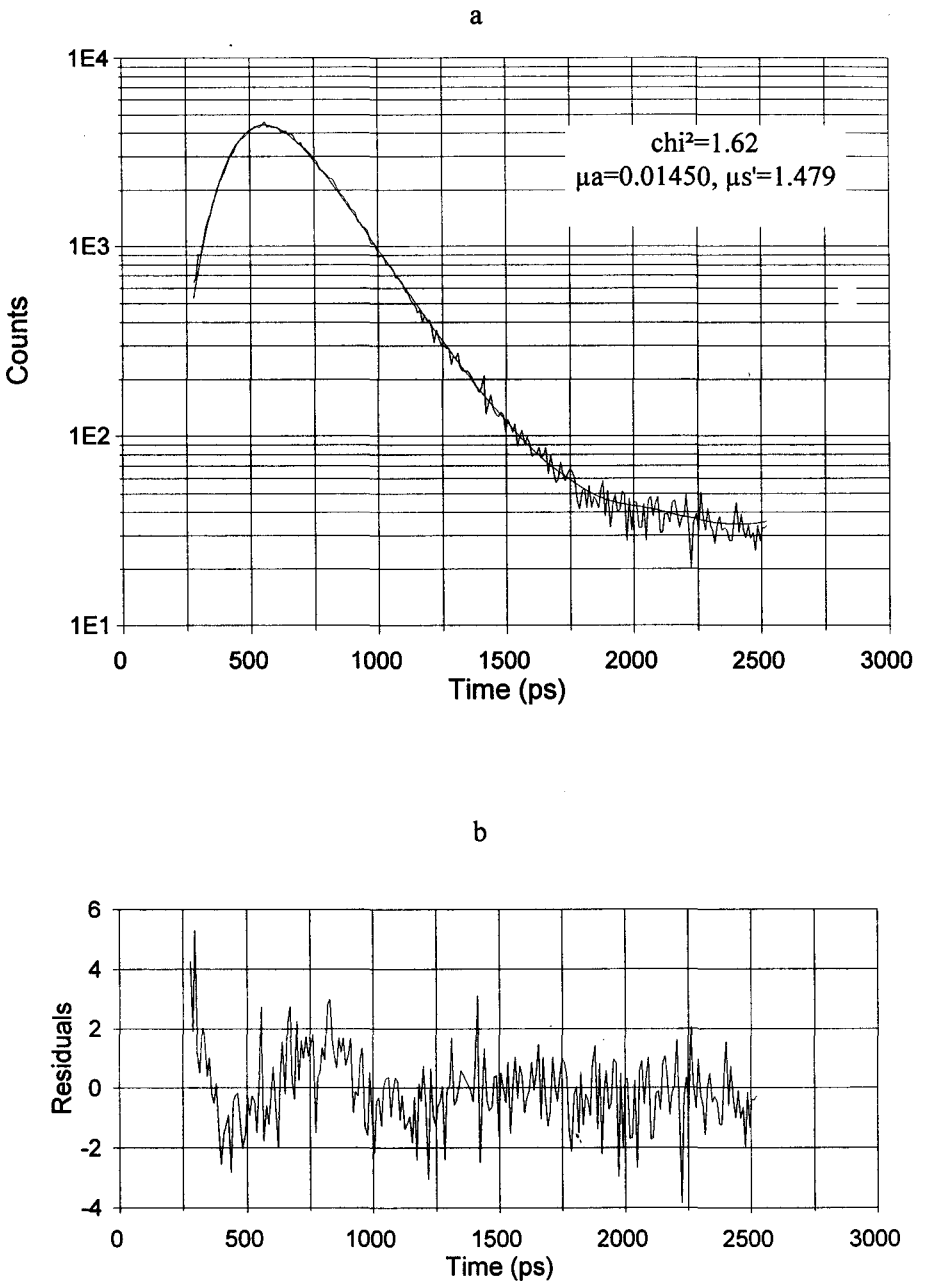

Figure 3.12: Data, fit (a) and residuals (b) for measurement at ρ = 10 mm on the palm of the hand at 750 nm.

variations can be expected depending on the individual and even on the exact location on the hand. Furthermore, as observed, it was expected that the scattering would decrease with increasing wavelength (Anderson 1993). Also from the extinction coefficients, a large increase in absorption was expected at 750 nm for deoxygenated blood compared to oxygenated blood (due to a larger extinction coefficient of deoxyhemoglobin compared to oxyhemoglobin at 750 nm). This increase was observed, although an increase at 810 nm was also observed. This was not expected as the absorption of oxyhemoglobin and deoxyhemoglobin are quite similar at 810 nm.

From these results the concentrations of Hb and HbO_2 could be estimated using equation (27 a and b) and these were used to calculate the hemoglobin saturation. These results are displayed in Table 3.14 along with the total concentration of hemoglobin.

	Condition: Oxygenation	**Condition: Deoxygenation**
[Hb] (μM)	12.1	37.8
[HbO_2] (μM)	51.0	42.0
Total concentration (μM)	63	80
SO_2 (%)	81	53

Table 3.14: Oxy- and deoxyhemoglobin concentrations and hemoglobin saturation under different oxygenation conditions as estimated by time domain measurements. Also shown is the total hemoglobin concentration.

There is a significant decrease in oxyhemoglobin concentration and an increase in deoxyhemoglobin concentration following arterial occlusion, as expected. This results in

a decrease in hemoglobin saturation, from 81% to 53%, following deoxygenation of the tissue. Varying the contribution of water to the background does not significantly affect the hemoglobin saturation. Increasing the concentration to 80% or decreasing it to 60% changes the predicted SO_2 by less than 1%.

3.6.3 Further *in vivo* Measurements

Since initial *in vivo* measurements met with success, further investigations of the temporal oxygenation changes induced by occlusion were performed. The same volunteer was measured under the same conditions in the same location on the palm. The first measurement had a collection time of two minutes and was performed under normal oxygenation conditions. Once more, arterial occlusion was induced using a blood pressure cuff at a pressure of 240 mmHg; after waiting 30 seconds for deoxygenation to begin, three consecutive measurements, each lasting 40 seconds were performed. Following the final measurement, the cuff was removed allowing blood flow to resume in the hand. Another measurement with a collection time of two minutes was performed one minute later. The one minute delay was to allow for the tissue to return to its normal state.

The results from these measurements are shown in Table 3.15. The scattering coefficient remained relatively constant throughout the measurements. As expected, it was measured to be lower at 810 nm than at 750 nm. Qualitatively, the absorption also changed as expected, it increased at 750 nm and decreased slightly at 810 nm during deoxygenation. The values for absorption and scattering were also similar to those measured in the preceding section.

Wavelength (nm)	Oxygenated or Deoxygenated	χ^2	μ_a (mm^{-1})	μ_s' (mm^{-1})
810	oxy	1.39	0.02072	1.3362
750	oxy	1.55	0.02024	1.4105
810	1st deoxy	1.23	0.01850	1.4174
750	1st deoxy	1.27	0.02211	1.4950
810	2nd deoxy	1.33	0.01845	1.4705
750	2nd deoxy	1.20	0.02247	1.4625
810	3rd deoxy	1.23	0.01851	1.4581
750	3rd deoxy	0.88	0.02259	1.4625
810	oxy	1.62	0.02110	1.4405
750	oxy	1.60	0.02147	1.5463

Table 3.15: Optical properties estimated from *in vivo* measurements on the hand at two wavelengths under normal conditions (oxy) and during various stages of arterial occlusion (deoxy).

Application of the same method as in the previous section allowed for the calculation of the oxy- and deoxyhemoglobin concentrations and the hemoglobin saturation from the estimated values of the absorption coefficients. The results from these calculations are shown in Table 3.16. There was a significant decrease in oxyhemoglobin concentration and hemoglobin saturation during arterial occlusion, as expected. However, in contrast to the previous section where an increased total

	Normal (pre-occlusion)	1st deoxy	2nd deoxy	3rd deoxy	Normal (post-occlusion)
[Hb] (μM)	23.9	34.8	36.2	36.4	27.4
[HbO_2] (μM)	56.1	37.9	36.5	36.5	54.6
Total concentration	80.0	72.7	72.7	72.9	82.0
SO_2 (%)	70	52	50	50	67

Table 3.16: Hemoglobin, oxy- and deoxyhemoglobin concentrations and hemoglobin saturation under different oxygenation conditions. Deoxygenation measurements were performed consecutively to reflect changes in the oxygenation state with time.

hemoglobin concentration was observed, there was a small decrease in total hemoglobin concentration during deoxygenation. Again, the concentration of deoxyhemoglobin increased during the measurement, as expected. Between the second and third measurement, from approximately 100 seconds to about 150 seconds after occlusion, no changes in the oxygenation status of the tissue were detected by the system. The measurement performed under normal conditions after arterial occlusion showed that the hemoglobin saturation and the concentrations returned to pre-measurement levels. The changes of the various parameters over time are better illustrated graphically, in Figure 3.13. Time to allow for storing of reflectance spectra during the measurement is estimated.

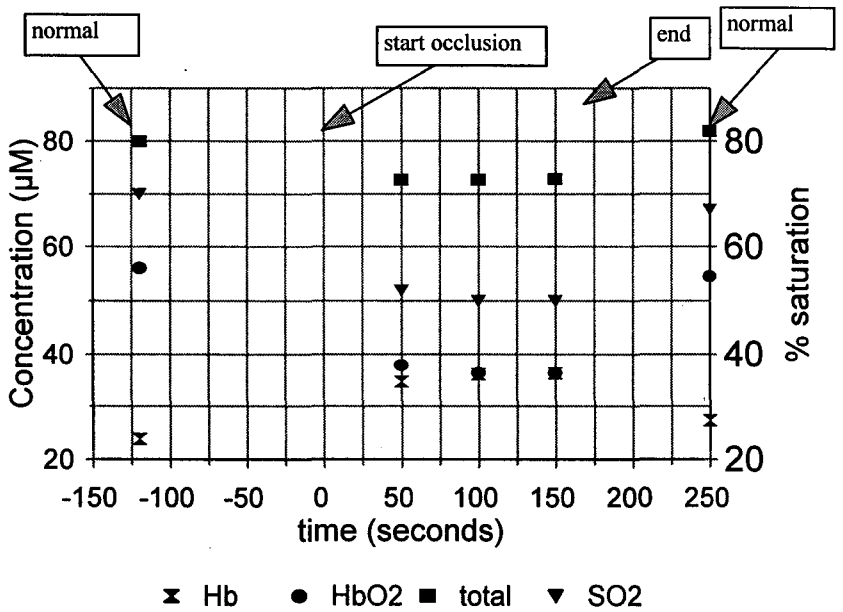

Figure 3.13: Variation of total hemoglobin, oxy- and deoxyhemoglobin concentrations and hemoglobin saturation with time under various stages of arterial occlusion.

Figure 3.13 shows the temporal changes of the four parameters. With the exception of the total hemoglobin concentration, the values change as expected with the oxygenation conditions induced. No changes between the second and third deoxygenation measurements are evident. These results will be investigated in more detail and will be compared to other measurements performed using other techniques in the next section. However, these measurements have demonstrated that the time domain system is capable of reflecting induced changes in oxygenation *in vivo*. The hemoglobin saturation values calculated from this method appear sensible and variations over time are detectable.

4 DISCUSSION

4.1 Polystyrene Spheres

The results obtained from the two experiments using varying concentrations of polystyrene spheres in water showed large deviations from the theoretical values and large variations between the different methods. The variation between the methods was surprising, as all three methods rely on the same theory to model the experimental reflectance. The primary aim of this section is to investigate reasons for the large overestimation of the scattering coefficient by the time-resolved system. Although comparisons will be made to other systems as a means of doing this, the nature of their deviations is not the focus of this thesis. The differences observed when measuring polystyrene were consistent with previous results and must be due to a systematic problem in the measurement method or in the analysis.

4.1.1 Effect of Source detector separation on estimated scattering coefficient

Since in section 3.4.2, it was found that the size of the phantom did not affect the estimated μ_s', it is clear that the size of the phantom was not a factor in the poor results. However, the scattering coefficient measured was dependent on the ρ value used. The errors for measurements performed at 10 mm were about 30%, while the errors on the two phantoms (s7 and b7) were only about 15% at 20 mm. In section 2.2.1(D), the errors

in fitting Monte Carlo data convolved with an IRF were determined to be about 11% at 10 mm and 8% at 20 mm. Therefore, only a portion of the overestimation observed here can be accounted for by limitations in the diffusion theory model.

Another factor that might affect the results obtained in the time domain is the presence of the wide IRF convolved with the reflectance. Although this is, in principle, accounted for by convolution of the theoretical data with the experimental IRF, it is possible that it is still altering the results. A better way to limit the effects of the IRF is to perform the fitting in the frequency domain as described in 2.2.3. Since measurements at two distances were available for the final phantoms in the series of polystyrene experiments, a relative distance frequency domain fit was performed on these data. The phase and amplitude were also calculated using the theoretical optical properties of the phantoms. The fitting range used for these data was from 0 to 600MHz. Previous results, section 2.2.3, suggested that a maximum frequency to which the data should be fit was about 1-3 GHz, but noise in the data limited this maximum to 600 MHz in this case. Results from these fits are shown in Table 4.1. The scattering values estimated are lower than the theoretical values by 6%. Thus, the results from this analysis are more

Phantom	**μ_a measured (mm^{-1})**	**μ_a theory (mm^{-1})**	**μ_s' measured (mm^{-1})**	**μ_s' theory (mm^{-1})**	**% error in μ_s'**
s7	0.00145	0.002	1.474	1.575	-6
b7	0.00211	0.002	1.511	1.615	-6

Table 4.1: Results of frequency domain fits on two polystyrene phantoms.

accurate than the results from either time domain fit. The absorption coefficient is fit with about the same accuracy as in the time domain. There was good agreement between the fit and the data over the entire fitting range. There were no significant differences between the phase and amplitude predicted by theory and the experimentally measured values for frequencies below 200 MHz. Differences were seen at larger frequencies, but they were not systematic. The frequency domain approach produced more accurate estimations of the scattering coefficient for these phantoms. When Monte Carlo data were fit using this approach for 20 mm reflectance relative to 10 mm reflectance, the optical properties returned were dependent on the maximum frequency to which the data were fit. The errors observed in these frequency domain fits were closer to those observed in the corresponding Monte Carlo fits than those seen in the time domain case. To investigate if the frequency domain fitting method improved the optical properties returned in all cases, results from other phantoms were analyzed using this technique, where data at multiple distances were available.

4.1.2 Further Measurements using Large Volume Phantom

The phantom that was used to investigate the effects of phantom size on μ_s' in section 3.4.2 was remeasured at four different distances. The theoretical optical properties of this phantom were $\mu_a = 0.002$ mm^{-1} and $\mu_s' = 0.910$ mm^{-1}. The resulting data were fit using a variety of approaches. The following fits were performed: four time domain fits, six two distance frequency domain fits and one frequency domain fit which used all four distances. The time domain and two distance frequency domain fits were performed in

the same manner as described previously. The multidistance frequency domain fit minimized the differences between the fit and the experimental data for three distances relative to 10 mm simultaneously. The results obtained from these different fitting techniques are displayed in Table 4.2. The estimates of the absorption by the time domain fitting technique do not vary systematically with the ρ value used. In contrast, the estimate of μ_s' improves as the source detector separation increases. This change was expected from 10 mm to 20 mm but it was thought that there would be little difference at larger ρ values. The diffusion approximation should perform as well at 20 mm as it does at 40 mm; however, it seems that this is not the case. The quality of the fits improves with distance as well. The χ^2 value decreases from 2.1 at 10 mm to 1.15 at 40 mm. This variation in the χ^2 value is not due to poorer statistics as the number of counts for each measurement was kept constant.

The fits performed in the frequency domain do not show the obvious trend that the time domain fits do. Of all the frequency domain fits, the four most accurate are those which make use of the reflectance data collected at 40 mm. The fit of 40 mm relative to 30 mm data produces extremely accurate results with errors in both coefficients less than 2%. The errors seen in the 20 mm relative to 10 mm data are much larger here than in the previous section (27% versus 6%). There does not seem to be an improvement in the values of the coefficients returned if the multidistance approach is used. Figure 4.1 shows the fits of phase and modulation versus frequency for the 40 mm relative to 20 mm data. There is good agreement between the fit and the data for most of the range, but at

the high frequency end deviations are apparent. Since the multidistance approach is a

Fitting Method	μ_a measured (mm^{-1})	μ_s' measured (mm^{-1})	% error in μ_s'
time (10 mm)	0.00265	1.274	40
time (20 mm)	0.00239	1.182	30
time (30 mm)	0.00255	1.148	26
time (40 mm)	0.00239	1.046	15
frequency (40/10mm)	0.00245	1.058	16
frequency (30/10mm)	0.00286	1.157	27
frequency (20/10mm)	0.00261	1.157	27
frequency (40/20mm)	0.00246	1.022	12
frequency (30/20mm)	0.00360	1.206	33
frequency (40/30mm)	0.00197	0.923	1
frequency (40, 30, 20/10mm)	0.00253	1.087	19

Table 4.2: Results of various frequency domain fits and time domain fits on large volume phantom. Theoretical properties are $\mu_a = 0.002\ mm^{-1}$ and $\mu_s' = 0.910\ mm^{-1}$.

new method, the graph of the multidistance fit is shown. Figure 4.2 shows this fit, the data and the theoretical results. From this, the differences between the experimental data and the theoretical data are evident. The modulation data appears to be in better agreement than the phase data over the entire fitting range.

a

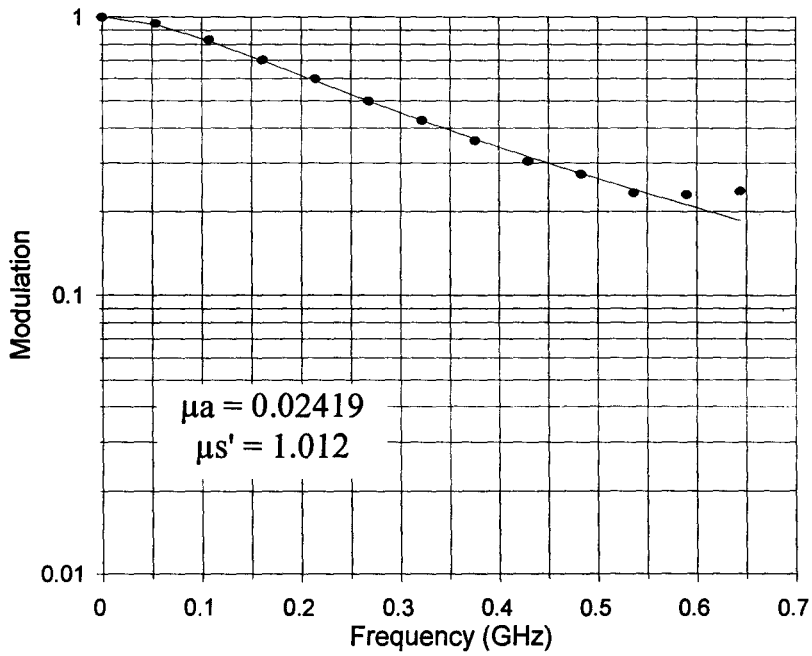

b

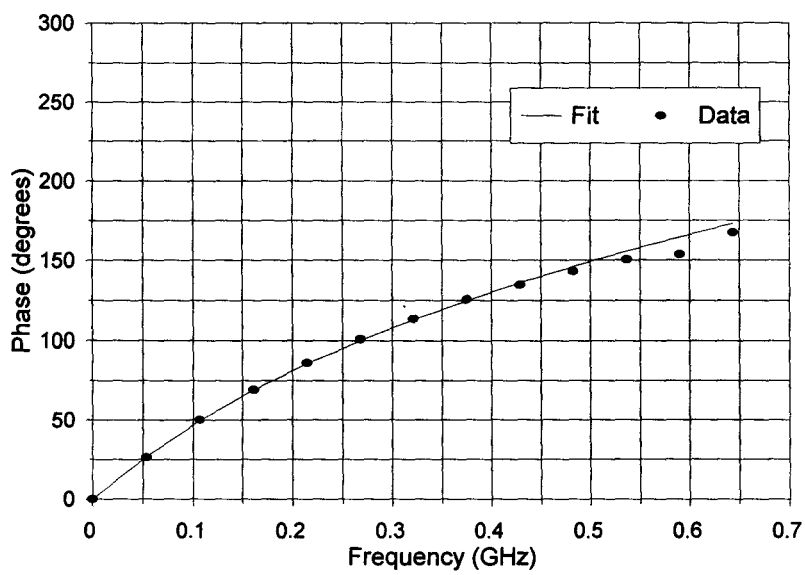

Figure 4.1: Example of a typical frequency domain fit on polystyrene phantom with theoretical optical properties of $\mu_s' = 0.910$ mm^{-1} and $\mu_a = 0.002$ mm^{-1}. Results are for 40 mm relative to 20 mm data (a) modulation and (b) phase.

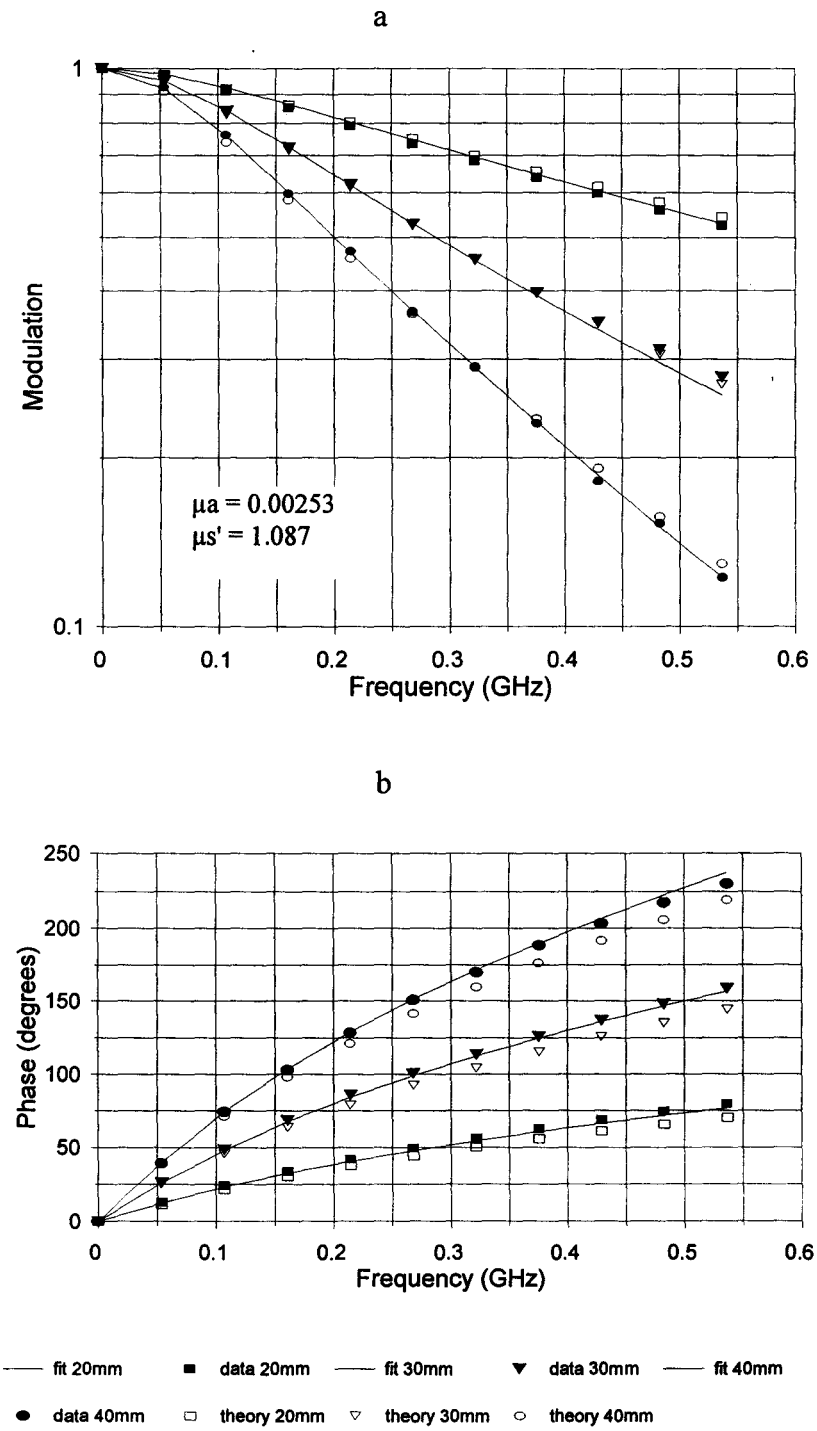

Figure 4.2: Results from fitting 3 distances simultaneously. Also shown are theoretical results (μ_s'= 0.910 mm^{-1} and μ_a = 0.002 mm^{-1}).

Another concern that must be addressed is the assumption that there is no mismatch in the indices of refraction between the black plastic probe and the suspension of polystyrene microspheres in water. To investigate these, results from measurements performed at 20 and 10 mm were analyzed using the frequency domain approach with varying mismatches. When the data were fit assuming no mismatch, i.e. n=1, the results were $\mu_s' = 1.157\ mm^{-1}$ and $\mu_a = 0.00261\ mm^{-1}$. Varying the relative n value by 15% had no significant effect on either optical property; results returned agreed with the initial estimates to within 1%. Therefore, if there was a small mismatch in the refractive indices it was not contributing a significant amount to the errors associated with estimating optical properties. In addition, to see any significant effect on the results, large mismatches, e.g. n=2, had to be assumed and it is highly unlikely that such a difference would exist under these experimental conditions.

To determine if there were difficulties associated with the measurement method, this phantom was measured using the frequency domain system described previously. This system measures phase and modulation at a constant frequency, 100 MHz, for varying ρ values. The time domain measurement when analyzed in the frequency domain produced results at varying frequency but at a constant source-detector separation. However, one of the frequencies at which data were available from this method happened to be 100MHz. Using the time domain method, the phase difference for a source detector separation of 10 mm, at 100 MHz can be calculated in three different ways, 20 versus 10, 30 versus 20 and 40 versus 30 mm. The average phase difference was found to be 24.8°

for these conditions. In the frequency domain method, the phase differences can be found by subtracting the phase measured at 9 mm from the measurement at 19 mm or the 11 mm result from the 21 mm result. So two phase differences can be calculated for ρ=10 mm at 100 MHz and these can be compared to the time domain values. The average phase difference from the frequency measurements was also 24.8° indicating that the two methods acquire the same phase information. The differences that exist between the methods were, therefore, not due to differences in the data collected.

4.1.3. Investigation of Total Attenuation Coefficient of Polystyrene

To verify that the characteristics of the suspension of polystyrene spheres were as calculated by Mie theory, direct measurements were performed to determine the variation of the total attenuation coefficient, μ_t with concentration of polystyrene. The total attenuation coefficient is the sum of the absorption and scattering coefficients. It can be theoretically calculated for a known concentration of polystyrene using Mie theory to predict the scattering and assuming an absorption equal to that of water. The total attenuation was determined by a narrow beam transmission measurement using a diode laser. To ensure that scattered light was not incident on the detector, the source and detector were separated by a large distance, about 1.5 m, and the acceptance angle of the detector was limited by the use of a collimator. A similar measurement was performed using a white light source. Both experimental and theoretical values of μ_t were determined relative to water. Figure 4.3 displays the measured versus theoretical results.

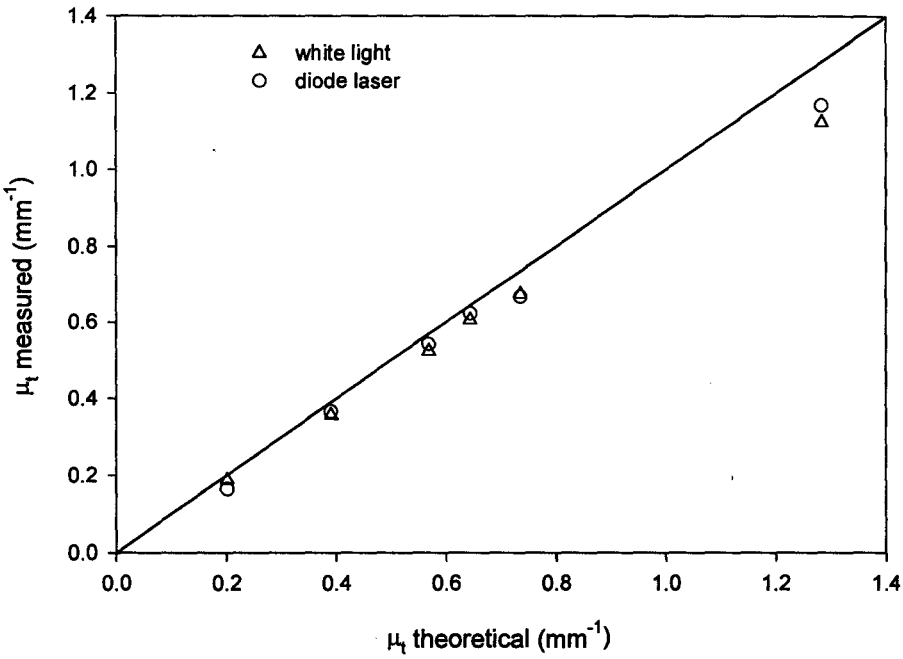

Figure 4.3: Measured versus expected μ_t values for varying concentrations of polystyrene spheres in water. Measurements were performed using two different light sources.

There was good agreement between measurement and theory for five of the concentrations measured. However, there was a systematic underestimation of the μ_t value that appeared to increase with increasing concentration. This is probably due to collimation problems which become more evident as the concentration and therefore the probability of scattering, of polystyrene increases. Overall, it appears that there is good agreement between the measured and theoretical μ_t values and therefore that spheres sizes were accurate and concentration calculations were performed correctly.

4.1.4 Comparison of Theoretical Data from Time Domain and CW Fitting Programs

Since there were large differences between the results obtained from the time domain

and the spatially resolved measurements, it was necessary to investigate differences in the forward calculation of reflectance used by the different routines. For typical optical properties used in the polystyrene experiments, μ_a = 0.002 mm^{-1} and μ_s' = 1.0 mm^{-1}, theoretical data were generated using the fitting routine employed by the spatially resolved system. In the time domain, theoretical data sets were generated for four different source detector separations. These data sets were Fourier transformed and the amplitude of the DC signal was calculated for each set. The DC amplitudes were normalized to the smallest ρ value, which was 6 mm. The spatially resolved amplitudes at the same four distances were similarly normalized. The results from this are shown in Table 4.3 and graphically in Figure 4.4.

ρ (mm)	DC Amplitude Spatial	DC Amplitude Time
6	1	1
8	0.4241	0.4248
10	0.2098	0.2101
12	0.1149	0.1151

Table 4.3: Theoretical predictions, from two different approaches for the amplitude of the DC component of the reflectance through a medium with μ_a = 0.002 mm^{-1} and μ_s' = 1.0 mm^{-1} at four different ρ values.

As expected, there was excellent agreement between the two different methods. The expressions for the reflectance used by each technique were the same except one

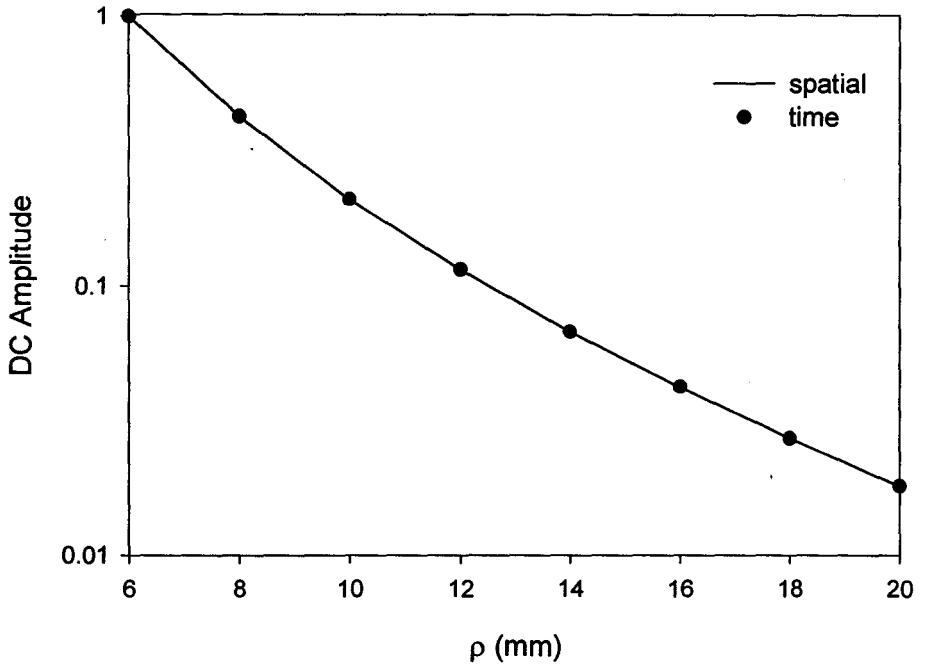

Figure 4.4: Variation of the predicted DC amplitude of the reflectance with ρ using two different forward calculations, one based in the spatial and the other in the time domain.

expressed reflectance as a function of ρ and the other as a function of time and ρ. Therefore, it was expected that the calculated DC amplitudes would be exactly the same. The variations observed were small and were most likely due to rounding errors in the Fourier transform of the time domain data. The differences between the two were small enough, less than 0.2%, to be considered insignificant.

4.1.5 Effect of Scattering Time Delay on Estimates of μ_s'

Thus far, none of the factors investigated could individually account for the large deviations observed between the measured and theoretical scattering coefficients. Although a portion of the error observed is probably due to limitations of the diffusion model for a source detector separation of 10 mm, this is unlikely to be much larger than

10% according to the fits of Monte Carlo data. A possible explanation for the discrepancies could be the existence of a scattering delay not accounted for with the current diffusion theory model. Yaroslavsky *et al.* (1997) suggested a modification to the diffusion theory to account for the small, yet finite amount of time spent by light undergoing a scattering event. If this is not accounted for, time domain measurements should underestimate the absorption and overestimate the scattering coefficient. This has been seen in other studies, (Madsen 1992a) and is also observed here. Yaroslavsky reported good agreement between Monte Carlo data and the modified diffusion model. The effect of the scattering delay was taken into account by scaling the speed of light used in the model and is therefore simple to include. It should also be noted that this effect would not be observed when spatially resolved measurements are performed as the time dependence of the light propagation is not considered. The renormalization of the speed of light is simple to include in the model according to equation 28:

$$c_{eff} = \frac{c_o}{n_{eff}}, \text{ where } \quad n_{eff} = n + t_1 \mu_s c_o \qquad (28)$$

where c_{eff} is the renormalized speed , n_{eff} is the modified index of refraction, n is the standard index of refraction of the medium and $t_1$is the mean scattering delay time. The problem is that the value of t_1 is not known. It is likely that t_1 is between about 100 and 1000 fs (Yaroslavsky *et al.* 1997); for the results from Madsen *et al.* (1992a) an upper limit on the t_1 value of about 214 fs is proposed. Although these measurements were not performed using polystyrene, a similar tissue simulating phantom was employed. The differences observed in this thesis could be accounted for by a mean scattering delay of

about 125 fs, which appears to be on the order of what might be expected. It would not be possible to include this as another parameter in the fitting procedure because the variables are coupled, i.e. μ_a and c always appear as a product. The development of a model based on the microscopic structure of the medium to predict t_1 has not been performed. However, this scattering delay seems to be a possible explanation for the errors observed in the time domain estimates of μ_s'.

4.2 Variation of Absorption with added ICG in the Frequency Domain

Although the results obtained through the time-resolved analysis of the data from the experiment using indocyanine green to vary the absorption of a polystyrene phantom were promising, a frequency domain analysis of the data was also undertaken. It was important to see if any advantage could be gained by employing the frequency domain analysis, especially for large ρ values where the time domain results were already accurate. The same approach was applied here as in section 4.1.2, six different distance combinations were fit, as well as a multi-distance (relative to 10 mm) approach. The data were fit to a maximum frequency between 500 MHz and 1 GHz, depending on the noise in the data. The theoretical scattering of this phantom was 1.093 mm^{-1} and the absorption was calculated using the measured absorption of ICG.

An example of a fit showing modulation and phase is shown in Figure 4.5 for 30 mm relative to 20 mm reflectance data. The estimated optical properties for this phantom are $\mu_a = 0.0138$ mm^{-1} and $\mu s' = 1.126$ mm^{-1} and the expected values are $\mu_a = 0.014$ mm^{-1}

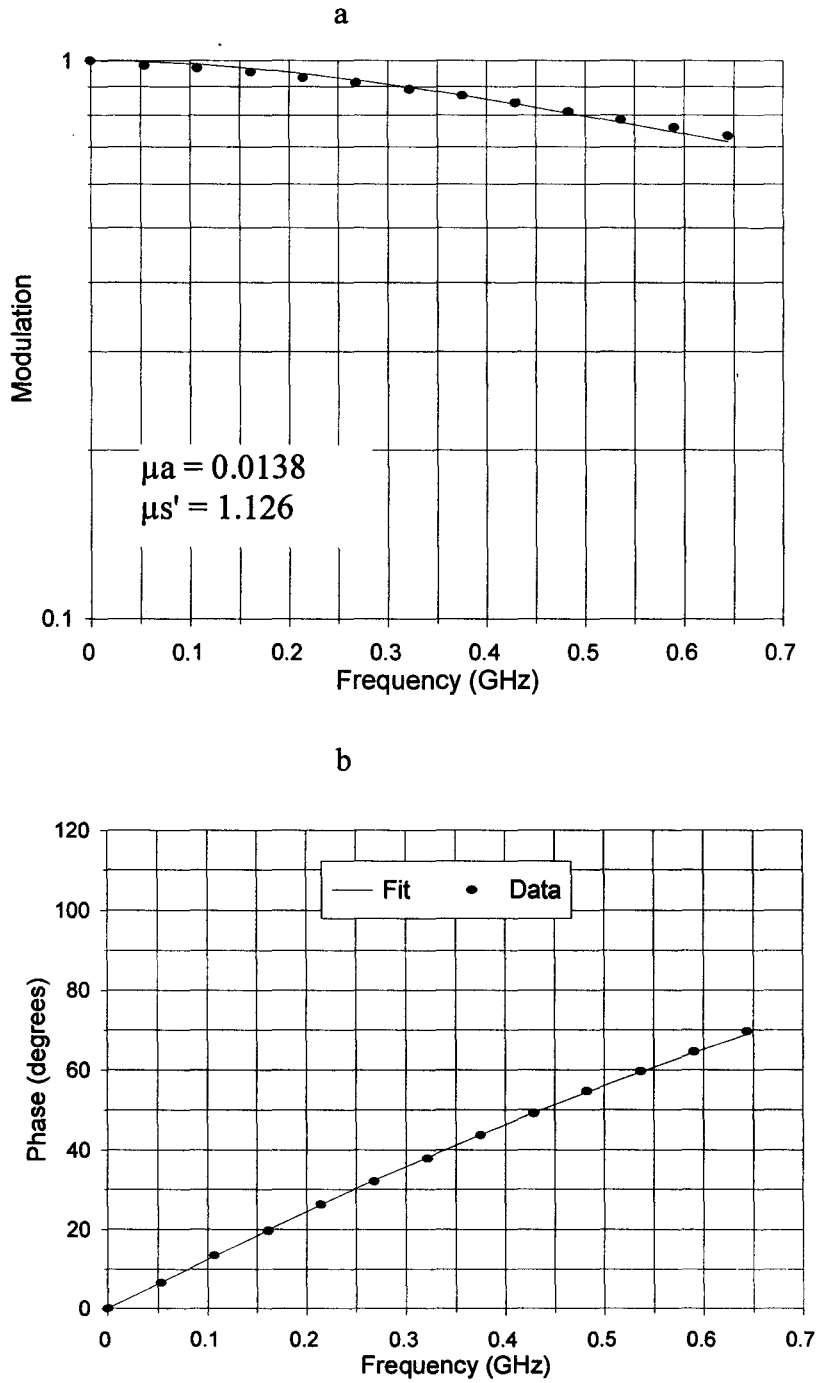

Figure 4.5: Frequency domain fits (a) modulation and (b) phase for measurements on polystyrene phantom with added ICG. The expected values for the optical properties are μ_a = 0.014 mm^{-1} and μ_s' = 1.093 mm^{-1}. The data is from 30 mm relative to 20 mm reflectance measurements.

and μ_s' = 1.093 mm^{-1}. There is good agreement between the fit and the data over the entire fitting range. A complete summary of the frequency domain results is displayed graphically in Figure 4.6. The top graph, Figure 4.6a shows the variation of measured μ_a with concentration of ICG for the frequency domain results and the transmission measurement, while Figure 4.6b shows the scattering coefficient estimated by the various fits and the theoretical μ_s' value.

From Figure 4.6a, it is clear that for the highest concentration of ICG, all estimates of absorption are similar, while the variation is much larger for lower μ_a values. Also, as seen in Figure 4.6b, most estimates of μ_s' are within about 10% of the theoretical value. A better way to examine this information quantitatively is to perform linear regression of the absorption versus the ICG concentration, as was done in section 3.5.2. The results from this are shown in Table 4.4 for all measurements, including the previous results from the time domain analysis. The results in italics indicate those slopes which agree with the slope predicted by the absorbance measurement, within uncertainty.

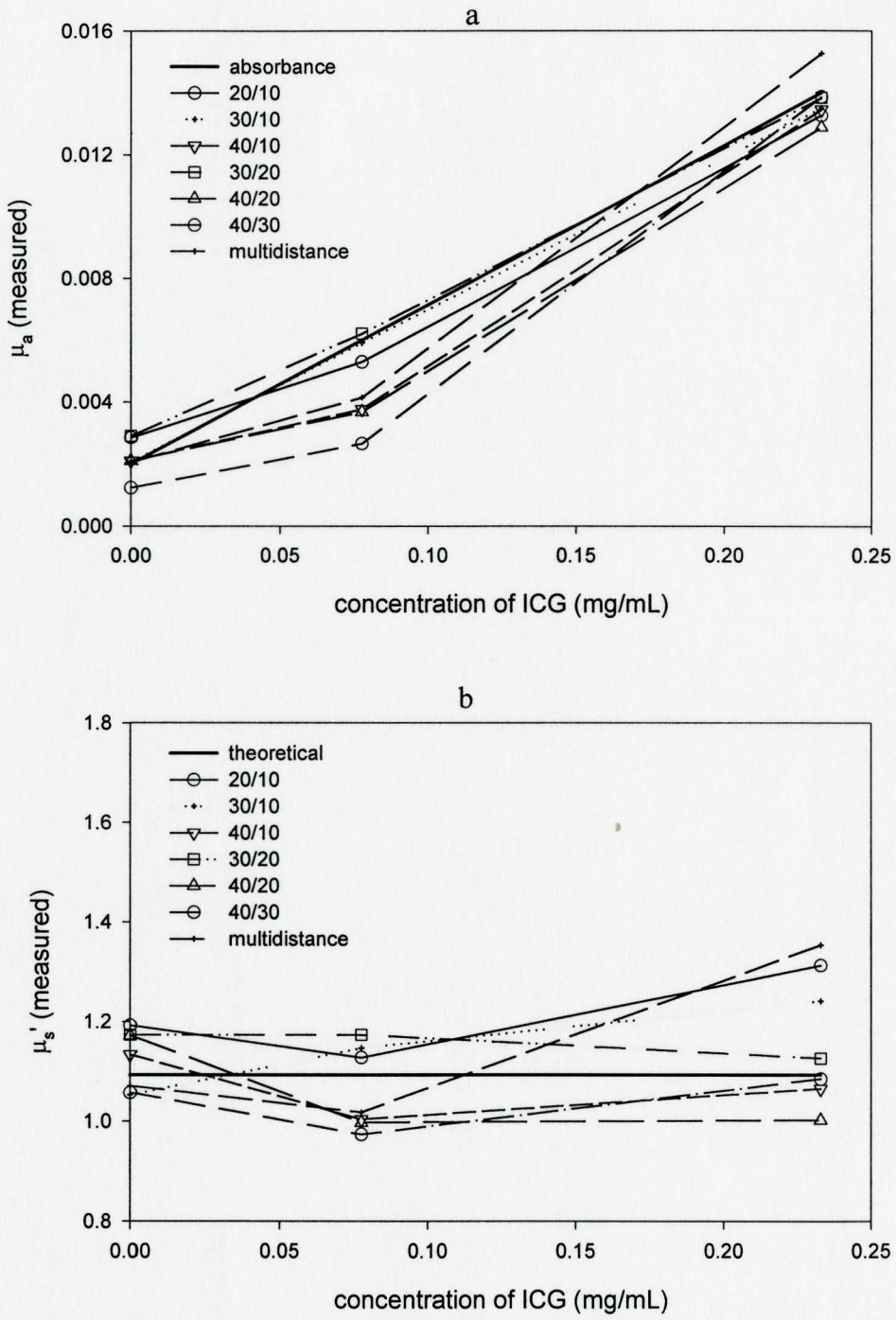

Figure 4.6: Variation of (a) absorption and (b) scattering with increasing concentration of ICG in a polystyrene phantom for various frequency domain results. Optical properties are in units of mm^{-1}

Method	Slope $\times 10^{-2}$ (mm %)$^{-1}$	Intercept (mm^{-1})	R^2
absorbance	5.2	0.0020	1
time (10 mm)	3.6 ± 0.2	0.0027 ± 0.0003	0.998
time (20 mm)	*5.1 ± 0.9*	*0.0018 ± 0.0015*	*0.968*
time (30 mm)	*5.1 ± 0.4*	*0.0018 ± 0.0007*	*0.994*
time (40 mm)	*5.3 ± 0.6*	*0.0015 ± 0.0014*	*0.977*
20/10	4.5 ± 0.1	0.0028 ± 0.0001	0.999
30/10	4.8 ± 0.1	0.0022 ± 0.0002	0.999
40/10	*5.1 ± 0.9*	*0.0013 ± 0.0016*	*0.967*
30/20	4.6 ± 0.3	0.0032 ± 0.0005	0.996
40/20	4.8 ± 0.3	0.0014 ± 0.0014	0.971
40/30	*5.6 ± 1.1*	*0.0022 ± 0.0019*	*0.962*
multi	*5.8 ± 1.0*	*0.0012 ± 0.0017*	*0.972*

Table 4.4: Results of linear regression of μ_a versus ICG concentration. Results in italics indicate slope predictions that agree with expected values with uncertainty.

In general, it does not appear that the frequency domain analysis is more accurate than the time domain results for ρ values larger than 10 mm. If there are no limitations on the source detector separation, i.e. there is adequate signal at large ρ values, time domain analysis is probably the best method to use to predict the optical properties of the sample. However, it must be noted that the ability of the time domain analysis to predict

μ_s' is dependent on the source detector separation used. Larger errors were observed in the time domain at 10 mm than at any larger ρ value. Also, for absorption similar to that of water, as seen in section 4.1.2 with the large volume polystyrene phantom, larger errors in μ_s' were observed for the time domain fits, from 15 to 26%, even at large ρ values compared to the errors observed in this section with added absorber, where μ_s' errors were about 10%. Another factor to consider is that frequency domain analysis has the advantage that it is less time consuming than the corresponding time-resolved fitting procedure.

4.3 *in vivo* Dual Wavelength Measurements

In the first *in vivo* measurements on the palm of the hand, the normal hemoglobin saturation was estimated to be 81% and following deoxygenation, this decreased to 53%. The total hemoglobin concentration was estimated to be about 63 μM under normal oxygenation conditions. Similar results were obtained in the second experiment, the normal SO_2 was calculated to be 70% and arterial occlusion reduced this value to about 50%. In this instance, the hemoglobin concentration was found to be about 80 μM. Much of the previous research in this area has been concerned with cerebral oxygenation. Obviously, the oxygenation status of the hand and the brain are likely to be different, however, for comparison some results will be discussed. Measurements performed on the rat brain found the normal hemoglobin saturation to be 97% and the total hemoglobin

concentration to be 62 ± 6 μM (Matcher and Cooper 1994). Although the hemoglobin concentration measured here was similar to this, the hemoglobin saturation measured in the hand was lower than in the brain. Similarly, Oda *et al.* (1996) estimated an SO_2 of about 85% in the rat head under normal conditions. More relevant to this thesis, the range of total hemoglobin concentrations encountered clinically is between 20 μM and 100 μM (Matcher and Cooper 1994) and the values estimated in the two experiments performed here fall within this range. Also, Fantini *et al.* (1994) performed a similar *in vivo* measurement using a frequency domain approach and a blood pressure cuff to occlude blood flow in the arm. The calculated hemoglobin saturation in the forearm, under normal conditions was about 80% and dropped to about 45% following occlusion. These results are comparable to those observed in this thesis. Actually, considering the differences between the experiments, different measurement techniques, subjects and placement of probe the agreement between the results is quite good. Yu *et al.* (1997) performed measurements on the finger and found the hemoglobin saturation, under normal conditions to vary between about 80% and 85%, again similar to results observed in this thesis.

The previous experiments described in this thesis have involved phantoms which are likely to satisfy the model assumptions of a semi-infinite homogeneous medium. How well the tissue volumes probed in these experiments abide by these assumptions is unclear. Although the volumes probed are probably large enough to be considered semi-infinite, it is unlikely that they could be considered perfectly homogeneous. The

presence of blood vessels and other structural heterogeneities would, in theory, compromise this assumption. Liu *et al.* (1995b) found that the absorption coefficient of tissue was a volume-weighted sum of the absorption coefficients of blood and background tissues, if the vessel diameters were less than about 800 μm. They also found that scattering heterogeneities did not significantly affect the determination of the absorption coefficient. Therefore, for tissue volumes that do not contain many vessels greater than 1 mm in diameter, the sample can be considered adequately homogeneous for the purpose of measuring μ_a.

Depending on the anatomical location of the measurements, it might be advisable to implement more complex models than the homogeneous semi-infinite medium. For example, measurements performed on the head may benefit from a layered model of the skull, as proposed by Okada *et al.* (1997). Also, recent models describing tissue as a two layered structure may provide a more accurate model in many situations (Kienle *et al.* 1998). Skin and many other organs have a layered structure which can be accounted for using diffusion models. Kienle *et al.* (1998) concentrated on situations where the top layer thickness is known and the underlying layer is considered semi-infinite, as would be the case for muscle with an overlying layer of fat and skin. They found that they could determine the optical properties of both layers when the thickness of the first layer was known. Furthermore, of the three techniques employed, time, steady-state or frequency domain, the time domain measurements showed the greatest potential for determination of the optical properties of multi-layered media. In some instances, a multi-layered

structure of the tissue may be necessary; this too is possible using diffusion theory models.

Measurements performed *in vivo* suffer from the further disadvantage that true values are not available, for either optical properties or for oxygenation parameters. Although both optical and oxygenation parameters determined in this investigation appear to be sensible, in terms of previous measurements and anatomical knowledge, it is impossible to quantify the errors associated with these measurements. Since these experiments have indicated that the system has potential for the noninvasive determination of hemoglobin saturation, it is now necessary to investigate how accurately it can do this. Design of experiments in which oxygenation status can be controlled and measured through another method would although for a better characterization of the system performance. For example, a liquid phantom containing a turbid material, blood and supplied with oxygen would allow for the measurement of an oxygenated system. Other researchers have then introduced yeast into such a system to consume oxygen and deoxygenate the phantom (Liu 1995a). Alternatively, nitrogen, in place of oxygen can be bubbled through the solution to produce deoxygenation (Cope 1991). In order to better quantify the accuracy of the system in the determination of oxygenation status of tissue, an experiment with controlled variables is necessary.

4.4 Uncertainties

There has been no discussion thus far of the uncertainties associated with the coefficients measured. Although systematic errors have been discussed, in terms of

comparisons to standard or theoretical values, other errors exist. The fitting routine itself was designed to return an error estimate for both optical properties. In general, since the fits and the data showed good agreement, these errors were small, usually less than 1% in either coefficient. Another error estimate, representative of the short term stability of the system, can be made from the series of ten measurements on Marley 8 (section 3.3.1). Taking the errors to be one standard deviation, instabilities of the system contribute an error of about 1.5% for both optical properties. This can be compared to the long term stability errors, which are about 5% for μ_a and about 10% for μ_s'. These are estimated from numerous measurements on the Marley 8 phantom over the course of a year. Therefore, although for shorter time periods the variability is not large, over longer time spans, larger errors are possible. Errors estimates associated with coupling to the solid phantoms were estimated to be about 5% for absorption and 4% for scattering from measurements performed in section 3.3.2. Inhomogeneities across the surface of the phantom did not introduce any more error than the errors seen in coupling of the probe and phantom.

Another approach to examining the errors associated with the estimated optical properties is to investigate the variability associated with one optical property when the other one is being varied. For example, in the experiment involving increasing concentrations of polystyrene spheres, the absorption coefficient should remain constant. However, variations of up to 30% in μ_a were observed. Similarly, in the experiment with increasing concentrations of indocyanine green, it was expected that μ_s' remains constant.

The variations observed in the scattering coefficient were about 12%. It is not unexpected that the variations observed in these experiments were larger than in other experiments, due to the fact that the other optical property was being varied in these two cases.

The final error source that was investigated was the effect of statistics on the standard deviations associated with either optical property. In section 3.3.2, it was found that for a typical number of counts, for example between 500 and 4000 counts in the peak channel, the errors associated with either coefficient were about 2%. For fewer peak counts, these errors increased to about 7% in μ_a and 4% in μ_s'. The differences observed between the estimates of optical properties from the reflectance collected for two seconds and those at thirty seconds, which were most likely to show a difference, were significant. The p-value for the absorption coefficients was 0.007 and the scattering coefficients was 0.020. Therefore, the average optical properties were different, in the measurements performed for two seconds, the errors observed were larger for the two second measurements. Statistics can contribute to significant errors in the optical properties estimated, however, this was only observed for much poorer statistics than were used in any of the experiments performed. Also, there were no differences observed between the intermediate and the longer counting times. It is therefore, not necessary to count for long time periods. Other random sources of error must be the largest contributors to variation; statistics is not the limiting factor for the experiments discussed in this thesis.

5 CONCLUSIONS

This thesis described the design and characterization of a system for the noninvasive determination of tissue optical properties. Determination of the optical properties of tissue provides knowledge regarding the physiological status of the sample. In the near infrared, light penetrates well into tissue, but undergoes both absorption and scattering. From the light that is scattered out of the tissue, the reflectance, it is possible to estimate the optical properties of the medium through the application of a suitable model. Under biological conditions, the diffusion approximation provides an adequately accurate model of the transport of light in tissue, in certain circumstances.

The principle of time domain measurements is as follows: when a short, narrow pulse of light is incident on a turbid medium, it is broadened and attenuated due to scattering and absorption. The reflectance is then collected and fit with the diffusion theory. It is assumed that the medium is homogeneous, semi-infinite and that there is no mismatch in the indices of refraction between the probe and the phantom. The fitted reflectance provides an estimate for the optical properties of the medium. By performing measurements at two wavelengths and exploiting the known differences in absorption between oxyhemoglobin and deoxyhemoglobin at those wavelengths, it is then possible to determine the hemoglobin saturation of the tissue. The hemoglobin saturation is the percentage of hemoglobin molecules that are bound to oxygen and is indicative of the oxygenation status of the tissue. The noninvasive determination of hemoglobin

saturation has applications in monitoring cerebral oxygenation of neonates and oxygen levels in the treatment locale for both photodynamic therapy and radiation therapy.

The system used in these experiments differs from the standard time domain apparatus because it employs inexpensive pulsed diode lasers as light sources and uses a miniature photomultiplier tube to collect the reflectance. Previous researchers have used lasers which are large, expensive, complex, and hence not ideal for clinical use. Furthermore, the photomultiplier tube used in these studies is much less expensive than the standard tube. The diode lasers operate at 750 nm and 810 nm, wavelengths at which there are distinct absorption differences between oxyhemoglobin and deoxyhemoglobin. Their low power ensures that they are safe for *in vivo* use, yet they provide adequate signal for measurements to be possible. The system can be controlled such that they alternately irradiate the sample and hence simultaneous dual wavelength measurements can be performed. However, before these measurements were undertaken, it was necessary to study the performance of the computer routines in estimating optical properties and the ability of the system to measure the optical properties of tissue simulating phantoms.

The fitting routine is based on the standard non-linear least squares fitting approach. In the time domain the process is complicated by the fact that the reflectance is convolved with the instrument response function, which is indicative of the temporal spreading of the signal due to the electronics and the PMT. In order to compensate for the presence of the IRF, the theoretical data are convolved with the experimental IRF and

compared to the experimental reflectance. Since this convolution must be performed with every iteration, the time domain fitting procedure can be time consuming.

In order to determine how well this routine performs, it was tested under a variety of conditions. Initially, the accuracy of the program in fitting diffusion theory data with the diffusion theory was determined. This confirmed that the program was functioning properly. Diffusion theory data with added noise were then fit under a variety of source detector separations and combinations of optical properties. The largest errors observing when varying ρ and fixing the optical properties, about 3% in either coefficient, were observed at ρ = 10mm. Under different combinations of μ_a and μ_s', the errors in both coefficients increased to about 4%. Despite the addition of noise to the data, it was still possible to determine the optical properties with acceptable accuracy.

Monte Carlo data were then fit under various conditions using the diffusion theory. The accuracy of the estimated optical properties depended on the optical properties themselves, the start time of the fitted region and the source detector separation. Fitting over the entire fitting range resulted in errors of about 8% in μ_a and 7% in μ_s' at 20 mm. Larger errors, 36% and 27%, were observed for μ_a and μ_s' at 10 mm. These errors could be decreased in either case to less than 4%, by removing the data collected at early times. This is because the early arriving photons are most likely to be in violation of the assumptions of the diffusion theory. To simulate a more realistic situation, Monte Carlo data were convolved with an experimentally measured IRF and fit using the diffusion model, modified to account for the IRF. Less dramatic improvements were seen in this case by varying the start time of the fit. In general, for either ρ value, it

was possible to determine μ_s' to within 10% and μ_a with an error of 5%. In general, errors are larger in μ_s' than μ_a and the estimated optical properties are higher than expected. The size of the error also depended on ρ; the error increased for smaller source detector separations.

Due to the time-consuming nature of the time domain routine, fitting in the frequency domain was investigated. This also makes accounting for the IRF a matter of algebra not convolution. The frequency domain and time domain diffusion equations are simply related through the Fourier transform. Diffusion theory data with added noise and Monte Carlo data, with and without an IRF were fit in the frequency domain. As in the time domain, better results were obtained at larger source detector separations and, by limiting the maximum frequency of the fit, improvements in the accuracy of the properties were observed. Limiting the high frequency components in the frequency domain is analogous to avoiding the steep rising edge of the pulse in the time domain. Overall, errors observed here were comparable to, or smaller than those observed in the time domain. The frequency domain approach does, in some cases, limit the significant influence of the IRF and improve the accuracy of the results. In addition, this technique is much faster than the time domain routine.

Preliminary experiments were performed using Intralipid and ink as a scatterer and an absorber respectively. Due to problems in quantifying the relationship between the concentration of either substance and the expected optical properties, these experiments did not prove particularly useful. Measurements were then performed on solid tissue simulating phantoms. Both the short term and long term stability of the

system were determined. Short term variations were about 1.5% for either coefficient. Long term stability was poorer, with variations of about 5% in μ_a and 10% in μ_s'. Statistics were not found to be a limiting factor in determining optical properties, except for cases with very poor statistics, i.e. less then a few hundred counts in the peak channel of the reflectance. The variation with source detector separation was also investigated; larger μ_s' values were measured at 10 mm than at 20 mm in all cases. Finally, the use of different boundary conditions was examined. Little difference was observed between the zero boundary condition (ZBC) and the more accurate extrapolated boundary condition (EBC). However, since small differences were observed and the EBC was no more difficult to model than the ZBC, this more physically plausible boundary condition was utilized.

To analyze the response of the system to variations in scattering, two experiments using a suspension of polystyrene spheres in water were performed. These spheres act as scattering centres and the scattering coefficient can be calculated if the concentration, sphere size and wavelength are known. Phantoms comprising spheres of two different diameters were measured at seven concentrations at a source detector separation of 10 mm. The variation of scattering versus concentration of spheres was overestimated by the time-resolved measurements by 25% and 32%, depending on the size of spheres used. However, the small differences between the sphere sizes are insignificant compared to the large deviations from expected results. The absorption coefficient remained relatively constant and was predicted more accurately for higher concentrations of polystyrene. Various factors were investigated in attempts to explain the large errors in μ_s' observed.

The limited size of the phantom was not found to introduce any additional errors in estimated optical properties. It was found that the source detector separation used affected the results; two measurements performed at 20 mm produced errors of about 15%. This improved accuracy at ρ = 20 mm is consistent with previous results. Frequency domain analysis performed using the above measurements at two different distances produced more accurate results; the errors in μ_s' were about 6%. Further measurements performed on polystyrene phantoms indicated improved accuracy in the time domain fits for larger ρ values, up to 40 mm. The accuracy of the frequency domain fits also showed a dependence on the source detector separation used.

However, despite these investigations, the large observed errors were still not explained. The assumption of no mismatch in the indices of refraction of the probe and the phantoms was examined and verified. The total attenuation coefficient of polystyrene was measured directly and found to agree with theoretical predictions. The data collected and the theoretical results from the time domain system were compared to other methods and found to be in agreement. One possible explanation for the large differences observed in the estimates of μ_s' is the presence of a scattering delay not accounted for by diffusion theory. The small time spent by a photon on the act of scattering is not accounted for by the model. This would result in an overestimate in μ_s' in the time domain, as was observed in all the time-resolved experiments discussed in this thesis.

The determination of hemoglobin saturation depends on an accurate estimation of the absorption coefficient at two wavelengths. Therefore, a similar experiment to quantify the accuracy of the system in estimating μ_a was essential. Indocyanine green, a

dye that absorbs well in the 800 nm region was used to accomplish this. A direct transmission measurement was used to determine the variation of absorption with concentration for this dye. The dye could then be added to a polystyrene phantom with a known scattering coefficient in varying concentrations to increase the absorption of the phantom. Measurements at four different distances from 10 to 40 mm were performed and analysis was performed in both the time and frequency domains. Using the transmission measurement as the standard, the most accurate results were obtained from time domain methods at 20, 30 and 40 mm and relative distance frequency method using 40 and 10 mm data or 40 and 30 mm data and a multi distance approach. For large ρ values and if there is significant absorption, time domain results produced errors of about 10% in μ_s' and 2% in μ_a. The frequency domain approach becomes advantageous if the only measurements available are at 10 mm, due to a lack of signal or if the absorption of the phantom is low. The other advantage that is always present is the increased speed of the frequency domain fitting routine.

The final test of the system was to determine if induced variations in oxygenation of tissue could be quantified. Measurements at two wavelengths, 750 nm and 810 nm, were performed on the palm of the hand of a volunteer. The oxygenation status of the hand was varied by application of a blood pressure cuff to induce arterial occlusion. It was then possible to determine the hemoglobin saturation of the tissue volume under normal conditions and under reduced oxygenation. The normal hemoglobin saturation of the tissue varied between 70% and 80% for different measurements and decreased to about 50% following arterial occlusion. It was found that oxyhemoglobin concentration

decreased after occlusion and deoxyhemoglobin concentration increased, as expected. The concentrations calculated and the saturation values observed were similar to those measured by other authors but no "gold standard" is available for comparison. The fact that the results seem reasonable is encouraging and shows that this technique deserves further attention.

Various aspects of the time domain method could be improved. In terms of measuring optical properties, the accuracy of the system in predicting μ_a is acceptable, however, the large errors observed in μ_s' are not. The best means of improvement would be the inclusion of the time scattering delay into the time dependent diffusion model. Once the average scattering delay time is known, this becomes a simple task. Unfortunately, at this point, it is unclear how to best determine this parameter without introducing further difficulties. Therefore, until the average scattering time delay can be easily measured or calculated, large overestimates in μ_s' when measuring in the time domain should be expected.

For future *in vivo* measurements, much work is still needed. Since only preliminary measurements to determine the viability of the system were performed here, much characterization of the system is necessary. Measurements were performed at a ρ value of 10 mm only, due to a lack of reflectance signal and hence were analyzed in the time domain only. In order to measure at larger source detector separations, it is necessary to modify the system to deliver more light to the sample. If a more sensitive detector was used in place of the photodiode to detect the trigger signal, more light could be delivered to the sample itself. The collection fiber is currently manufactured in-house

and consists of six 400 μm fibers and a better bundle would result in better signal collection. These would be two simple ways to increase the amount of light delivered to the system without significantly increasing the cost. If measurements at larger distances were available, then two distance frequency domain analysis could be performed. This may lead to more accurate results but would certainly increase the speed at which results were obtained, an important condition if the system is to be used in a clinical environment. For repeated measurements of oxygenation status over time, automation of the collection and storage of data would be helpful to decrease the time spent on this process. As well, in the current technique the background absorption is estimated. There may be advantages to introduction of a third laser at a different wavelength. Measuring the absorption at three wavelengths would allow for the background absorption to be calculated based on measurement. This is only possible if the wavelength dependence of the background absorption is known.

The model used assumes that the tissue volume is a homogeneous semi-infinite slab. The effect of blood vessels in the area is probably not a factor if the diameters are small, although the layered structure of the tissue may not be well represented by this model. Better results have been observed when a layered model of the skin has been used. It would be simple to model the tissue as a two layered structure where the thickness of the top layer, i.e. the skin, is known and the underlying layer, the soft tissue, is considered semi-infinite. Before inaccuracies in the model can be quantified, it is necessary to have a system in which the oxygen status can be controlled. Other researchers have used various phantoms incorporating oxygen and blood, as well as yeast

to consume the oxygen. It would also be possible to diffuse gases through a liquid phantom to alter the oxygenation state. A method to quantify the hemoglobin saturation of a phantom must be developed so that comparisons between measured and expected oxygenation parameters can be made. Following the addition of these improvements, the full potential of the system for the *in vivo* noninvasive determination of hemoglobin saturation can be investigated.

6 REFERENCES

Aldrich, C.J., *et al.* 1994. The effect of maternal oxygen administration of human fetal cerebral oxygenation measured during labour by near infrared spectroscopy. *Br J Obstet Gynaecol, 101,* 509-513.

Anderson, R.R. 1993. Optics of the Skin. H.W. Lim & N.A. Soter (Eds.), In *Clinical Photomedicine.* New York: Marcel Dekker, Inc.

Bevington, P.R., and Robinson, D.K. 1992. *Data Reduction and Error Analysis for the Physical Sciences.* New York: Mcgraw-Hill Inc.

Bonner, R.F., *et al.* 1987. Model for photon migration in turbid biological media. *Journal of the Optical Society of America, A4,* 423-432.

Brazy, J.E., Lewis, D.V., and Mitnick, M.H. 1985. Noninvasive monitoring of cerebral oxygenation in preterm infants: Preliminary observations. *Paediatrics, 75,* 217-225.

Bruulsema, J.T., *et al.* 1997. Correlation between blood glucose concentration in diabetics and noninvasively measured tissue optical scattering coefficient. *Optics Letters, 22,* 190-192.

Chance, B. 1991. Optical method. *Annu Rev Biophys Chem, 20,* 1-28.

Chance, B., *et al.* 1990. A phase modulation system for dual wavelength difference in spectroscopy of haemoglobin deoxygenation in tissue. *Proc Soc Photo-Opt Instrum Eng, 1204,* 481-491.

Chance, B., *et al.* 1988a. Time-resolved spectroscopy of hemoglobin and myoglobin in resting and ischemic muscle. *Annals of Biochemistry, 174,* 698-707.

Chance, B., *et al.* 1988b. Comparison of time-resolved and -unresolved measurements of deoxygenation in brain. *Proceedings of the National Academy of Science of the USA, 85,* 4971-4975.

Cheong, W.F., Prahl, S.A., and Welch, A.J. 1990. A Review of the Optical Properties of Biological Tissues. *IEEE J Quant Elect, 26,* 2166-2185.

Cope, M. ,1991. Ph.D. Thesis. The Development of a Near Infrared Spectroscopy System and its Application for Non Invasive Monitoring of Cerebral Blood and Tissue Oxygenation in the Newborn Infant. University College.

Cope, M., and Delpy, D.T. 1988. System for long term measurement of cerebral blood and tissue oxygenation on newborn infants by near infrared transillumination. *Med Biol Eng Comput, 26,* 289-294.

Cubeddu, R., Pifferi, A., and Taroni, P. 1996. Experimental test of theoretical models for time-resolved reflectance. *Medical Physics, 23,* 1625-1633.

Delpy, D.T., *et al.* 1988. Estimation of optical pathlength through tissue from direct time of flight measurement. *Physics in Medicine and Biology, 33,* 1433-1442.

Duderstadt, J.J., and Hamilton, L.J. 1976. *Nuclear Reactor Analysis.* New York: John Wiley & Sons.

Fainchtein, *et al.* 1997. *In-situ* determination of concentration and degree of oxygenation of hemoglobin in neural tissue by pulsed photoacoustic spectroscopy. *Proc Soc Photo-Opt Instrum Eng, 2979,* 417-428.

Fantini, S., *et al.* 1995. Frequency-domain multichannel optical detector for noninvasive tissue spectroscopy and oximetry. *Optical Engineering, 34,* 32-42.

Farrell, T.J., Patterson, M.S., and Wilson, B.C. 1992. A diffusion theory model of spatially resolved, steady-state diffuse reflectance for the non-invasive determination of tissue optical properties *in vivo*. *Medical Physics, 19,* 879-888.

Ferrari, M., *et al.* 1992. Time-resolved spectroscopy of the human forearm. *J Photochem Photobiol B: Biol, 16,* 141-153.

Ferrari M., *et al.* 1991. Near infrared time-resolved spectroscopy and fast scanning spectrophotometry in ischemic human forearm. *Proc Soc Photo-Opt Instrum Eng, 1431,* 276-283.

Ferrari, M., *et al.* 1986. Effect of carotid artery compression test on regional cerebral blood volume, haemoglobin oxygen saturation and cytochrome-c-oxidase redox level in cerebrovascular patients. *Adv Exp Med Biol, 200,* 213-222.

Ferrari, M., *et al.* 1986. Cerebral blood volume and haemoglobin oxygen saturation monitoring in neonatal brain by near infrared spectroscopy. *Adv Exp Med Biol, 200,* 203-212.

Ferrari, M., *et al.* 1985. Continuous non invasive monitoring of human brain by near infrared spectroscopy. *Adv Exp Med Biol, 191,* 213-222.

Firbank, M., *et al.* 1996. An investigation of light transport through scattering bodies with non-scattering regions. *Physics in Medicine and Biology, 41,* 767-783.

Flock, S.T., Wilson, B.C., and Patterson, M.S. 1989. Monte Carlo modeling of light propagation in highly scattering tissues. II. Comparison with measurements in phantoms. *IEEE Transactions on Biomedical Engineering, 36,* 1169-1173.

Flock, S.T., Wilson, B.C., and Patterson, M.S. 1988. Hybrid Monte Carlo-diffusion theory modeling of light distributions in tissue. *Proc Soc Photo-Opt Instrum Eng, 908,* 20-28.

Groenhuis, R.A.J., Ferwerda, H.A., and Ten Bosch, J.J. 1983a. Scattering and absorption of turbid materials determined from reflection measurements. 1. Theory. *Applied Optics, 22,* 2456-2462.

Groenhuis, R.A.J., Ten Bosch, J.J., and Ferwerda, H.A. 1983b. Scattering and absorption of turbid materials from reflection measurements. 2. Measuring method and calibration. *Applied Optics, 22,* 2463-2467.

Hale, G.M., and Querry, M.R. 1973. Optical Constants of Water in the 200-nm to 200-μm Wavelength Region. *Applied Optics, 12,* 555-563.

Hall, E.J. 1988. The Oxygen Effect and Reoxygenation. In S.M. Gay & S. Robinson (Eds.), *Radiobiology for the Radiologist.* (pp. 137-160). Philadelphia: J.B. Lippincott Co.

Hampson, N.B., Camporesi, E.M., and Stolp, B.W. 1990. Cerebral oxygen availability by NIR spectroscopy during transient hypoxia in humans. *Journal of Applied Physiology, 69,* 907-913.

Haskell, R.C., *et al.* 1994. Boundary conditions for the diffusion equation in radiative transfer. *Journal of the Optical Society of America A11,* 2727-2741.

Hemenger, R.P. 1977. Optical properties of turbid media with specularly reflecting boundaries: applications to biological properties. *Applied Optics, 16,* 2007-2012.

Hielscher, A.H., *et al.* 1996. Time-resolved photon emission from layered turbid media. *Applied Optics, 35,* 719-728.

Hielscher, A.H., *et al.* 1995. Influence of Boundary Conditions on the Accuracy of Diffusion Theory in Time-Resolved Reflectance Spectroscopy of Biological Tissues. *Physics in Medicine and Biology, 40,* 1957-1975.

Jacques, S.L., and Flock, S.T. 1991. Effect of surface boundary on time-resolved reflectance: measurements with a prototype endoscopic catheter. *Proc Soc Photo-Opt Instrum Eng, 1431,* 12-20.
Jacques, S.L., and Prahl, S.A. 1987. Modeling Optical and Thermal Distributions in Tissue during Laser irradiation. *Lasers Surg Med, 6,* 494-503.

Jobsis, F.F. 1977. Non-invasive infra-red monitoring of cerebral and myocardial oxygen sufficiency and circulating parameters. *Science, 198,* 1264-1267.

Kelleher, J.F. 1989. Pulse oximetry. *Journal of Clinical Monitoring, 5,* 37-62.

Kienle, A., *et al.* 1998. Noninvasive determination of the optical properties of two-layered turbid media. *Accepted for publication in Applied Optics, 37.*

Kienle, A., and Patterson, M.S. 1997a. Improved solutions of the steady-state and time-resolved diffusion equations for reflectance from a semi-infinite turbid medium. *Journal of the Optical Society of America, A14,* 246-254.

Kienle, A., and Patterson, M.S. 1997b. Determination of the optical properties of semi-infinite turbid media from frequency-domain reflectance close to the source. *Physics Medicine and Biology, 42,* 1801-1819.

Kienle, A., and Patterson, M.S. 1996. Determination of the optical properties of turbid media from a single Monte Carlo simulation. *Physics in Medicine and Biology, 41,* 2221-2227.

Kohl, M., and Cope, M. 1994. Influence of glucose concentration on light scattering in tissue-simulating phantoms. *Optics Letters, 19,* 2170-2172.

Lakowicz, J.R., Lazko, G., and Grycynshi, I. 1988. Gigahertz frequency-domain fluorometry: Resolution of complex decays, picosecond processes and future developments. *Photochemistry and Photobiology, B2,* 295-311.

Lindberg, L.G., Lennmarken, C., and Vegfors, M. 1995. Pulse oximetry-clinical implications and recent technical developments. *Acta Anaesthesiol Scan, 39,* 279-287.

Liu, H., *et al.* 1995a. Determination of optical Properties and blood oxygenation in tissue using continuous NIR light. *Physics in Medicine and Biology, 40,* 1983-1993.

Liu, H., *et al.* 1995b. Influence of blood vessels on the measurement of hemoglobin oxygenation as determined by time-resolved reflectance spectroscopy. *Medical Physics, 22,* 1209-1217.

Madsen, S.J., *et al.* 1994. Portable, high-bandwidth frequency-domain photon migration instrument for tissue spectroscopy. *Optics Letters, 19,* 1934-1936.

Madsen, S.J. ,1993. Ph.D. Thesis. Experimental Studies of Time-Resolved Light Propagation in Turbid Media. McMaster University.

Madsen, S.J., *et al.* 1992a. Experimental tests of a simple diffusion model for the estimation of scattering and absorption coefficients of turbid media from time-resolved diffuse reflectance measurements. *Applied Optics, 31,* 3509-3517.

Madsen, S.J., Patterson, M.S., and Wilson, B.C. 1992b. The use of India ink as an optical absorber in tissue-simulating phantoms. *Physics in Medicine and Biology, 37,* 985-993.

Madsen, S.J., *et al.* 1991. Time resolved diffuse reflectance and transmittance studies in tissue simulating phantoms: a comparison between theory and experiment. *Proc Soc Photo-Opt Instrum Eng, 1431,* 42-50.

Maier, J.S., *et al.* 1994. Possible correlation between blood glucose concentration and the reduced scattering coefficient of tissues in the near infrared. *Optics Letters, 19,* 2062-2064.

Matcher, S.J., and Cooper, C.E. 1994. Absolute quantification of deoxyhaemoglobin concentration in tissue near infrared spectroscopy. *Physics in Medicine and Biology, 39,* 1295-1312.

Moulton, J.D. ,1990. M.Eng. Thesis. Diffusion Modeling of Picosecond Laser Pulse Propagation in Turbid Media. McMaster University.

Mudgett, P.S., and Richards, L.W. 1972. Multiple scattering calculations for technology II. *J Coll Interface Sci, 39,* 551-567.

O'Connor, D.V., and Phillips, D. 1984. *Time-correlated Single Photon Counting.* London: Academic Press.

Oda, M., *et al.* 1996. A simple and novel algorithm for time-resolved multiwavelength oximetry. *Physics in Medicine and Biology, 41,* 551-562.

Okada, E., *et al.* 1997. Theoretical and experimental investigation of near-infrared light propagation in a model of the adult head. *Applied Optics, 36,* 21-31.

Papazoglou, T.G., *et al.* 1995. Limitations of diffusion approximation in describing femtosecond laser transillumination of highly scattering media of biological significance. *Applied Physics Letters, 67,* 3712-3714.

Patterson, M.S. 1995. Noninvasive Measurements of Tissue Optical Properties: Current Status and Future Prospects. *Comments Mol Cell Biophys, 8,* 387-417.

Patterson, M.S., *et al.* 1991a. Frequency-domain reflectance for the determination of the scattering and absorption properties of tissue. *Applied Optics, 30,* 4474-4476.

Patterson, M.S., *et al.* 1991b. Diffusion equation representation of photon migration in tissue. in *Microwave Theory and Techniques Symposium (IEEE,* New York), 905-908.

Patterson, M.S., *et al.* 1990. Applications of time-resolved light scattering measurements to photodynamic therapy dosimetry. *Proc Soc Photo-Opt Instrum Eng, 1203,* 62-75.

Patterson, M.S., Chance, B., and Wilson, B.C. 1989a. Time resolved reflectance and transmittance for the non-invasive measurement of tissue optical properties. *Applied Optics, 28,* 2331-2336.

Patterson, M.S., Schwartz, E., and Wilson, B.C. 1989b. Quantitative reflectance spectrophotometry for the noninvasive measurement of photosensitizer concentration in tissue during photodynamic therapy. *Proc Soc Photo-Opt Instrum Eng, 1065,* 115-122.

Pogue, B.W. ,1996. Ph.D. Thesis. Frequency-Domain Optical Spectroscopy and Imaging of Tissue and Tissue-Simulating Media. McMaster University.

Prahl, S.A., *et al.* 1992. Determination of optical properties of turbid media using pulsed photothermal radiometry. *Physics in Medicine and Biology, 37,* 1203-1217.

Reichman, J. 1973. Determination of absorption and scattering coefficients for nonhomogeneous media 1. Theory. *Applied Optics, 12,* 1811-1815.

Reynolds, L., Johnson, C., and Ishimaru, A. 1976. Diffuse reflectance from a finite blood medium: applications to modeling of fiber optic catheters. *Applied Optics, 15,* 2059-2067.

Schmidt, J.M., Zhou, G.X., and Walker, E.C. 1990. Multilayer model of photon diffusion in skin. *Journal of the Optical Society of America, A7,* 2141-2153.

Severinghaus, J.W., and Kelleher, J.F. 1992. Recent Developments in pulse oximetry. *Anesthesiology, 76,* 1018-1038.

Sevick, E.M., *et al.* 1991. Quantitation of Time- and Frequency-Resolved Optical Spectra for the Determination of Tissue Oxygenation. *Analytical Biochemistry, 195,* 330-351.

Svaasand, L.O., *et al.* 1993. Properties of Photon Density Waves at Boundaries. *Proc Soc Photo-Opt Imstrum Eng, 1888,* 214-226.

Svaasand, L.O., and Ellingson, R. 1983. Optical properties of human brain. *Photochemistry and Photobiology, 38,* 293-299.

Tinet, E., Avrillier, S., and Tualle, J.M. 1996. Fast semianalytical Monte Carlo simulation for time-resolved light propagation in turbid media. *Journal of the Optical Society of America A13,* 1903-1915.

Tremper, K., and Barker, S. 1989. Pulse oximetry. *Anesthesiology, 70,* 98-108.

van de Hulst, H.C. 1980. *Light Scattering by Small Particles.* New York: Dover.

van Staveren, H.J., *et al.* 1991. Light scattering in Intralipid-10% in the wavelength range of 400-1100 nm. *Applied Optics, 30,* 4507-4514.

Wang, L.H., and Jacques, S.L. 1993. Analysis of diffusion theory and similarity relations for light reflectance by turbid media. *Proc Soc Photo-Opt Instrum Eng, 1888,* 107-116.

Weishaupt, K.R., Gomer, C.J., and Dougherty, T.J. 1976. Identification of singlet oxygen as the cytotoxic agent in the photo-inactivation of a murine tumor. *Cancer Research, 36,* 2326-2329.

Wickramasinghe, Y.A.B.D., Crowe, J.A., and Rolfe, P. 1986. Laser source and detector with single processor for a near infra-red medical application. *IEEE Progress Reports on Electronics in Medicine and Biology,* 209-215.

Wilson, B.C., Patterson, M.S., and Flock, S.T. 1987. Direct versus Indirect Techniques for the Measurement of the Optical Properties of Tissues. *Photochemistry and Photobiology, 46,*601-608.

Wilson, B.C., and Patterson, M.S. 1986. The Physics of Photodynamic Therapy. *Physics in Medicine and Biology, 31,* 327-360.

Wilson, B.C., and Adam, G. 1983. A Monte Carlo model for the absorption and flux distributions of light in tissue. *Medical Physics, 10,* 824-830.

Wyatt, J.S., *et al.* 1986. Quantification of cerebral oxygenation and haemodynamics in sick newborn infants by near infrared spectroscopy. *Lancet, 8515,* 1063-1066.

Yaroslavsky, I.V., *et al.* 1997. Effect of the scattering delay on time-dependent photon migration in turbid media. *Applied Optics*, *36,* 6529-6538.

Yu *et al.* 1997. Noninvasive investigation of skin local hypothermia influence upon local oxygenation and hemoglobin concentration. *Proc Soc Photo-Opt Instrum Eng,* 2979, 375-377.